REPUBLIQUE ALGERIENNE DEMOGRATIQUE ET POPULAIRE

Ministry of Higher Education and Scientific Research

Abdelhamid Ibn Badis University of Mostaganem

Faculty of Science and Technology

Department of Process Engineering

Faculty of Science and TechnologyAbdelhamid Ibn Badis University, Mostaganem

Submitted in accordance with the requirements for the degree of

PhD in 3rd cycle BMP

in Process Engineering

SPECIALITY: ***Chemical Engineering***

By

Bilal BELMEKKI

Control of oxidative processes in plasma reactors

Date of presentation: 26/02/2025

In front of the thesis jury composed of:

President:	**Fatiha ABDELMALEK**	Professor	Mostaganem University
Examinators:	**Amine KHELIFA**	Professor	Mostaganem University
	Abdelmadjid RAIS	Professor	Sidi Belabes University
	Abdelkader CHOUAIH	Professor	Mostaganem University
Invited	**Ahmed ADDOU**	Professor	Mostaganem University
Thesis director:	**Mouffok Rédouane GHEZZAR**	Professor	Mostaganem University

ACADEMIC YEAR: 2024/2025

Acknowledgment

First, I would like to thank **Allah**, who gave me the power, the will, and the conscience to complete this work.

Thanks to my dear parents, **Hadj HAMOU** and **Hadja NOURIA**, for the moral support they gave me and all the sacrifices they made for me during my years of study, and I ask Allah to protect them. To my sisters, brothers, and all members of my small family to the big one, from very close to far, thank you for your support and the pride you have shown me.

I would like to express my sincere thanks to my thesis supervisor, **Mouffok Redouane GHEZ-ZAR**, Professor at the University of Mostaganem, for his availability, patience, involvement, and invaluable advice. As well as the scientific, academic, and personal knowledge he provided me with both during and outside the preparation of my thesis. He has my deepest respect. I would like to express my deepest gratitude to him for having made this work so motivating and enriching.

This work was carried out at the Laboratoire des Sciences et Techniques de l'Environnement et de la Valorisation (**S.T.E.V.A**) under the supervision of Professor **ABDELMALEK Fatiha** of the University of Mostaganem, whom I would like to thank for the honor of welcoming me to her laboratory and providing me with the means to carry out my research. I particularly appreciated her pertinent advice and broad understanding. I would like to express my sincere gratitude. I would like to thank her once again for agreeing to examine my research work as president of the jury.

I would particularly like to thank Professor **KHELIFA Amine** for having opened the doctoral program that enabled me to complete my post-graduate studies. I would like to express my sincere gratitude to him for the honor he has bestowed on me by examining my work despite his various scientific and pedagogical duties.

I would like to express my deepest gratitude to Mr **ABDELMADJID RAÎS**, Professor at the University of Sidi Belabbes, who honors me with his presence by agreeing to examine this work despite his busy schedule.

A lot of thanks are addressed to Mr. **CHOUIAH Abdelkader**, Professor at the University of Mostaganem, for the honor he has bestowed on me by examining my work despite his various scientific, academic, and pedagogical duties.

I would like to thank Professor **Ahmed ADDOU** for his relevant advice, expertise, knowledge, and experience, which he transferred to me during the preparation of my research thesis in the STEVA laboratory. A second thanks is addressed to him for accepting to examine my research thesis.

I would like to thank all the members of the STEVA laboratory, including staff, PhD students, and technicians, as well as my PhD colleagues and friends from other departments and faculties, who supported, helped, and accompanied me during my PhD years.

Contents

Abstract

The aim of this thesis is to control plasma-liquid interactions by means of a chemical engineering approach based on some well-known but sometimes new approaches.

The first control step consists of comparing the operating regimes of each Gliding Arc Discharge plasma reactor and considering a new reactive device capable of positioning itself with the other reactors according to the needs expressed by the user. The operating principle of this new reactor is inspired by the Venturi flow principle, and its spatiotemporal discharge mode enables the production of molecules for industrial use. It is a plasma reactor that operates efficiently from both a production and an economic point of view. For the safety front, the investigations indicate a high level of safety (SIL2) compare to the other plasma reactors. Adopting the double film theory and following a more modern approach to the mathematical treatment of mass transfer, it was possible to calculate the operating regime of each plasma reactor handling liquid media. Based on this evaluation, the new reactor with the best efficiency-safety ratio was selected to produce Catechol from phenol molecules at Lab and Industrial scales using the novel GAD-VNT plasma reactor.

The conceptualization of the chemical control of plasma reactions has opened up great perspectives on easy, economical, and safe industrial organic synthesis.

Tables list

Figures list

Equations List

Chemical reactions list

General introduction

Faced with the growing importance of environmental considerations in the early 2000s, chemistry has never had a good reputation. However, a real movement is underway to move towards “green” chemistry, where researchers have shown great interest in the subject. The trend was towards increasing the energy efficiency of processes, replacing organic solvents with aqueous solvents, and seeking increasingly efficient and eco-friendly technologies and catalysts.

In parallel, a new technology has shown a good evolution of use in the field of water treatment because of its primordial efficiency. These technologies are cold plasmas, which can be produced under different processes, such as corona discharge, dielectric barrier discharge (DBD), jet discharge, and sliding discharge (GAD). In these technologies, the plasma is created at room temperature and atmospheric pressure by means of two electrodes, between which a strong potential difference is imposed. In this state of matter, which remains at room temperature, very energetic species are then created: electrons of several eV, excited molecules, free radicals, and ions. These reagents are capable of initiating chemical reactions that are difficult to achieve in ordinary chemistry. As these plasmas can be produced under normal pressure and temperature conditions, the need for expensive or energy-intensive facilities is reduced. In some cases, plasma can replace them and act precisely as a catalyst, thanks to the exotic species it contains. Therefore, the use of plasmas in chemistry could go in the direction of "green" chemistry by reducing the consumption of energy and catalysts in the processes. Plasma can also create new reaction pathways that could simplify currently complex synthesis protocols thanks to radicals that are difficult or even impossible to produce by chemistry.

In fact, the use of plasmas in organic synthesis has remained limited due to its low selectivity in the sense of producing a pure chemical compound that meets the requirements of the target market. They are very effective in the destruction of pollutants, but more selective chemical reactions have so far remained out of their reach.

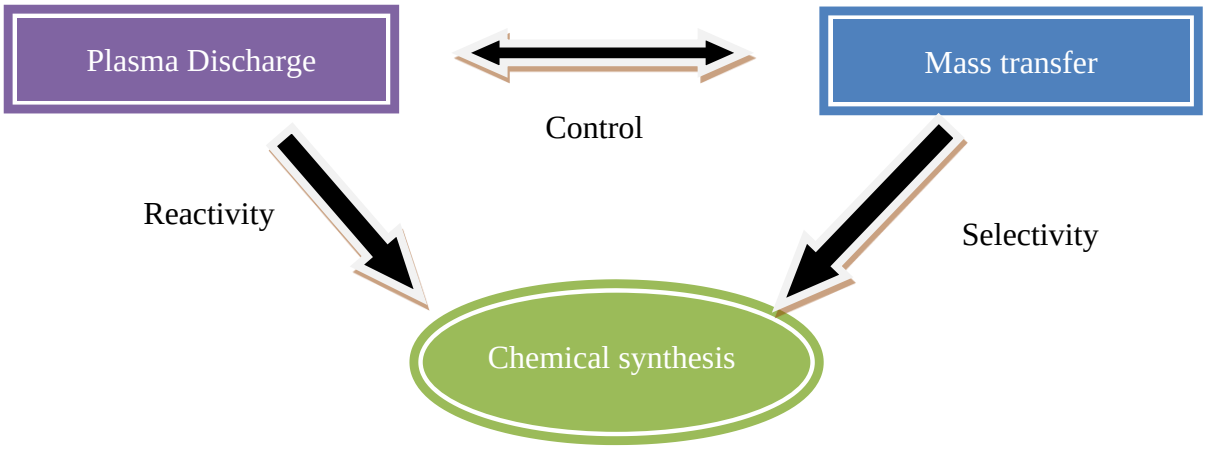

Figure 1. Synergy of disciplines

In order to find executable solutions for controlling oxidative processes based on reactivity, mass transfer, and simulation of these processes (Figure 01), we have developed this document, which is divided into 04 chapters: a chapter on the literature review, a chapter on the methodology and materials used, and finally two chapters on the results obtained. Thus:

Chapter I, "State of art", first highlights a review of the literature on plasmas in general and, in the background the Glidarc discharge used in our study, as well as the state of the art on this type of plasma processes, its applications, its advantages and its limitations. In a second time, it presents the basic concepts and the solutions proposed for the control of this process.

The second chapter "Materials and methods" presents the different plasma glidarc configurations present in the STEVA laboratory, including the description of the new reactor with its design parameters. As well as, the main methods and analysis techniques used during our work.

Chapter 3, "Classification of plasma GAD reactors", presents the chemical and physical properties of the configurations studied, such as gas-liquid transfer coefficient, acidity, conductivity, total oxidant agents, nitrite, and nitrate ion concentrations. These results were used to study the reaction-mass transfer competition in the four plasma GAD configurations, and subsequently, the induction of this competition on the performance of these devices was established, such as depollution, chemical conversion, selectivity, and safety contribution.

Chapter 4, "Catechol production process using plasma reactor", presents the thesis project, announcing the proposal of a new process dedicated to the industrial production of catechol. The invention is based on the use of the glidarc plasma reactor in the new configuration proposed

in Chapter II (GAD-V). This process has shown relevant performance in terms of production rate, selectivity, and economic interest.

Finally, the overall conclusion of this paper will point the way to future optimization and intensification of cold plasma technology in industrial processes.

CHAPTER I. Plasma reactors – State of the art

Generalities

Plasma, often referred to as the fourth state of matter, is a highly ionized gas consisting of ions, electrons, and neutral particles. The term "plasma" was coined by Irving Langmuir in the 1920s while studying electric discharges in vacuum tubes [1]. He used the term to describe the ionized gas because of its composition analogy to the blood plasma, which carries cells and nutrients. The plasma state is formed when a gas is energized to the point where electrons are freed from atoms. This ionization process can occur through various means, such as heating or exposure to strong electromagnetic fields, and can lead to magnetic confinement phenomena in fusion reactors due to their excellent electrical conductivity. Plasma is prevalent in both natural and artificial environments where the natural one occurs abundantly in the universe and helps study astrophysical phenomena, while artificial plasmas developed in laboratories have diverse applications in medicine and scientific research. Unlike solids, liquids, and gases, plasma does not have a definite shape or volume and is influenced by electromagnetic fields. These unique properties make it a significant area of study in various scientific fields.

1. Plasma classification

Within the plasma, the thermodynamic equilibrium between species is not fully defined. However, stationary states occur, in which each particle species has an energy characterized by a temperature T, as presented in Figure 2. This is defined by the average kinetic energy [2]. Heavy species have comparable average kinetic energies, represented by the macroscopic temperature Tg. Electron energies, on the other hand, can be at much higher temperatures (Te). Based on the energy distribution among the particles and the difference between the electron and the heavy species temperature, plasmas are categorized into two main types: thermal and non-thermal plasmas. This classification is dictated by whether or not local thermodynamic equilibrium (LTE) is established. A medium is said to be in local thermodynamic equilibrium when the temperature of the electrons is identical to that of the gas.

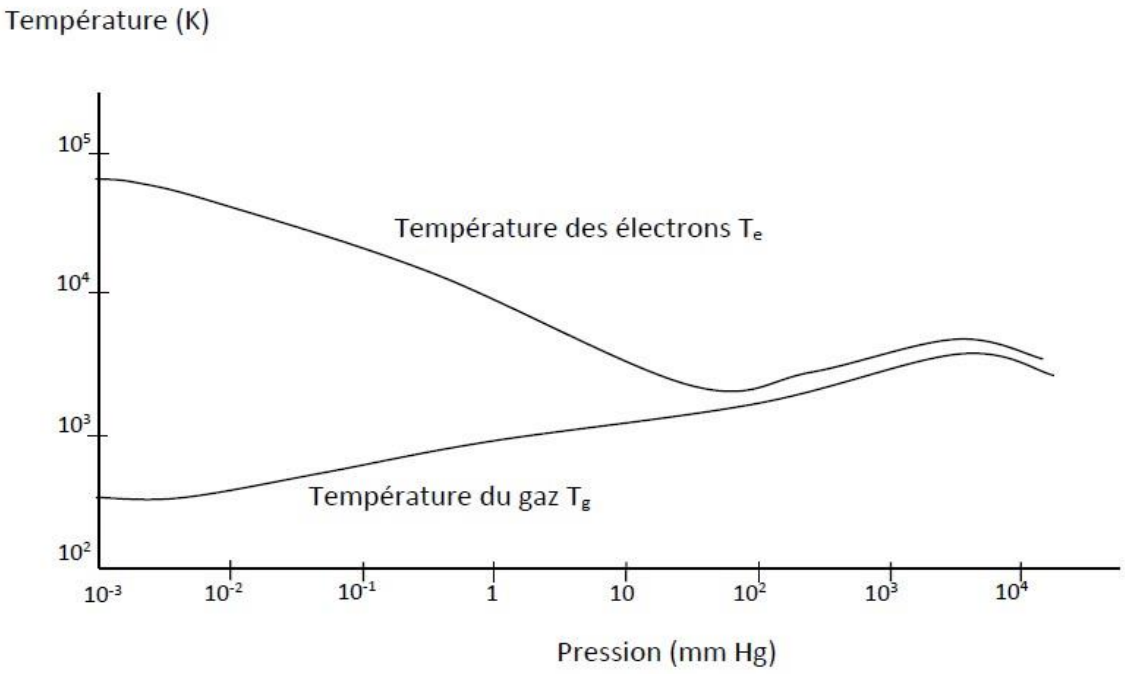

Figure 2. Temperature of electrons and heavy species in plasma [120]

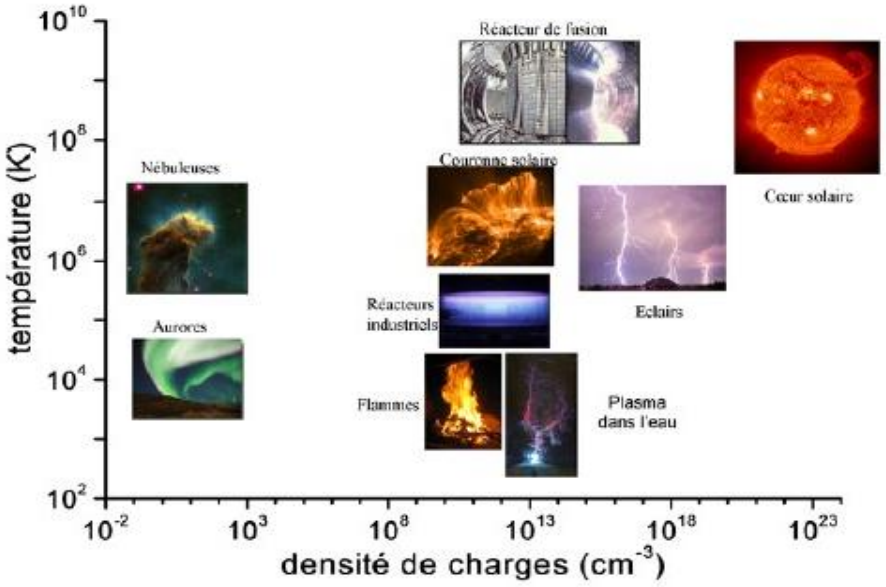

Figure 3. Classification of displacement in a logarithmic diagram according to electron temperature and charge density [121]

1.1 Thermal plasma

Thermal plasmas are obtained at high pressures and temperatures [3]. They are rich in highly energetic ions and electrons. The energy involved can be considerable, requiring powers of up to 50MW [4, 5].

When a plasma is ignited in the laboratory, the energy generated by the electric field is first accumulated by the electrons. For this reason, the initial temperature of the electrons is higher. Subsequent collisions transfer this energy to the ions (heavier particles). This balances the temperatures inside the plasma [6].

The temperature difference between electrons and heavy particles is defined as being proportional to the square of the ratio of electric field to pressure. In hot plasmas, this ratio is low, and the temperatures of electrons and ions are close together, around 10,000 K. This indicates a local thermodynamic equilibrium between the electrons and the heavy species, and the temperatures of the electrons and ions are in equilibrium, and close to each other. In this case, we can speak of thermal plasma.

Natural thermal plasmas

-**The Sun and Other Stars**: The cores of the Sun and other stars are examples of natural thermal plasma. These are incredibly hot regions where nuclear fusion occurs, creating a plasma that is in thermal equilibrium.

Laboratory thermal plasma

- **Arc discharges:** these are self-sustaining direct-current discharges with a relatively low voltage drop at the cathode (around 10 KV)

- **Radio-frequency or microwave plasma discharges:** used when it is important to contact between the plasma and the electrodes. A high-voltage electric current is passed through a solenoid, creating an axial magnetic field.

1.2 Non-thermal plasma

These plasmas are easier to obtain and more stable at atmospheric pressure [7-9]. They are characterized by the lack of thermodynamic equilibrium between electrons and gas molecules. The well-known ratio between electric field and pressure is high, meaning a big difference between the temperature of electrons and heavy species ($Te = 10^4$-10^5, $Tg = 10^2$ -10^3 K). Electrons will not be able to transfer their energy to heavy particles because of the low energy supplied in these processes compared with hot plasmas. In this case, the electrons accelerated by the electric field collide inelastically with the heavy species and transfer part of their kinetic energy to them, giving rise to reactive species such as metastable species, radicals, and ions. These created reactive species are subject to use in various applications such as medicine, depollution, surface treatment, etc.

Natural Non-Thermal plasmas:

- **Auroras (Northern and Southern Lights):** Auroras are beautiful natural displays of light in the polar regions caused by the interaction between the solar wind (a plasma from the Sun) and the Earth's magnetosphere. When charged particles from the solar wind collide with gases in the Earth's atmosphere, they create a cold plasma.

Laboratory thermal plasma:

- **Crown discharges:** faint glow discharges appearing at atmospheric pressure on tips or edges where the electric field is sufficient [10].

- **Pulsed corona discharges:** an improvement on corona discharges, they enable micro-discharges to be formed without the need for an arc [11].

- **Dielectric barrier discharges:** the addition of a dielectric material prevents arcing [12].

- **Glidarc discharge:** obtained by electrical treatment of the gliding arc type [13].

2. Non-thermal plasma technologies

In contrast to low-pressure plasmas, which need vacuum conditions, atmospheric plasma technologies generate and apply plasma at or near atmospheric pressure. These technologies are extensively employed across many sectors due to their adaptability, effectiveness, and capacity to function without intricate vacuum systems. Below are some of the most prominent atmospheric plasma technologies.

2.1 Dielectric barrier discharge (DBD)

DBD plasma is produced by applying a high-tension alternative to two electrodes. At least one of them is recovered by a semi-conducting material or insulator called an electrical barrier. This later ensures a temporary discharge function and prevents the creation of an arc.

When the voltage applied to the electrodes is sufficiently high, avalanche ionization phenomena emerge. The naturally occurring electrons in the gas are being accelerated by the electrical field and collide to produce new electrons; this is the avalanche phase. These charges propagate along the field lines, leaving a trained ionized streamer corresponding to the micro-discharge channel with a wavelength of about 100 μm [14].

Current flowing through the channel leads to an accumulation of charges on the dielectric (Figure 3). When the field induced by these charges masks the applied field, the discharge is extinguished.

This charge deposit delimits an area of the dielectric where the field is weakened. This means that future micro-discharges will have to propagate alongside it. The presence of the dielectric not only inhibits the arc but also spatially distributes the filaments. The plasma will, therefore, cover the entire available surface.

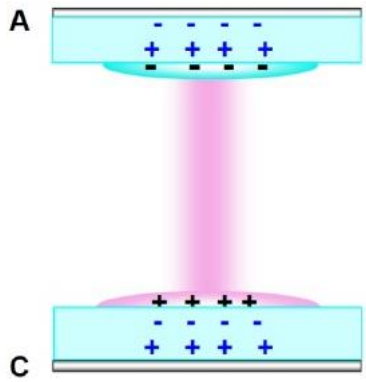

Figure 4. Schema of Dielectric Barrier Discharge [15]

2.2 Corona discharge

A corona discharge is achieved by applying a suitable potential difference between two asymmetrical electrodes, such as tip/plane, tip-cone, and wire-tube coaxial as active and passive electrodes, whose respective radii of curvature are very different in order to obtain a much stronger electric field in the vicinity of one of the two electrodes. As a result, two different zones can be distinguished: the luminous ionization zone located around the electrode with the smaller radius of curvature and the diffusion zone where the ions move along the field lines. Figure 4 presents the corona discharge with two different electrodes [14, 16].

The creation of the ionized channel (streamer) is identical to that observed in a DBD. However, the discharge is extinguished in areas where the electric field is too weak to maintain ionization [14].

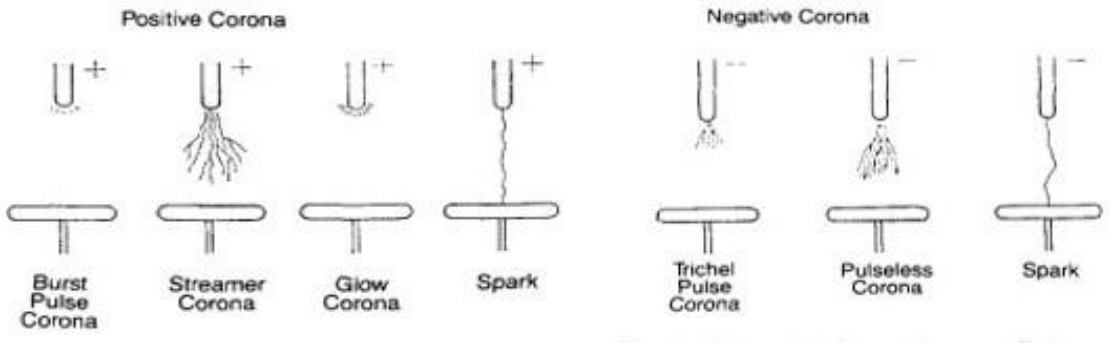

Figure 5. Schematic of different types of corona discharge [17]

2.3 Jet discharge

Atmospheric Pressure Plasma Jets (APPJ) are devices that generate a focused stream of plasma in open air. Usually, it consists of two electrodes: a high-voltage electrode and a grounded electrode. Depending on the design, the grounded electrode might be placed outside or integrated into the setup, while the high-voltage one is often placed inside the dielectric tube (see figure 05).

The majority of jets operate using noble gases, such as argon or helium, mixed with trace amounts of reactive gases, like air, water, or oxygen. The gas is fed into a dielectric tube at a controlled rate to maintain a stable jet. When the high voltage is applied, the electric field ionizes the gas atoms or molecules, stripping electrons from them. Note that the sharp tip of a needle electrode offers the advantage of enhancing the electric field locally. This creates a mixture of free electrons, ions, and neutral particles, forming the plasma. The free electrons gain energy from the electric field and collide with neutral gas atoms, causing further ionization

in a process called electron avalanche. This cascade of ionization events leads to the rapid formation of plasma.

An important disadvantage of plasma jets is that the surface area of the treatment is relatively small, considering that wounds eligible for plasma treatment might be as large as several squared centimetre. Obviously, this could be solved by moving the jet along the treatment area or install several jets in parallel system, that was already studied by Kong et al [18,19]..

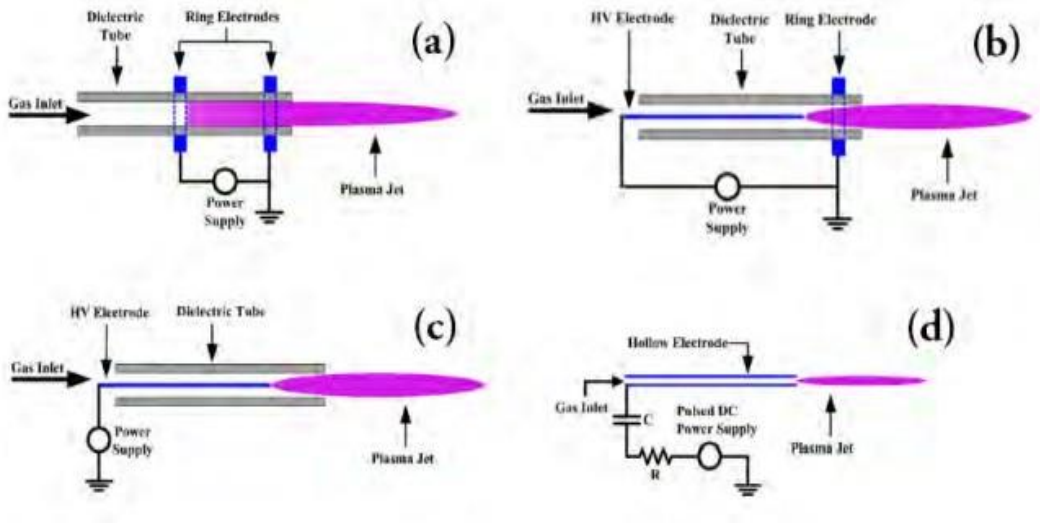

Figure 6. Schematics of different plasma jet designs [20]

2.4 Gliding arc discharge

The "Glidarc" is a non-thermal plasma obtained by electrical effluvage of the sliding arc type, a simple and inexpensive process developed by Czertnichwski [21, 22]. Unlike dielectric barrier and corona discharges, which require very high voltage values, this technique involves applying a relatively low potential difference of 5 to 10 KV between two diverging electrodes arranged symmetrically around a gas stream. An electric arc is ignited at the minimum distance between the electrodes and slides, under the effect of the flow, along them, lengthening thanks to their divergence [23], as shown in Figure 6. In the arcing zone, the energy supplied by the high-voltage generator, expended in the arc by the Joule effect, compensates for the power evacuated by thermal conduction. As this phase is in thermodynamic equilibrium, the temperature of the electrons is equal to that of the heavy particles.

When the arc propagates along the electrodes, the electrical power dissipated by the Joule effect no longer compensates for the power evacuated by thermal conduction. The discharge then evolves into a non-equilibrium plasma. The temperature of the electrons, 10000 K, is higher than that of the heavy species, 1500-3000 K. During this second phase, electrical treatment begins. 75-80% of the total energy involved in the discharge is expended in the non-equilibrium

phase. It is these reactive species that are partly responsible for the chemical properties and lethal effect of Glidarc [24].

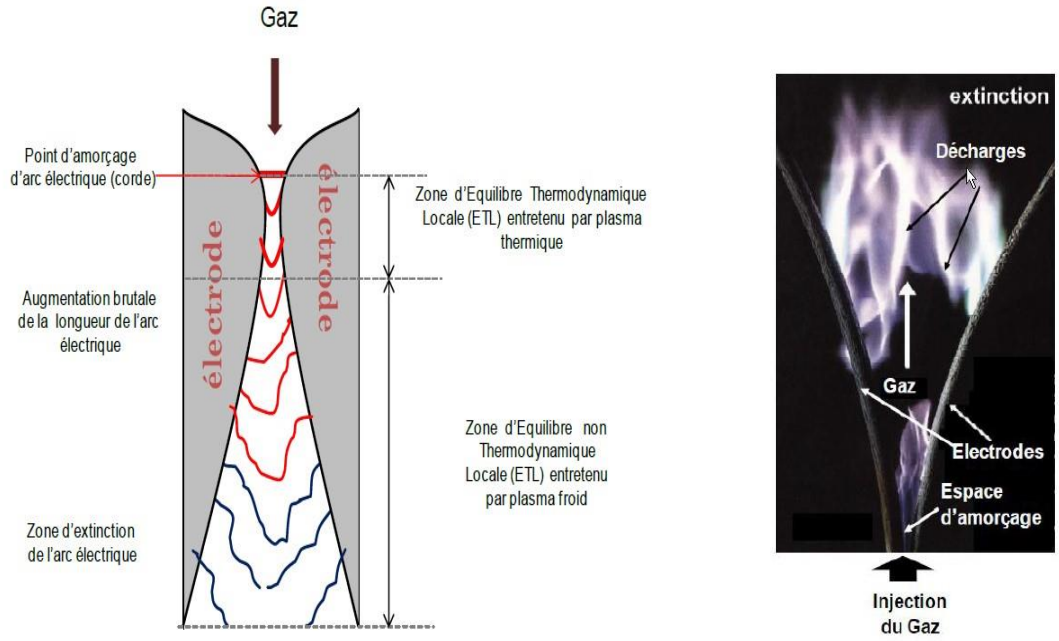

Figure 7. Plasma Gliding Arc Discharge, (a) electrode profile and evolution of the sliding arc, (b) photograph of the evolution of the sliding arc [25]

3. Plasma gliding arc discharge applications

Historically, non-thermal plasmas have been studied at low pressure in discharge tubes. Their use under reduced pressure is still widespread in micro-fabrication (etching, thin-film deposition, plasma-assisted chemical vapor deposition, etc.) but requires complex and costly installations. As a result, atmospheric-pressure plasmas such as glidarc plasmas are increasingly used today. In addition, glidarc plasma can operate at high gas flow rates, enabling larger volumes to be processed and making it suitable for various applications. First, Czertnichwski developed the gliding arc for gas treatment [21, 22], then further researches were conducted on environmental remediation, material processing, medical applications, and chemical synthesis.

Figure 8. Cold Plasma Gliding arc discharge applications [21]

3.1 Environmental remediation

Gliding arc plasma has shown significant efficacy in environmental applications such as VOC abatement and organic Pollutant Degradation. The high energy electrons and reactive species (such as O, $^{\bullet}$OH, and N) produced in the plasma interact with VOC molecules, breaking them down into less harmful molecules such as CO_2 and H_2O, reducing their environmental impact [26-29]. Furthermore, water contaminated with organic pollutants, including pesticides, dyes, and medications, can also be treated using gliding arc discharge. The reactive oxygen and nitrogen species (RONS), such as hydroxyl radicals ($^{\bullet}$OH) and nitrogen oxide ($^{\bullet}$NO) generated in the plasma can effectively break down the outlined contaminants under a complex mechanism going from oxidation to mineralization processes [26, 30-33].

3.2 Material processing and surface treatment

In recent years, plasma GAD has been widely used for surface modification of materials such as polymers and membranes. The high reactivity of the produced plasma, such as technology, allows the grafting of functional groups like hydroxyl, carboxyl and amine onto the treated

material surface, enhancing their mechanical and adhesion properties, wettability, and biocompatibility [34-37].

The plasma treatment of metal surfaces is also becoming a promising process for anticorrosion activities and affects their mechanical properties. The relatively low temperature of the gliding arc discharge makes it suitable for treating temperature-sensitive materials. This process, especially with nitrogen-containing gases, has greatly enhanced the hardness, wear resistance, and corrosion resistance of metal surfaces [38-44].

In addition, several studies have used gliding arc discharge for plasma-enhanced chemical vapor deposition (PECVD), wherein reactive species from the plasma help deposit thin films of materials onto substrates [45-49]. This process is critical in applications such as semiconductor manufacturing, solar cells, and protective coatings.

3.3 Medical applications

Gliding arc discharge has been explored for medical applications, such as wound healing, cancer therapy, infection control, etc. The antimicrobial properties of this technology were widely studied for different bacteria groups, and it showed a high level of microbial inactivation, even for resistant ones, due to the high amount of produced plasma oxidants [50-52]. Additionally, the antimicrobial properties of plasma help prevent infection, making it suitable for treating chronic wounds, burns, and ulcers. The plasma-generated reactive species can also promote angiogenesis, cell proliferation, tissue regeneration, and inflammation reduction [54-59]. GAD plasma has been investigated for its potential in cancer therapy, where the reactive oxygen and nitrogen species (ROS and RNS) generated by plasma can induce oxidative stress in cancer cells that trigger their apoptosis (programmed cell death), offering a non-invasive treatment option [60-64].

3.4 Chemical synthesis

Plasma-based chemical synthesis, mainly through Gliding Arc Discharge (GAD) plasma, has emerged as an auspicious approach for enhancing reaction kinetics and enabling chemical transformations that are challenging to achieve through conventional thermal processes. The synthesis of ammonia (NH_3) via plasma-assisted nitrogen fixation is one of the emerging applications of gliding arc plasma. In this process, nitrogen (N_2) from the atmosphere is dissociated into reactive nitrogen species, which then combine with hydrogen to form ammonia. This process offers an alternative to the traditional Haber-Bosch process, potentially reducing energy consumption and greenhouse gas emissions [65-69]. In addition, Plasma can facilitate the

hydrogenation of CO_2 into methane (CH_4) or other hydrocarbons, offering a pathway for renewable fuel production [70-76]. This process contributes to carbon capture and utilization (CCU) strategies, turning CO_2 into valuable products while reducing its environmental impact.

3.5 Agriculture applications

Plasma technology, particularly Gliding Arc Discharge (GAD) plasma, has emerged as a promising tool for improving agricultural productivity. This technology can be used to generate plasma-activated water that is highly concentrated by reactive species such as oxygen and nitrogen radicals. Oxygen reactive species like hydrogen peroxide H_2O_2 inactivate harmful pathogens such as bacteria, viruses, and fungi and help for better plant health. Nitrogen species, such as nitrates (NO_3^-) and nitrites (NO_2^-), which are essential nutrients for plant growth [77-85]. By irrigating crops with plasma-activated water, farmers can effectively deliver bioavailable nitrogen to plants, reducing the need for synthetic fertilizers

4. Plasma GAD challenges

Plasma gliding arc discharge technology offers numerous advantages, particularly in chemical synthesis, environmental applications, and agriculture; the laboratory scale has shown promising results; however, scaling them up for industrial processes is the most challenging part. Several limitations must be addressed to improve its efficiency, selectivity, scalability, safety, and commercial viability. These challenges are primarily related to technical, economic, and operational aspects of GAD systems [86-89].

1. Energy efficiency: In GAD systems, a significant portion of the energy is dissipated as heat rather than contributing to generating reactive species. This inefficiency can lead to higher operating costs, especially in large-scale industrial applications.
2. Low Selectivity in Chemical Reactions: The versatile population of produced plasma species, such as rectors, makes it difficult to control the selectivity of chemical reaction pathways. This complexity can result in the formation of undesired by-products, reducing the efficiency of the target reaction and the quality of the final product, which then requires a hard purification process and higher operational cost.
3. Uniformity of plasma medium: Maintaining uniform distribution of reactive species over a large volume is another significant limitation, especially for large-scale systems. This lack of uniformity affects the performance of plasma-based processes. Moreover, the plasma arc

creates localized high-temperature zones, resulting a partial reactions or incomplete conversion that is highly undesirable for chemical synthesis processes.

4. Material degradation: The intense energy and reactive environment generated in GAD plasma systems can cause material degradation over time, leading to equipment wear and reduced operational efficiency. Finding materials that can withstand the harsh conditions inside a plasma reactor is a key obstacle in scaling up the technology.
5. Safety Concerns: The high voltage, intense radiation, and presence of free radicals in GAD plasma systems raise the probability of hazardous operability risks. The long exposition to the reactive oxygen and nitrogen species and UV radiations generated by plasma can pose health risks and occupational diseases.
6. Economic considerations: The cost-benefit duality in such as processes have to be comparatively studied with the conventional processes, including costs of implementation, equipment, maintenance, energy consumption, and final product pricing.

5. Plasma GAD characterizations

5.1 Consumed energy

The energy consumed in a gliding arc discharge (GAD) plasma system depends on several factors, including input power, operating voltage and current, gas flow rate, gas nature, electrode configuration, and overall system efficiency.

Generally, the gliding arc plasma operates with a high voltage of around 9 kV and a moderate current of 100 mA [90]. The electrical power input P is 0.9 kW, calculated using the following formula:

$$P = V * I \qquad \textbf{(Eq. 1)}$$

A specific energy consumption is usually calculated to examine the plasma consumed energy in different reactors. It can be expressed as the amount of energy consumed per unit volume of gas treated or per unit mass of gas treated.

$$\text{Specific Energy Consumption (SEC)} = \frac{P}{Q} \qquad \textbf{(Eq. 2)}$$

Q: is the gas flow rate ($m^3\ h^{-1}$)

For a gas flow rate of 700 $l.h^{-1}$, a 1.29 kW h m^{-3} was consumed. The SEC provides a measure of the energy efficiency of the GAD process for different gases and flow rates.

In such reactors, the energy is not totally conserved, and some energy is lost as heat due to the resistance of the electrodes and the surrounding gas. The efficiency of converting electrical energy into plasma energy can vary but is generally less than 100%.

Unlike corona discharge, this technique consumes more energy (1.29 kW h m^{-3}) [90], resulting in a higher production of active species. These criteria make it ideal for industrial applications in pollution control.

5.2 Processes occurring in plasma GAD

Plasma Gliding Arc Discharge (GAD) technology in gas-liquid systems presents a unique platform for numerous physical and chemical phenomena. This part explores the key processes occurring in the plasma gas region, gas-liquid interface, and liquid region.

5.2.1 Gas region

The unique properties of plasma arise from the collective behaviour of the charged and neutral particles, leading to various physical and chemical processes. Table I.1 shows the different types of processes that occur within plasma and can, therefore be grouped in terms of excitation, ionization, dissociation, recombination, and other reactions [91].

Table 1. The principal reaction types in plasma phases [95]

Reaction process	Reaction type	Reaction	N°
Excitation	By heavy particle	$A + B \rightarrow A^{\cdot} + B$	**(R 1)**
	By photon	$A + h\vartheta \rightarrow A^{\cdot}$	**(R 2)**
	By electron	$A + e^{-} \rightarrow A^{\cdot} + e^{-}$	**(R 3)**
	By transfer	$A + B^{\cdot} \rightarrow A^{\cdot} + B$	**(R 4)**
Deexcitation		$A^{\cdot} \rightarrow A + h\vartheta$	**(R 5)**
Ionisation	By heavy particle	$A + B \rightarrow A^{-} + B + e^{-}$	**(R 6)**
	By photon	$A + h\vartheta \rightarrow A^{+} + e^{-}$	**(R 7)**
	By attachment	$A + e^{-} \rightarrow A^{-}$	**(R 8)**
Charge transfer		$A + B^{+} \rightarrow A^{+} + B$	**(R 9)**
Dissociation	By photon	$A_2 + h\vartheta \rightarrow A + A$	**(R 10)**
	By electron	$A_2 + e^{-} \rightarrow A + A + e^{-}$	**(R 11)**
	By transfer	$A_2 + B \rightarrow A + A + B$	**(R 12)**
Recombination	Between atoms	$A + A + B \rightarrow A_2 + B$	**(R 13)**
	Electron/ion	$e^{-} + A^{+} \rightarrow A + h\vartheta$	**(R 14)**
	Ion/ion	$A^{-} + B^{+} \rightarrow AB$	**(R 15)**
	Between radicals	$R^{\cdot} + H^{\cdot} \rightarrow RH$	**(R 16)**
	Ion/molecules	$A^{+} + B \rightarrow AB^{+}$	**(R 17)**

These reactions can be grouped into three main processes: the primary process, closely linked to the physics of the discharge; the secondary process close to chemical plasma part; and the third one for liquid interaction (figure 9) [25].

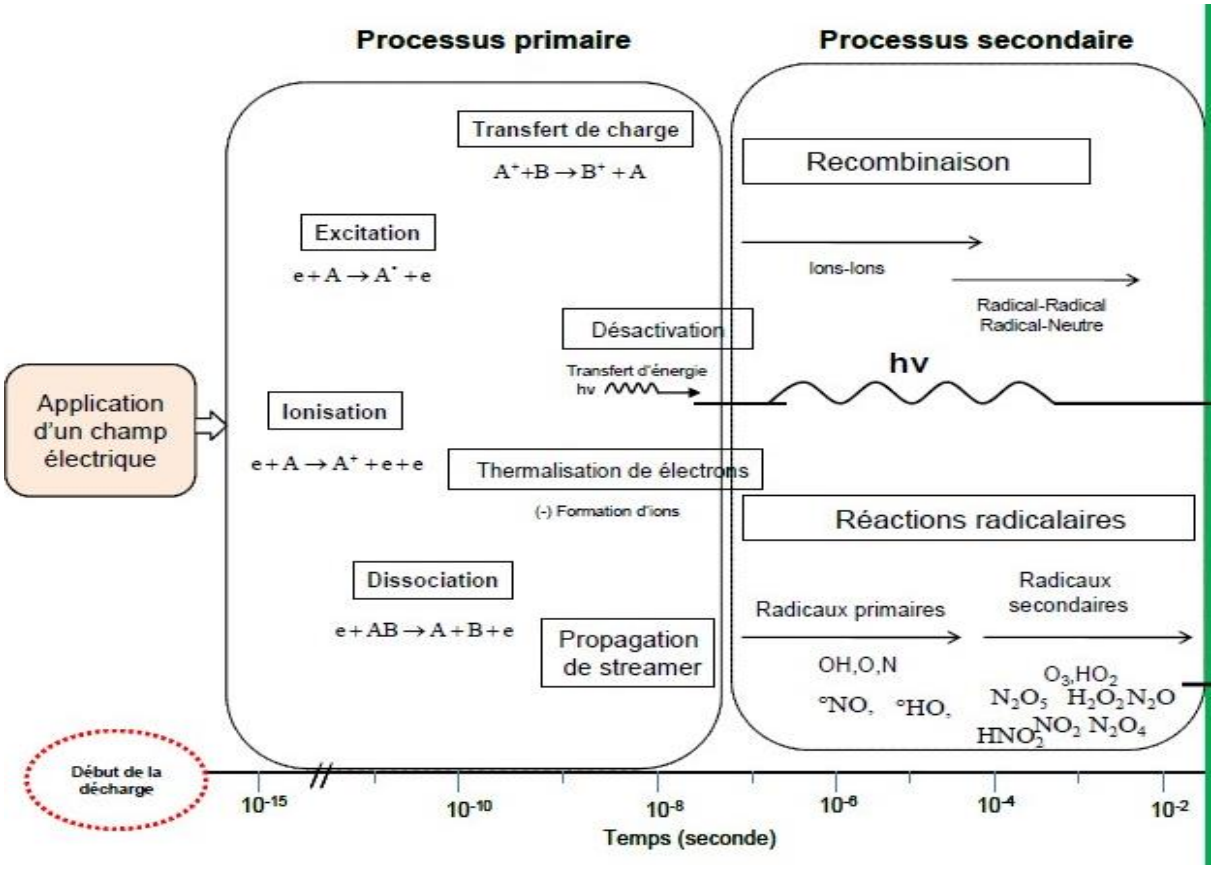

Figure 9. Mechanism of plasma reactive spices in plasma gas [25]

The primary process gathers the ionization and excitation reactions that the produced electrons start by applying the appropriate potential difference, followed by the charge transfer and streamer propagation reactions. The time scale of the primary process-governing phenomena is on the order of nanoseconds (ns). The type of discharge, the type of current used, the shapes, and the structure of the electrodes all affect how effective this procedure is [24, 92, 93]. At this level, the principal produced species are electrons, atomic radicals, and ionic species with both positive and negative charges.

The second process is the logical progression of the first one and remains the chemical part of plasma, where the most important reactions occur. These reactions are of oxidative species production, such as radical and recombination reactions. The maximum time required for these species' creation is less than a millisecond (ms). Once active and reactive species have formed in the gas phase, they may either move into the liquid phase to form new reactive species or

increase the concentration of certain species. These interactions with the liquid represent the third process (tertiary process.).

5.2.2 Interface

The plasma gliding arc is a biphasic reactor in which the plasma species generated in the gas phase are transferred into the liquid, driving various chemical reactions such as oxidation, reduction, and the formation of new compounds. The interfacial area, solubility, and transfer regime are the key parameters determining the performance of such reactors.

The mass transfer process in GAD involves both diffusion and convection, which are influenced by the turbulence caused by the plasma discharge and the characteristics of the liquid.

Generally, the reactive species in biphasic plasma reactors move from the gas bulk to the gas-liquid interface by diffusion; this phenomenon is governed by Fik's law:

$$J = -D \times \frac{dC}{dX} \qquad \textbf{(Eq.3)}$$

Where, J is the molar flux of the reactive species, D is the diffusion coefficient, and $\frac{dC}{dX}$ is the concentration gradient at the gas-liquid interface.

However, the mechanical movement of the arc and the high-velocity gas flow increase in plasma GAD reactors generate a convection turbulence regime. This later enhances the mass transfer by increasing the gas-liquid contact area and accelerating the reactive species' movements.

When the plasma species are brought into contact with a liquid, after a time "t," the concentrations of this element remain constant but different in each phase: the system is then in thermodynamic equilibrium [96, 97]. Henry's law, which describes the thermodynamic equilibrium obtained, is given by Henry's constant "He" according to the relation.:

$$H_e = \frac{C_g}{P} \qquad \textbf{(Eq.4)}$$

Once equilibrium has been established, conditions near the gas-liquid interface are difficult to observe or explore experimentally, if not impossible. To overcome this, hypotheses and theories have been developed to study the transfer between the two phases. One such theory is the double film model (Lewis and Whitman) [130]. Proposed by LEWIS and Whitman, this model is applicable to two-phase gas-liquid or liquid-liquid systems. In this model, solute transfer to the liquid phase is essentially by molecular diffusion.

The conditions for applying Whitman's double-film model are similar to our own. Therefore, this model will be used in the next chapters to explain and simulate the mass transfer in plasma GAD reactors. This model is also simple to implement [98-101].

5.2.3 Liquid region

Plasma GAD introduces additional complexity due to interfacial reactions at the gas-liquid boundary. Short-lived species produced in the discharge (radicals, excited molecules, electrons, UV radiation) react directly on the solution surface to form new species [25]. Among these reactions is the dissociation of the water molecule by electron impact to form •OH radicals and stable species such as H_2O_2 following the reactions:

$$e^- + H_2O \rightarrow H^{\cdot} + {}^{\bullet}OH + e^- \quad \textbf{(R 18)}$$

$$e^- + 2H_2O \rightarrow H_2O_2 + H_2 + e^- \quad \textbf{(R 19)}$$

The presence of UV radiation in the discharge also contributes to the formation of ˙OH and H˙ radicals by dissociation of the water molecule:

$$H_2O + h\vartheta \leftrightarrow H^{\cdot} + {}^{\bullet}OH \quad \textbf{(R 20)}$$

The stable species formed can transfer from the gas to the liquid phase and react with water molecules. This process occurs either when the discharge is in direct contact with the liquid or in the post-space discharge phase when the discharge is not in direct contact with the solution.

H_2O_2 formed in the gas phase or at the gas-liquid interface (in the case of humid air) can penetrate the liquid due to its high Henry's law constant. However, it can be rapidly decomposed in the presence of UV radiation following the reaction [102]:

$$H_2O_2 + h\vartheta \leftrightarrow 2\ {}^{\bullet}OH \quad \textbf{(R 21)}$$

Stable nitrogen species created in the gas phase may also strongly absorb into the liquid phase due to their high solubility.

Among these NO_x, absorbed nitrogen dioxide (NO_2) and its dimeric form, N_2O_4, react with water molecules to form nitric and nitrate acids, which are responsible for the acidity of the treated aqueous medium, releasing protons and ions that are also responsible, along with other species, for increasing the medium's conductivity. This mechanism is described by the following reactions [102, 103]:

$$2NO_2 + H_2O \rightarrow HNO_2 + H^+ + NO_3^- \quad \textbf{(R 22)}$$

$$N_2O_4 + H_2O \rightarrow HNO_2 + H^+ + NO_3^- \quad \textbf{(R 23)}$$

In the case of •NO, its absorption is generally negligible due to its low Henry's partition constant (He =1.8 10^{-5} mol m^{-3} Pa^{-1}).

Finally, in the liquid phase, there may be reactions between oxygen and nitrogen species:

$$O_3 + HNO_2 \rightarrow O_2 + H^+ + NO_3^- \quad \textbf{(R 24)}$$

$$H_2O_2 + HNO_2 \rightarrow H_2O + H^+ + NO_3^- \quad \textbf{(R 25)}$$

$$H_2O_2 + 2O_3 \rightarrow 3O_2 + 2\ {}^{\bullet}OH \quad \textbf{(R 26)}$$

These reactions can lead to the formation of peroxynitrite, which is difficult to detect. Ferhat and his colleagues have conducted investigations to determine with certainty the presence of this long-lived plasma species [122]. This species demonstrates the post-discharge effect of plasma by slowly decomposing into hydroxyl and nitrogen dioxide radicals according to the following reaction:

$$HONOO \leftrightarrow {}^{\bullet}OH + NO_2^{\bullet} \quad \textbf{(R 27)}$$

The plasma species transferred to the liquid reflects the oxidative power of these reactors in liquid phases, a parameter that can be measured using the total oxidant measurement method.

In case the liquid to be treated contains molecules to be treated, the oxidizing species produced enter into oxidation reactions with these substrates. The oxidizing species likely to convert these molecules are the highly reactive and non-selective •OH radical, the O• radical, ozone, nitrogenous species (NO_x), etc. These species can also include UV radiation and electron radiation. UV radiation and electrons can also be added to these species. Figure.10 presents A proposed global scheme of plasma-chemical reactions.

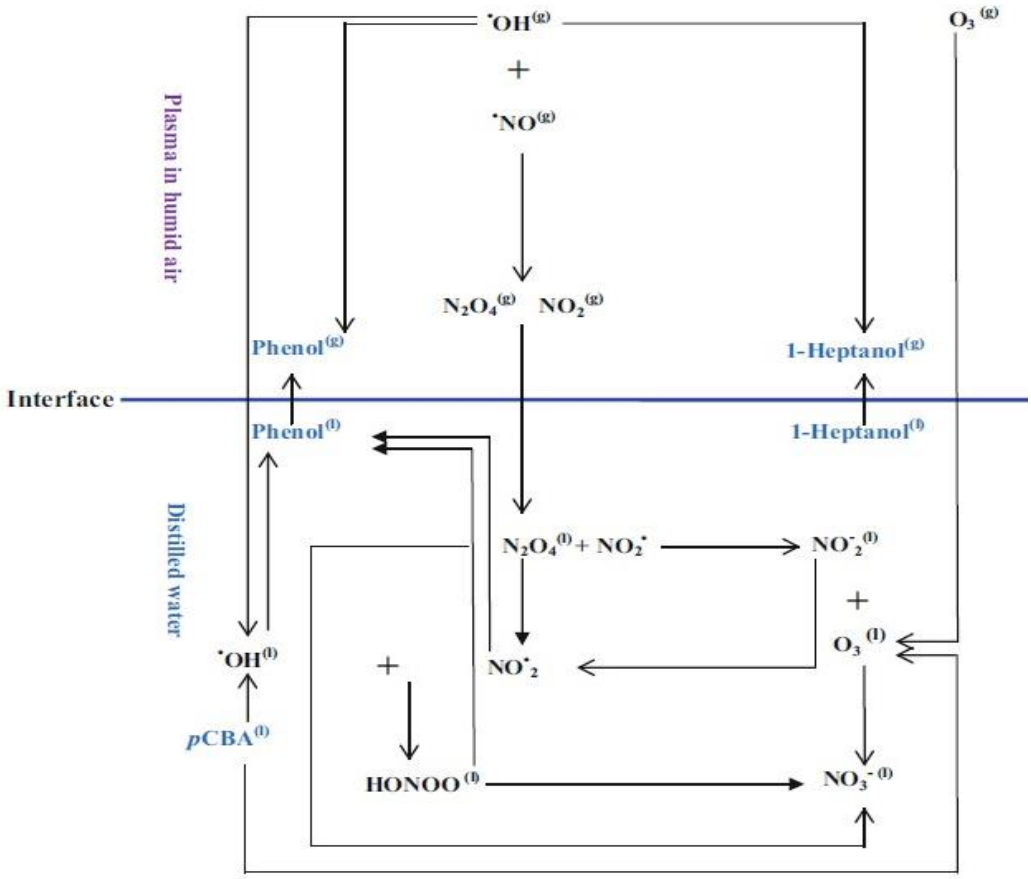

Figure 10. A proposed global scheme of plasma-chemical reactions [26]

The reactivity of species differs according to their redox potential, where the hydroxyl radicals $^{\bullet}OH$ remains the most reactive species due to their high oxidation potential $E^{o}(^{\bullet}OH/H_2O) = 2.8\ V/SHE$ which is among the strongest oxidizing potentials in water. Both of $^{\bullet}OH$ and $NO^{\bullet}$ radicals are responsible for the dual power of GAD, acidification and oxidation. Several studies have demonstrated the potential of this technique for removing pollutants from wastewater [91, 104, 32]. Discharge generates active oxidizing species; some of these are long-lived and are responsible for time-dependent and spatiotemporal post-discharge reactions (TPD & STPD) which develop in the liquid phase [104, 105]. These reactions continue after the GAD discharge has stopped (in TPD) or being far from the plasma sources (in STPD), ensuring the "continuity" of degradation. The peroxynitrite formed in the discharge is said to be responsible for post-discharge phenomena in aqueous solutions. This active species has strong oxidizing properties ($E^{o}(HONOO/NO_2^{\bullet}) = 2.02\ V/SHE$).

5.3 Chemical composition of plasma gliding arc discharge

The chemical composition of the plasmagenic medium is highly dependent on the type of gas used. Air is a very complex plasma gas, given its composition (oxygen, nitrogen and/or H_2O,

etc.). In the plasma plume, these molecules undergo both elastic and inelastic choc with highly accelerated electrons, resulting in excitation, ionization, dissociation and attachment reactions producing highly reactive radical species. Emission spectroscopy carried out on non-thermal plasma discharges reveals the presence of oxygen radicals such as $^{\bullet}OH^{\cdot}$, $^{\cdot}HO_2$, $O^{\cdot}$, H_2O_2, O_3, …, and nitrogen radicals and ions such as $NO^{\bullet}$, $NO_2^{\bullet}$, N_2O_5, HONOO, etc. [25, 94].

5.3.1. Reactive oxygen species (ROS)

These species are generated through various ionization, dissociation, and excitation processes involving oxygen, vapor water molecules and other species present in the gas [94].

$$O^{\cdot} + H_2 \rightarrow H^{\cdot} + {}^{\bullet}OH \quad \textbf{(R 28)}$$

$$H^{\cdot} + H_2O \rightarrow H_2 + {}^{\bullet}OH \quad \textbf{(R 29)}$$

$$HO_2^{\cdot} + O_3 \rightarrow {}^{\bullet}OH + O_2 + O_2 \quad \textbf{(R 30)}$$

$$^{\bullet}OH + O_3 \rightarrow O_2 + HO_2^{\cdot} \quad \textbf{(R 31)}$$

$$^{\bullet}OH + H_2O^{\cdot} \rightarrow H_2 + HO_2^{\cdot} \quad \textbf{(R 32)}$$

$$O_2 \rightarrow O^{\cdot} + O^{\cdot} \quad \textbf{(R 33)}$$

$$^{\bullet}OH + H_2O^{\cdot} \rightarrow H_2O_2 + H^{\cdot} \quad \textbf{(R 34)}$$

$$OH^{\cdot} + {}^{\bullet}OH \rightarrow H_2O_2 \quad \textbf{(R 35)}$$

$$HO_2^{\cdot} + H_2O^{\cdot} \rightarrow H_2O_2 + {}^{\bullet}OH \quad \textbf{(R 36)}$$

$$H_2O + e^- \leftrightarrow H^{\cdot} + HO^{\cdot} + e^- \quad \textbf{(R 37)}$$

$$2H_2O + e^- \leftrightarrow H_2O_2 + H_2 + e^- \quad \textbf{(R 38)}$$

$$H_2O + h\vartheta \leftrightarrow H^{\cdot} + {}^{\bullet}OH \quad \textbf{(R 39)}$$

5.3.2 Reactive nitrogen species

The presence of nitrogen (as a reminder, the composition of air is, in very simplified terms, 21% dioxygen and 79% dinitrogen) induces by the same mechanisms the production of nitrogen oxides called NOx, according to the following reactions: [94, 95]

$$N_2 + O_2 \leftrightarrow NO^{\cdot} + NO^{\cdot} \quad \textbf{(R 40)}$$

$$NO^{\cdot} + O_2 + e^- \rightarrow NO_2^- + O^{\cdot} \quad \textbf{(R 41)}$$

$$NO^{\cdot} + O^{\cdot} + M \rightarrow NO_2^- + M + e^- \quad \textbf{(R 42)}$$

$$N_2 + O^{\cdot} \rightarrow NO^{\cdot} + N^{\cdot} \quad \textbf{(R 43)}$$

$$N^{\cdot} + O^{\cdot} \rightarrow NO^{\cdot} \quad \textbf{(R 44)}$$

$$N^{\cdot}(2D) + O_2 \rightarrow NO^{\cdot} + O^{\cdot} \quad \textbf{(R 45)}$$

$$NO_2 + OH^{\cdot} \rightarrow H^+ + NO_3^- \quad \textbf{(R 46)}$$

$$NO^{\cdot} + OH^{\cdot} \rightarrow HNO_2 \quad \textbf{(R 47)}$$

$$HNO_2 + H_2O_2 \rightarrow HNO_2 + H_2O \quad \textbf{(R 48)}$$

In addition, the species created in the gas phase of the discharge can be grouped into two main families, depending on their lifetimes (see Table 2).

Table 2. Plasma species in Gas-Liquid environment

Parent speices	Primary speices	Secondary speices
H_2O, N_2, O_2, e	$^{\bullet}OH, H^{\bullet}, O^{\bullet}, N^{\bullet}, NO^{\bullet}, NO_2^{\bullet}, \ldots$	$H_2O_2, NO_X, O_3, HONOO, \ldots$

- The family of highly reactive, short-lived and unstable species: In this family we can have atomic and polyatomic radicals (e.g. in a moist air plasma, we can have $OH^{\cdot}$, $O^{\cdot}$etc).
- The long-lived species family: These species are more stable than short-lived species (in a dry air plasma, O_3 and NO_X are typical examples). The species formed in the gas phase are highly dependent on the nature of the plasma gas.

Figure.11 shows the probable zones of these two families.

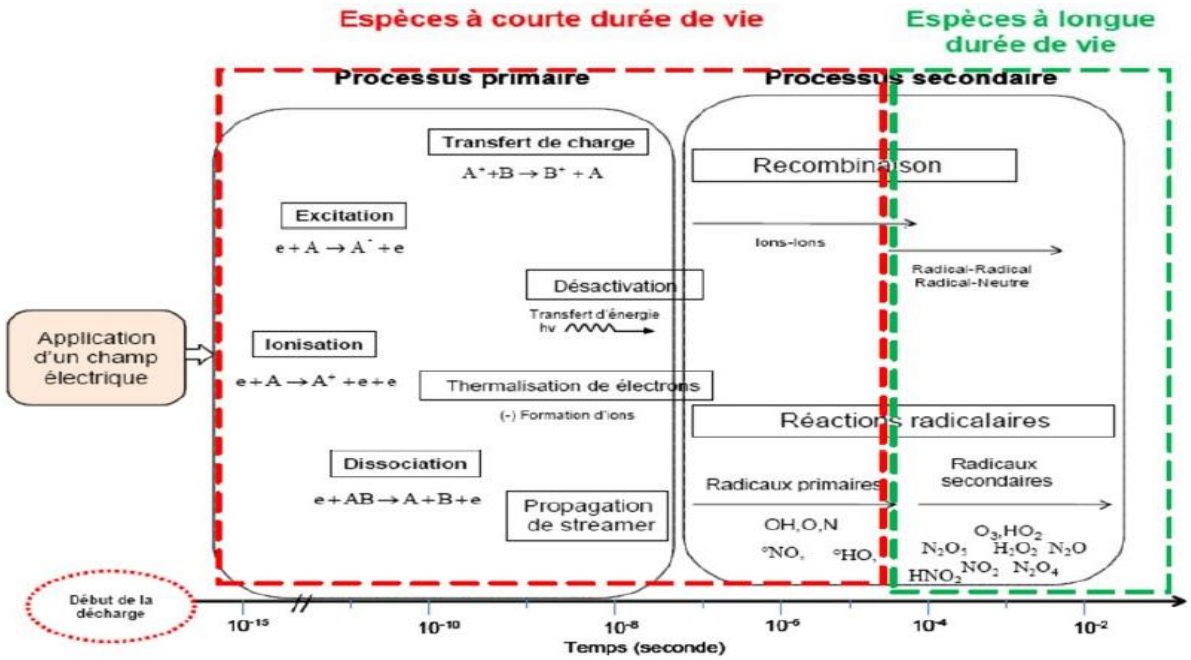

Figure 11. Distribution of species into two large families according to their lifetime [25]

6. Plasma GAD processes control

Effective control of the processes taking place in gliding arc discharge (GAD) plasma reactors offers a powerful solution to the challenges and limitations inherent in these systems. By implementing precise control mechanisms, GAD reactors can be optimized for a variety of applications, from water treatment and environmental remediation to chemical synthesis and industrial production. Controlling oxidation processes enables significant reductions in energy consumption and promotes more guided reaction pathways, reducing the likelihood of unwanted by-products, particularly in chemical synthesis and pollutant degradation. Controlling gas flow, mixing, and surface enhancement ensures a more efficient transfer of reactive species into the liquid, resulting in higher conversion rates. It also helps to protect materials, increasing their durability and service life. Achieving an optimum balance between energy efficiency, mass transfer, and reaction selectivity is key to the widespread adoption and scalability of this technology for industrial purposes. Below are several key control measures that can significantly improve the performance and efficiency of GAD reactors.

6.1 Energy consumption control

The consumed energy can be controlled using various strategies, the most effective being the use of pulsed power systems [106-109]. This strategy delivers energy in short bursts while maintaining the plasma state. This minimizes component heating and enables better control of

arc stability. Energy consumption can be reduced by using high-frequency alternating current, which results in less heating of the electrodes and reactor walls, thus reducing energy loss through heat dissipation. In addition, implementing a power management protocol can also be an effective strategy, reducing power when fewer reactive species are required, which can help reduce unnecessary energy consumption.

6.2 Mass transfer control

Optimizing plasma gas-liquid interactions, such as the transferred amount of reactive species, offers more control over the oxidative power of these technologies; thus, the higher the transferred quantities, the higher the conversion rate is reached, and vice versa. This can be achieved by designing the right configuration for the right operation. According to "technique de l'ingenieur", there are several gas liquid systems with different properties such as interfacial area, mixing mode, and treated volumes [100]; thus, if there is a need for fast oxidation like for water depollution, the higher surface area and well-mixed reactor is required because it ensures higher absorption amount of oxidative species. However, if higher selectivity is required for chemical synthesis, a moderate to lower surface area with a well-mixing system is preferable. Venturi and agitated tanks present the highest interfacial area, while the lowest one refers to the pulverization column. However, the difference in mixing and discharge types can show different properties in terms of conversion rate and consistency.

Furthermore, the mass transfer in these reactors can also be controlled by the optimization of the feeding gas flow rate. Thus, the higher flow rates reduce the residence time time of the gas molecules in the plasma plum and improve the transfer of reactive species into the liquid. However, this may lead to incomplete ionization and insufficient reactive species generation. Conversely, a flow rate that is too low can result in poor transport of reactive species but better gas ionization. A balancing plasma generation and mass transfer phenomena is highly required.

For continuous treating systems, the liquid circulation parameter can greatly affect mass transfer operations. Circulating the liquid phase offers more liquid volumes to be exposed to the plasma, helping to better reactive species absorption. This strategy is highly recommended for systems showing lower mixing properties.

6.3 Reactive species generation control

Several strategies can handle the control of the generated plasma reactive species type and amount; the first one consists of controlling the feed gas composition, which influences the types and concentrations of reactive species generated in the plasma, such as using higher concentrations of oxygen lead to high production of oxygen reactive species (ROS) while using

higher nitrogen concentration led to a higher amount of nitrogen reactive species (RNS). The second strategy consists of separating the plasma reactive species based on their lifetime and reactivity. For example, using direct discharge will concentrate our medium by highly reactive and short-life species; this allows for a fast and intense reactivity of the plasma device. However, using spatiotemporal post-discharge offers more long-lived and lower reactive species; this offers more control over the conducted operation and selectivity [105]. Last but not least, the optimization of powered energy can control the composition of the generated plasma population species. For example, using energy lower than the breaking down energy band of molecules will not lead to its ionization and offer lower reactivity of the produced entities. For instance, nitrogen molecules have an energy band of 9.8 eV. Thus, more RNS will be generated if the provided energy is higher than the breaking down band energy of nitrogen molecules. Elsewhere, more ROS are generated [91]. Furthermore, a selective gas filter could be a great option for controlling the plasma gas population; the filter needs to be installed in the generated gas output before its interaction with the targeted molecules, such as using a filter will reduce their interaction with the treated liquid or material and allows for more ROS concentrated medium. The control of the plasma-produced reactive species offers more control of the plasma reactivity and selectivity that could be beneficial, especially for chemical reactions and plasma medicine.

6.4 Reaction pathways and selectivity control

Controlling reaction pathways and selectivity in plasma reactors is a complex operation that requires a comprehensive understanding of the interplay between various operational parameters such as medium acidity, conductivity, and total oxidant amount. The conductivity in these reactors is a parameter that reflects the quantity of the produced charged entities in the solution. It influences the transport of charge and mass in the system. A balanced conductivity ensures that desired reactive species interact with target compounds without promoting excessive ion recombination or side reactions.

In addition, the acidity of the solution medium has a significant influence on the reactivity of dissolved species and the progression of chemical reactions. Generally, plasma oxidative reactions are conducted in an acidic medium that is fast and is auto-acidified by the plasma reactor itself, according to the production of nitric and nitrate acids. This acidity promotes the formation of strong oxidizing species such as hydroxyl radicals ($^{\bullet}OH$) and enhances their stability in solution; these species are responsible for the oxidative power of this system. In basic conditions, hydroxide ions affect the stability of plasma reactive species, leading to the formation

of lower reactive species and water [110, 111]. This action reduces the reactivity of such reactors by reducing the concentration of free radicals available for oxidation reactions. Thus, the pH optimization of the treated solution helps control the oxidative power better.

Despite their efficiency in breaking down chemical pollutants, the use of plasma reactors for chemical synthesis is still far from the expected performances in terms of selectivity and final product purity, referring to the high reactivity shown by the produced plasma spices, which react rapidly in parallel reaction with the treated molecules, leading to parasite reactions and undesired by-products. The use of selective scavengers can be a promising tool to overcome the unselective plasma problem. Scavengers are specific compounds that have a high affinity and are translated by a high constant rate to the reactive spices to be controlled or eliminated, preventing them from participating in unwanted reactions. For example, Ter-butanol and methanol are the best chemicals used for scavenging hydroxyl radicals; they work by reacting quickly with these radicals, neutralizing them before they have the opportunity to react with the treated molecules [112, 113]. For nitrite and NO_x radicals, sulfamic and sodium azide acids have shown great scavenging rates and high selectivity [114]. Meropoulis and Aggelopoulos have studied the effect of adding selective scavengers for $^{\bullet}OH$, H_2O_2, O_3 And solvated electrons on the degradation rate of dye molecules both in gas-liquid DBD and plasma bubble [115]. Rather than improving the selectivity of chemical reactions, scavengers also enhance the overall efficiency of the process by neutralizing reactive species that could lead to side reactions.

Furthermore, catalysts can be used to control reaction pathways in plasma reactors. Their properties in transferring volumetric to surface reaction allow them to be an efficient tool for controlling oxidative reactions. Their process consists of the adoption of both plasma reactive species and the treated molecules to a specific adsorptive pore with a specific diameter; this is the limiting step of the plasma catalysis process, allowing selective adsorption. Then, making the adsorbed reagents too close to a specific condition allows for the initiation of the desired reaction with a minimum activated energy and less to no undesired by-products by skipping side reactions, ensuring a fast and selective reaction mechanism. Then, the product is desorbed to the bulk-liquid medium. Photocatalysts are highly recommended in reactors due to the high amount of UV light emitted by plasma. These later serve to activate reactive sites in the catalyst surface. Here, the band gap of the catalyst plays a crucial role in the determination of the reaction pathways, selectivity, conversion rate, and consumed energy [116-119].

These strategies can be easily studied using simulation software; they provide insights into plasma dynamics, chemical kinetics, mass, and heat transfers that are difficult to capture ex-

perimentally. These insights allow for the precise control of reaction pathways and the development of more efficient and scalable plasma GAD reactors for a wide range of applications, from chemical synthesis to environmental remediation.

Conclusion

A clear and brief explanation of the thermal classification of plasma processes is presented in this chapter, as well as the main technologies that have been developed in the context of cold plasma. Focusing on the plasma gliding arc discharge, which was the main system used in the presenting thesis, the different applications, challenges, and limitations have been strongly discussed. This system has shown promising results, so it can be proposed to integrate industrial processes in the applications of water and surface treatment to chemical production. However, its integration with the industrial sector needs to be well controlled in terms of selectivity, conversion rate, safety, eco-friendship, and economic roadmaps.

For this, the different processes present in plasma gliding arc discharge have been widely discussed, such as plasma energy consumption, species generation both in gas and liquid phases, mass transfer, and different chemical reactions. These processes directly affect the plasma GAD conditions; controlling them serves to control the reactor outcomes.

Finally, different strategies have been proposed as control solutions for the processes present in these systems; these solutions serve to optimize the energy consumed, ensure the good transfer of the oxidizing charge, avoid parasitic reactions and undesirable by-products

CHAPTER II. Material and methods

Introduction

In this chapter, we will detail the new configuration proposed in this work as well as the old configuration present in the STEVA laboratory. In the second part, we will develop the operating mode used in the aqueous solution treatment experiments. We will also describe the analytical techniques used to study the liquid phase (by-products, ions, etc.) and the gas phase (discharge characterization). Finally, we will look at the analysis and preparation techniques used to determine phenol conversion rates, AG25 discoloration rates, demineralization rates, and selectivity.

1. Model reagent

In our work, we have chosen model reagents with different properties, such as phenol, which is uncolored and moderately soluble in water, and acid green 25 (AG25), which is highly soluble in water and visible.

AG25, phenol and its by-products used in this study (Table.3) are of analytical quality. They were used without prior purification. Solutions were prepared with ultra-pure water obtained using a Human Power1 New Water Purification System.

All reagents used in this study are listed in Table.3:

Table 3. Reagents used in this study

	Product	Supplier	Quality
Aromatic	Phenol	SIGMA-ALDRICH	≥ 99.5 %
	Hydroquinone	SIGMA-ALDRICH	≥ 99.5 %
	1,2-Dihydroxy-benzène (Catechol)	SIGMA-ALDRICH	≥ 99 %
	1,3-Dihydroxy-benzène (Resorcin)	SIGMA-ALDRICH	≥ 99 %
	2-Nitrophénol	SIGMA-ALDRICH	≥ 99 %
	2,4-Dinitrophénol	SIGMA-ALDRICH	≥ 99 %
	p-Benzoquinone	BIOCHEM	≥ 99 %
Dye	Acid Green 25 (Anthraquinone dye)	SIGMA-ALDRICH	≥ 99 %

1.1 Physicochemical properties of the used chemical products

This study focuses on acid green, phenol and its derivatives, whose physicochemical properties are presented in Table.4.

Table 4. Physicochemical properties of phenol and its derivatives

Product name	Chemical structure	Brute formula	Appearance	Molecular weight ($g.mol^{-1}$)	Solubility in water at 20 °C ($g.L^{-1}$)	Saturation vapour pressure at 20 °C (Pa)	λ_{max}
Phenol (Acide phénique) (Acide carbolique)	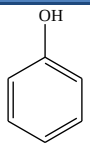	C_6H_6O	Uncolored to yellow or light pink crystals	94,11	76	53	270
1,2-Dihydroxybenzène (Catechol)	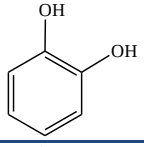	$C_6H_6O_2$	Uncolored crystals	110,11	430	20	254
1,3-Dihydroxybenzène (Resorcine)	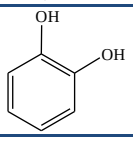	$C_6H_6O_2$	White crystals	110,11	1400	0.065	270
1,4-dihydroxybenzène (Hydroquinone)	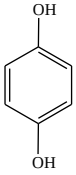	$C_6H_6O_2$	Uncolored crystals	110,11	59	0,12	254
1,4-Benzoquinone (p-Benzoquinone)	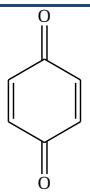	$C_6H_4O_2$	Yellow crystals	108.10	10	10	254
2-Nitrophenol	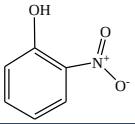	$C_6H_5NO_3$	Pale yellow crystals	139.10	2,5	15	247
4-Nitrophenol	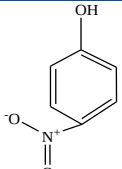	$C_6H_5NO_3$	Uncolored to pale yellow crystals	139.10	12,4	0,0032	247
Acid Green 25 (Anthraquinone dye)	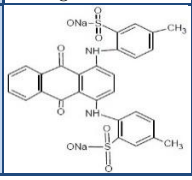	$C_{28}H_{20}N_2Na_2O_8S_2$	blackish green powder	622.6	36	9.73×10^{-23}	643

2. Experimental devices

The first version of plasma GAD reactors (Glidarc I & II.) used in previous studies are batch system reactors, meaning that the contact surface between the plasma and the solution to be treated is limited and remains invariable.

To propose reactors for industrial use with high treatment efficiency and performance, various Glidarc geometries have been envisaged to ensure continuous treatment, enabling massive treatment, such as the Glidarc Failing Film and Spray Tower reactors [90, 122]. However, the performance of these reactors is somewhat limited in terms of time and contact surface compared with batch systems. These details will be developed in Chapter III.

Consequently, a new Glidarc geometry will be developed to meet the requirements of industrial processes, such as massive processing and high yield. This is a spiral-tube reactor assisted by a venturi system contactor, enabling a gas-liquid plasma fluid flow to be co-current along the spiral tube, ensuring long contact times and large surface areas.

2.1 GAD-Batch

The LEICA laboratory team at ROUEN University, under the direction of Professor J.L. BRISSET, has developed a more efficient reactor, Figure 12. This closed reactor centralizes the diffusing species towards the target to be treated, condenses the water vapors, has a higher capacity, prolongs treatment times, and consequently offers greater reactivity.

This adaptation has made it possible to treat a large number of recalcitrant organic pollutants in the aqueous phase and liquid industrial waste [123]. However, there are technical limitations to extrapolating it to a pilot or industrial scale.

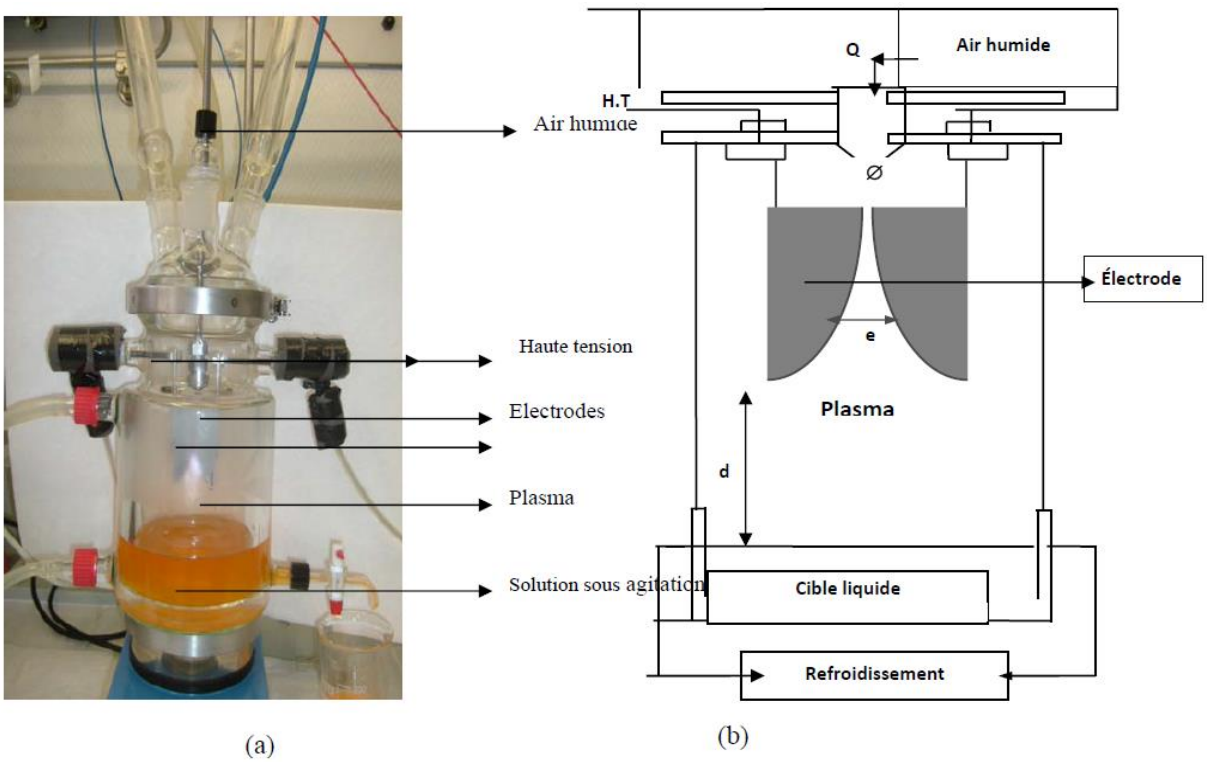

Figure 12. Plasma GAD-II, (a) reactor photograph, (b) reactor description diagram [123]

2.2 GAD.FF

To overcome these problems, another generation of 'Glidarc' called 'Glidarc III' (figure.13) has been developed by Ghezzar et al. 2013 [90] to treat liquids in the film state and continuous flow and loop systems: the glass cell has been replaced by a stainless-steel plate on which straight channels are machined. This plate forms the functional part of the device, i.e., the core of the reactor. It can be tilted at different angles from 0° to 90°. It is the seat of the absorption reaction between the ionized gas (plasma) and the falling liquid film channeled along the channels.

The liquid to be treated is drawn from a reservoir by a peristaltic pump. The 'Glidarc' III has been optimized by varying the following parameters, which are more extensive than the original configuration: channel width, pump speed, and plate angle.

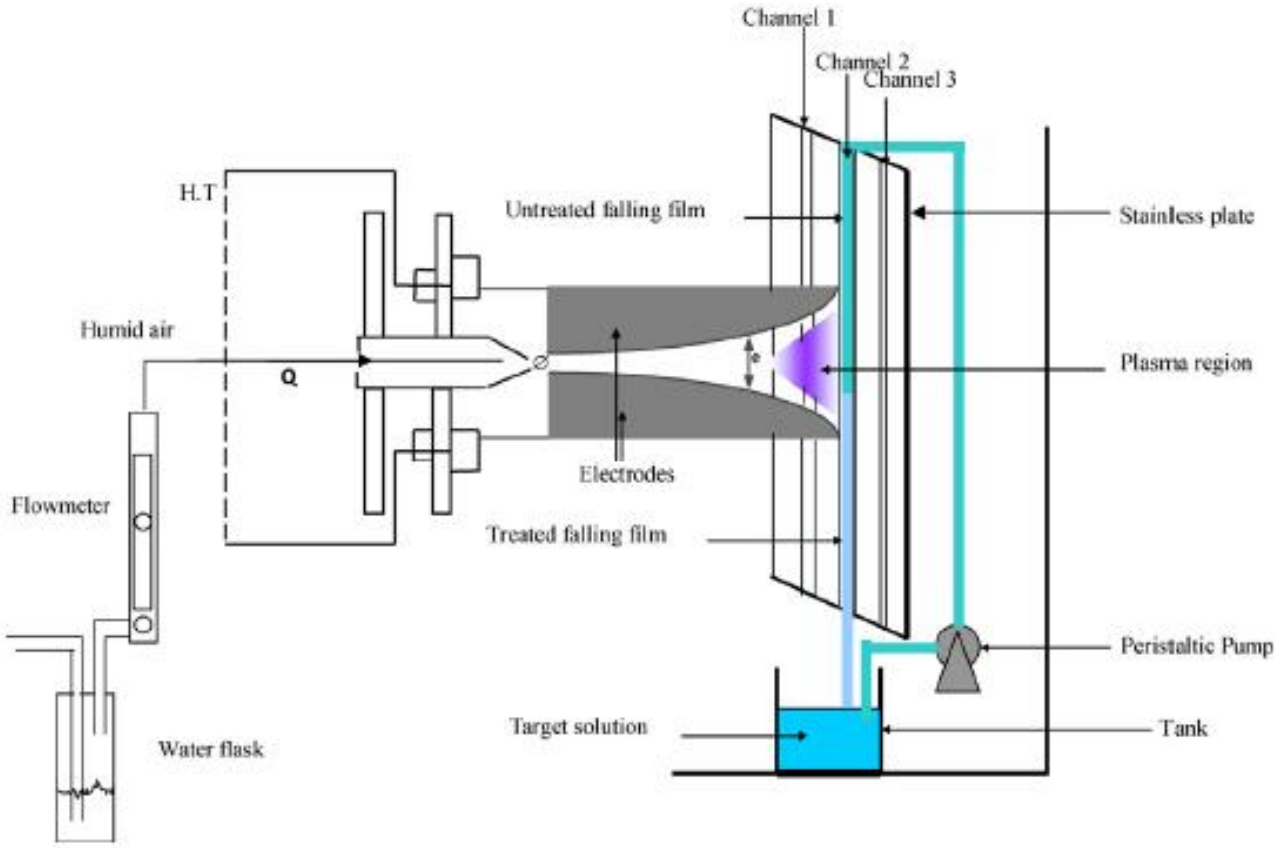

Figure 13. Schemes description of plasma GAD-Failing Film [90]

2.3 GAD-ST

Figure 14 shows the GAD spraying tower reactor in which the gas phase is nonthermal plasma at atmospheric pressure. This phase is in countercurrent with the droplets of the liquid that fall along the column. In the spatial post-discharge mode (ex-situ) produced by the presented plasma reactor, the discharge takes place far from the target (70 cm) to treat the pollutant remotely. Therefore, the electrodes have a longer service life, and the risk of electric shock is minimized. The parameters affecting plasma efficiency are relevant for all current GAD devices [33, 90]. They are optimized in the previous work [124, 91, 118] and have been kept the same in this work. (i) diameter of the plasma gas inlet nozzle: Φ= 1 mm; (ii) distance between electrodes (e): e = 3 mm; (iii) plasma gas: the used plasma gas was essentially air saturated with water in order to minimize treatment costs and generate active •NO and •OH radicals; (iv) plasma gas flow(Q): 700 L h^{-1}; and(v) the injected power 'P' into the discharge is constant during the treatment period. The power was estimated at 100 W based on the relationship proposed by Doubla et al. [125].

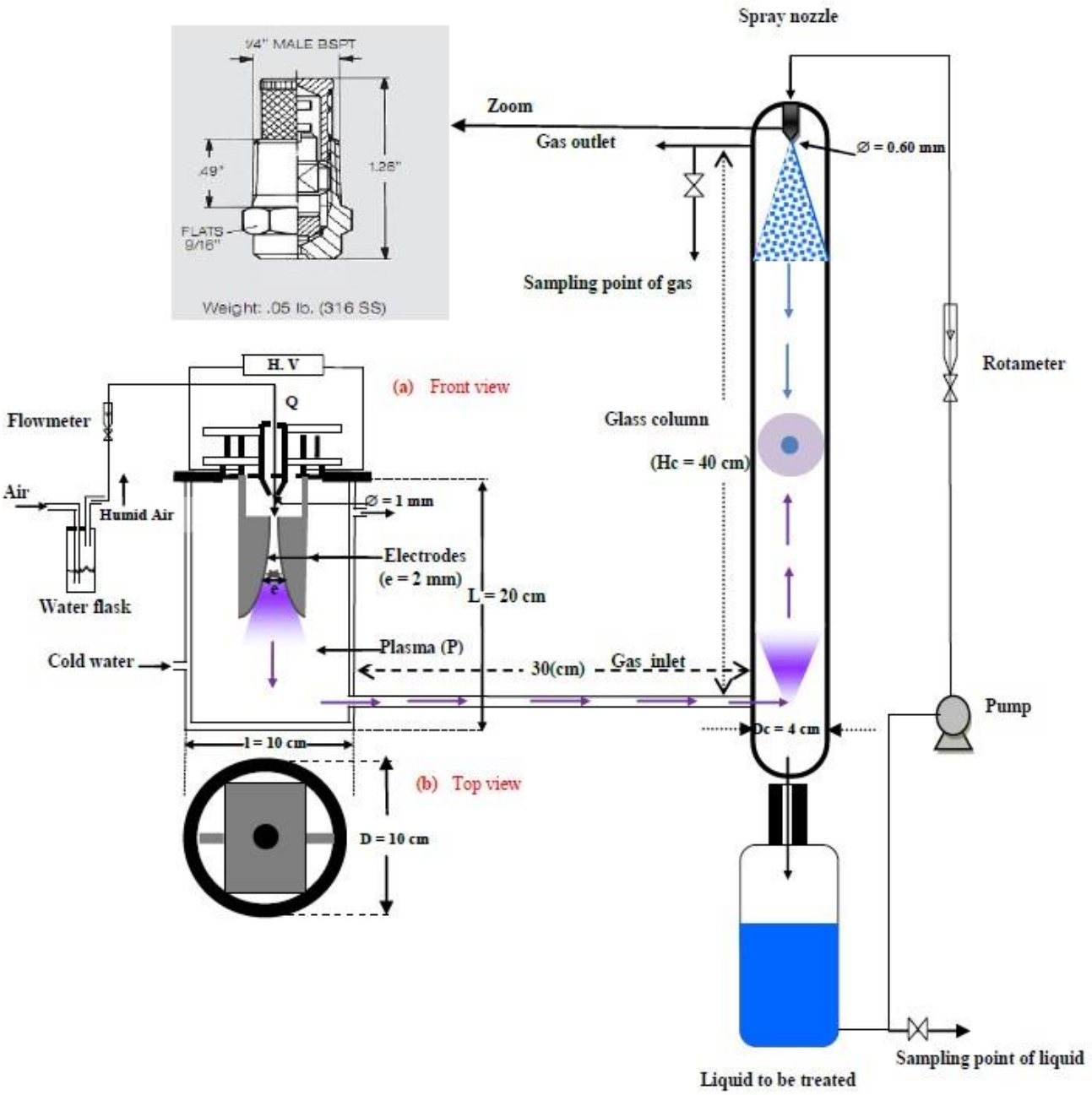

Figure 14. Schemes description of plasma GAD-Spray Tower [105]

2.4 GAD-V

The GAD-VNT (Gliding Arc Discharge-Venturi) system operates on the same fundamental principle of plasma generation as the GAD-ST. However, it introduces a different gas-liquid interaction mechanism in this configuration. Figure 15 shows an overview of the assembly we designed and installed in our STEVA laboratory; the atmospheric plasma gas produced by the gliding arc discharge is directed to a Venturi system, where it is mixed with the liquid solution being processed. The gas and liquid phases flow in co-current mode through a 100 cm spiral

pipe, designed to increase fluid residence time and enhance mass transfer processes between the plasma and liquid phases.

This extended residence time enables more effective interaction between the reactive species generated in the plasma and the liquid components, thus improving overall treatment efficiency. The respective flow rates of the liquid and plasma phases are $9.6\times10\text{-}3\ m^3\ h^{-1}$ for the liquid (Q_L) and $0.9\ m^3\ h^{-1}$ for the gas (Q_G), ensuring a stable flow regime for the mixing process. After treatment, the gas phase (air) is discharged into the atmosphere, while the liquid phase is recirculated into the stirred tank for further treatment or subsequent stages. This configuration is designed to optimize mass transfer performance, exploiting the Venturi system's ability to create efficient mixing and enhance dissolution of plasma-reactive species in the liquid. The spiral configuration also contributes to this by increasing the contact surface and maximizing interaction time.

The pilot plant consists of three main components, as shown in Figure 15: a Glidarc-VNT reactor that produces plasma gas, a venturi-tube system in which the absorption phenomenon takes place, and a tank containing the solution to be treated.

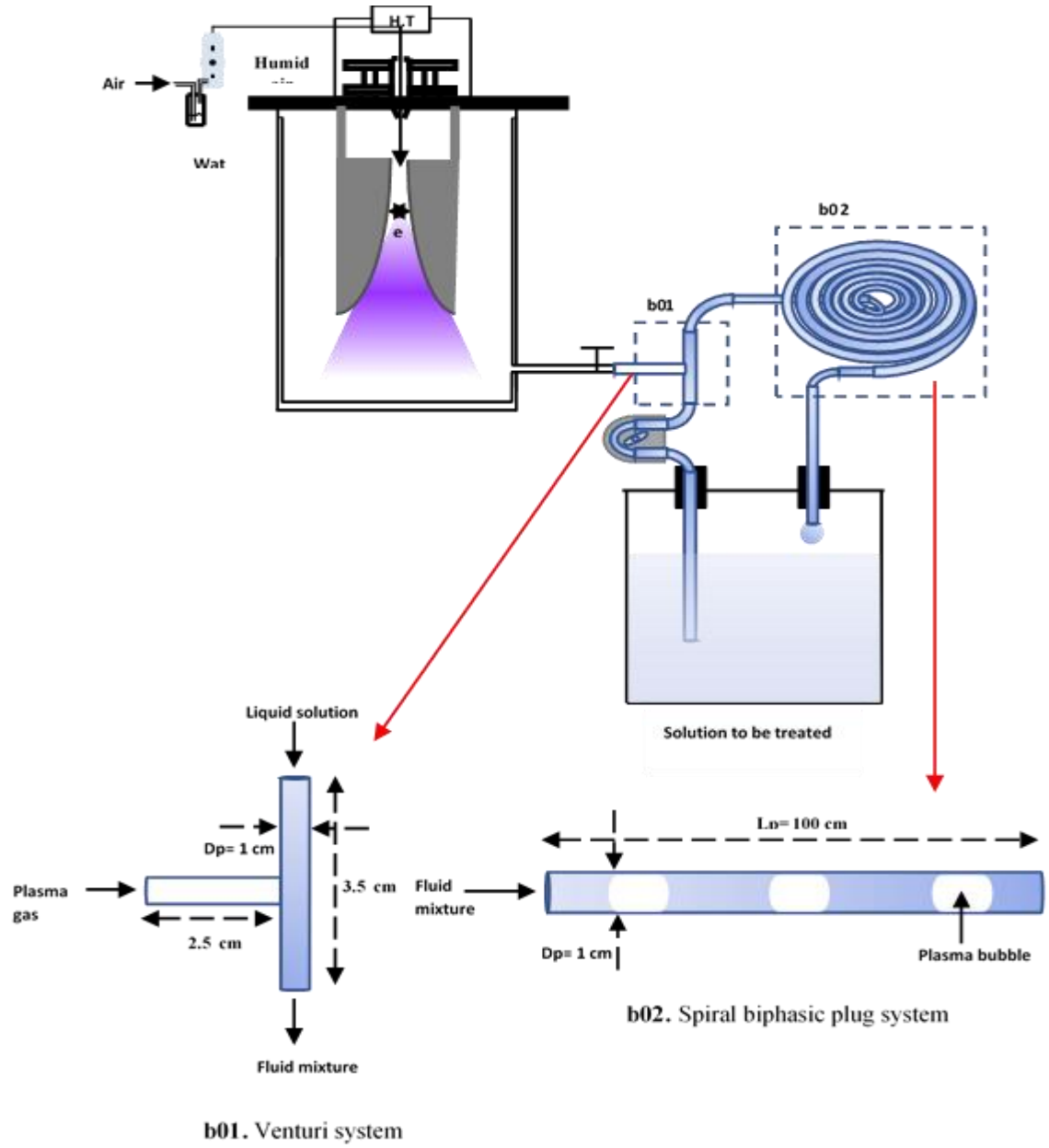

Figure 15. Glidarc V- (GAD.Venturi) pilot installation

2.4.1 Plasma reactor

Plasma gas inlet nozzle diameter (ϕ)

The nozzle is directly related to the jet flow of the plasma gas. The narrower the nozzle, the more mobile the active species and the greater their diffusion into the target. In all 'Glidarc' generations ϕ = 1 mm.

Inter-electrode distance (e)

Depending on the distance between electrodes, the volume of the plasma plume is more or less significant. For example, an electrode spacing (e) of 3 mm results in a considerable volume. On the other hand, e = 5 mm is the maximum distance at which the arc is extinguished.

Plasma gases

Plasma-generating gases can be oxygen, nitrogen, air or other. In this work, water-saturated air was chosen as the plasma gas to minimize processing cost and to generate the reactive species $^{\bullet}NO$ and $^{\bullet}OH$.

Gas flow rate (Q)

When the flow rate is in the range (700, 900) L h-1, the plasma plume is pink, a color characteristic of oxygen plasma, and plasma species migrate rapidly towards the target to be treated. Below this interval, i.e. at 360 L h-1, the plume becomes pale yellow, the characteristic color of a nitrogen plasma, and active entities diffuse slowly.

Distance between electrode and liquid surface (d)

In previous generations of reactors, bringing the electrodes closer to the target leads to faster species diffusion, thus minimizing treatment time. However, this distance must be relative to the flow rate of the plasma gas to avoid quenching of the plum. In this new reactor, (d) is 20 cm of pipe length connecting the reactor to the venturi system. The main operating parameters of the plasma reactor are:

The wet air flow rate is 900 m^3 h^{-1}, with a nozzle diameter of 1 mm and an electrode-target distance of 20 cm.

2.4.2 Venturi-tube system

This system is made up of two parts, such as the venturi contactor, which mixes the plasma gas and the liquid to be treated, and the spiral tube, which ensures a long residence time for improved reactor efficiency.

Venturi contactor

The venturi contactor is made of polyvinyl chloride (PVC), an inexpensive material that resists chemical attack. Figure.15a present the zoom diagram of the venturi contactor with more detailed parameters. This contactor: is a microsystem with an external diameter (D_V) of 0.005 m that offers a better gas-liquid interfacial area (a_V) about 0.08 m^{-1} after the creation of discrete volumes from the immiscible phases. The plasma gas fraction was calculated to be 13.83%, that is closed to the standard value mentioned in “Technique de l’ingenieur” [100].

Spiral pipe

Figure.15b present the zoom diagram of the spiral pipe with more detailed parameters. This pipe considered as the place of the plasma-liquid reaction, the dispersion generated by the venturi system circulate throughout the spiral pipe of length $L_p = 100$ cm and diameter $D_p = 1$ cm with a residence time of t_s = 20 s for liquid and gas flows of Q_L = 0.01 $m^3 s^{-1}$ and Q_G = 0.7 $m^3 h^{-1}$, respectively. This tubing has been manufactured from a flexible PVC material reinforced with polyester thread for added strength and durability. Clear PVC pipe is resistant to chemicals, oils and UV rays, making it an ideal choice for a variety of applications.

What's more, this material has the advantage of being transparent, allowing us to visualize fluid flows inside the pipe.

The venturi system designed in this way offers a number of advantages over other liquid effluent treatment processes. The system is simple in technology, requires low capital outlay, and can handle high flows of gas and liquid.

Solution tank

It is a Pyrex glass tank used as solution container of 300 ml, assisted by three circulating holes such as of liquid pumping outlet, fluidic inlet and pored gas outlet.

- **The gas plasma circuit**

Plasma gas from the Glidarc reactor is fed into the venturi-tube system by a centrifugal compressor located outside the STEVA lab. The flow rate to the column is 700 L h^{-1}. This flow rate can be adjusted at two levels:

♦ In the compressor installation, a pressure reducer to lower the pressure.

♦ On the pilot plant level, a valve enables finer adjustment of the air flow into the Glidarc reactor,

Plasma gas from the Glidarc reactor is transported to the venturi contactor through a 20 cm long gas pipe.

The plasma gas velocity was chosen to be as close as possible to the values likely to be encountered in industry. In industry, velocities measured in ducts, manifolds and chimneys are generally between 8 and 12 m s^{-1} for natural circulation and between 10 and 20 m s^{-1} for forced circulation.

In practice, the installation sets two limits for plasma gas velocity:

♦ An upper limit above which the gas flow is greater than the liquid flow, causing the venturi system to malfunction due to the absence of treated liquid in the pipe.

♦ A lower limit below which the gas flow is no longer sufficient, resulting in an undesired flow of liquid to the Glidarc plasma reactor, which can also be a major hazard due to the presence of the electric arc.

In both cases, we are no longer in the domain of a gas phase dispersed in li-quid. The tests carried out indicate that the upper velocity limit is 15 m s^{-1}, and the lower limit is 7 m s^{-1}. This velocity range is indeed close to the industrial case. After passing through the column, the gas is returned to the atmosphere, where it can be sampled for analysis of the gas phase.

- **The liquid circuit**

If the plasma gas is open-circuit, the solution to be treated can be either open-circuit or closed-circuit. This solution comes from a 2.5 L recovery tank, partially filled before the system is started up. An emptying tank of the same capacity is also provided for draining the rinsing water from the venturi system after use. It can also be used as a reserve or for optimization purposes.

The piping from the tanks is divided into three branches, each fitted with an opening valve for selecting the tank and operating mode. A needle valve connected to the solution inlet circuit of the venturi contactor is installed at the outlet of each recovery tank, and another needle valve connected to the solution outlet circuit is installed at the inlet of each recovery tank.

For open-circuit operation, we close the inlet valve of the tank containing the solution to be treated and open the inlet valve of the second tank; this mode of operation is used in continuous-mode treatment.

For closed-circuit operation, the second tank is isolated, and we open the inlet and outlet valves of the tank containing the solution to be treated. This mode of operation is used for batch mode treatment.

A peristaltic pump is installed on the water pipe upstream of the column to provide sufficient pressure to ensure proper gas dispersion in the liquid flow. This flow rate is measured using a pump-specific chart.

It is then important to always have the same height of water in the tank to obtain a constant load and detect leaks.

After passing through the pipes, the solution is mixed with the plasma gas, ensuring a fluid phase with a gas fraction of 13.83%.

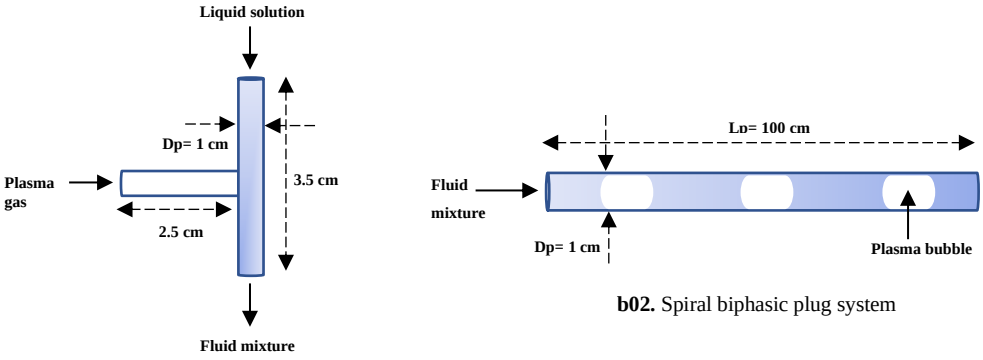

b01. Venturi system

b02. Spiral biphasic plug system

Figure 16. Venturi system Diagram

To ensure a dispersed fluidic phase. It is, therefore, necessary to use an optimum liquid flow rate that is sufficient to guarantee good absorption of the plasma species. This flow rate must not be too high, however, so as not to bypass the normal circuit to the Glidarc reactor. In our case, we used a flow rate of 58 ml min^{-1}.

For the liquid phase analyses, both tanks were equipped with sampling taps.

3. Experimental protocol used in water treatment experiments.

3.1 Sample preparation

Samples of the model reagent (Phenol or AG25) chosen for the Glidarc plasma treatment experiments under different configurations were prepared at concentrations of 1 and 0.8×10^{-3} mol L^{-1}, respectively, in different reactor volumes for each configuration.

After treatment of the solutions by the Glidarc discharge, the volume of the solution is collected in a 100 mL vial for the different liquid phase analyses. For a non-reactive medium (water), three analyses were performed to determine the properties of each configuration such as (1) pH and conductivity analysis, (2) analysis of nitrite and nitrate ion concentrations, and (3) analysis of total oxidants. For a reactive medium, a volume (approximately 2 mL) is taken from the 100 mL for an analysis of the residual phenol concentration and its by-products by High Pressure (or Performance) Liquid Chromatography (HPLC); the same volume was taken from the AG25 solution treated by plasma for a UV-Visible spectrophotometric analysis in order to measure the residual concentration of the latter. In order to obtain a value that is as accurate as possible,

the samples are analyzed within 8 hours of the experiment. The remaining volume is then used in the following order: (1) Total Organic Carbon (TOC) analysis, (2) pH and conductivity analysis, in order to limit cross-contamination between the different techniques. The final volumes are kept in the refrigerator for possible additional analyses.

3.2 Estimating solution evaporation rates in Glidarc experiments

The use of Glidarc will blow the solution significantly. In order to measure the evaporation rate, a phenol solution (10^{-3} mol L^{-1}) is treated by the Glidarc reactor without electrical discharge (only gaseous airflow). The concentration of phenol solution is measured after a 60-minute treatment by a UV-visible spectrophotometer at a wavelength of 270 nm; this operation is done for all Glidarc configurations present in the STEVA laboratory. Phenol is moderately volatile and has a Henry constant $K_H = 4.56\times10^{-2}$ Pa m³ mol^{-1} at 20°C; significant evaporation of the solution can lead to a decrease in the concentration of the reagent in solution. This can lead, if not corrected, to a false estimate of the final residual concentration. Knowing the concentration of phenolic solution at the start and end of treatment, it is possible to calculate an "Evaporation rate" noted by X_{ev}, whose formula is (eq.1):

$$X_{ev} = \frac{C_f}{C_0} \qquad \textbf{(Eq.5)}$$

Where, C_f and C_0 are respectively the final and initial concentrations of the phenol solution. The evaporation rates in the four configurations do not exceed 3%.

3.3 Determination of the composition of the treated solution

HPLC analysis allows us to determine the concentrations of phenol and its derivatives. In order to be as accurate as possible, calibration curves were plotted for each of the organic compounds that may be present in the solution of phenol treated by GAD plasma. The same procedure was done for green acid 25 to determine its residual concentration using a UV-Visible spectrophotometer. The conversion rate (T_x) is then given by the following expression (eq.2):

$$T_x(\%) = \frac{(C_0 - C_t)}{C_0} \times 100 \qquad \textbf{(Eq.6)}$$

Where, C_t corresponds t_o the residual concentration of reagents after a treatment time “t”.

4. Analysis method

The physico-chemical analyses carried out concerned plasmagenic species in the liquid phase and chemically treated compounds in solution before and after glidarc plasma treatment for all four configurations. In the following, we provide an overview of all the techniques used in this work.

4.1 Gas-phase measurements

4.1.1 Plasma gas composition

In order to determine the different excited species, present in the gas phase during the discharge, an optical emission spectrophotometry (OES) study was carried out. This non-invasive, easy-to-use technique detects reactive species in a plasma by analyzing the light emitted by the discharge. In a plasma discharge, molecules or atoms are excited, and their return to a stable state result in the emission of a photon whose energy depends on the electronic transition involved. By studying the emission spectra, it is possible to identify the species present in the plasma discharge. The principle of the technique is based on the excitation of an atomic or molecular species, resulting in the passage of an electron from a lower energy level (E_i) to a higher energy level (E_j). Once at the excited level, the electron will tend to return, by radiative cascade, to a lower, more stable energy level (relaxation phenomenon). This de-excitation gives rise to the emission of photons, the wavelengths of which are characteristic of the emitting element and the energy gaps between levels.

In our work, an optical emission spectrometer (Spectrapro-500i, Action Research Corporation) fitted with a CCD detector (Spectrum) was used. Measurements were carried out with 1200 and 3600 grating and slit apertures ranging from 10 to 100 μm. To maximize the signal-to-noise ratio, each Spectrum acquisition was made by accumulating 10 measurements. The optical fiber was focused as much as possible at the center of the Glidarc plasma tongue, i.e., approximately 2 cm from the nozzle. The center was chosen to be the most representative of the species present in the gas phase. The analysis was carried out in ambient air without contact with a liquid.

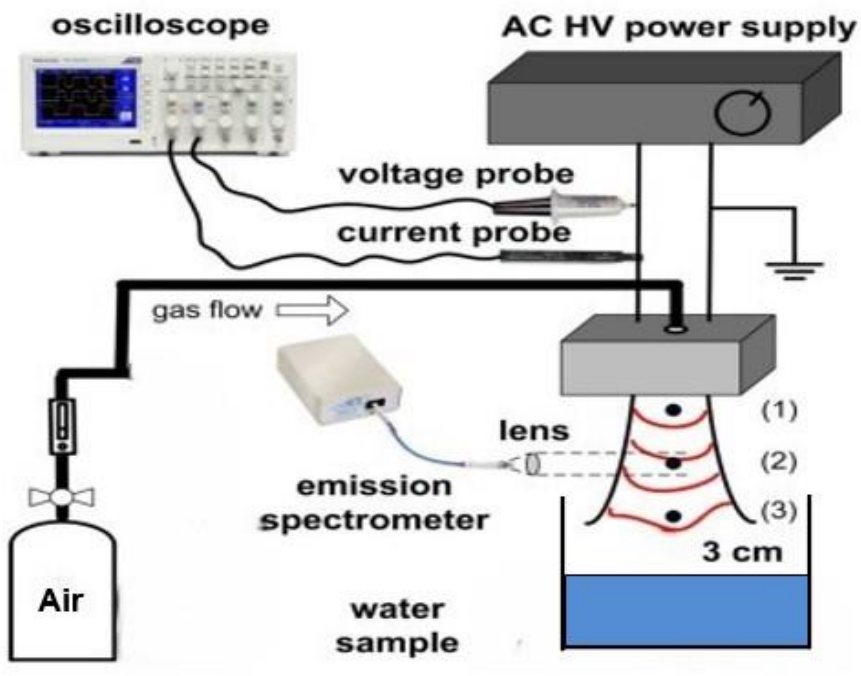

Figure 17. Schematic diagram of the experimental setup of OES analysis of the plasma gliding arc discharge (9000 V, 30 mA and 700 L min^{-1} air flow rate)

4.2 Liquid-phase measurements

4.2.1 PH and Conductivity

Glidarc treatment of an aqueous target leads to the diffusion of various ionic species from the plasma into the solution to be treated, thereby increasing the solution's conductivity. Generally speaking, these solutions are acidic, although acidification can result from plasma discharge in the presence of nitrogen, leading to the formation of nitric and nitrous acids, as explained in Chapter 3.

Therefore, PH and conductivity analyses are monitored in parallel with the same solution.

4.2.2 Plasma speices quantification

Measurements are taken on liquid samples taken at the outlet of the recovery tank.

The stable species measured in the liquid phase are:

- Nitrite and nitrate ions
- Total oxidants

4.2.2.1 Volumetric method for measuring total oxidants in the liquid phase

The total oxidants measured by the volumetric potassium iodide (KI) method are the species capable of oxidizing iodide ions (I^-) to diode (I_2). These species have higher potentials than the I_2/I^- redox couple (E°= 0.621 V).

These include hydroxyl radical ($E^o(^{\bullet}OH/H_2O) = 2.8\,V/SHE$), ozone ($E^o(O_3/O_2) = 2.07\,V/SHE$), dissolved $NO_2^{\bullet}$ ($E^o(NO_2^{\bullet}/N_2O) = 1.22\,V/SHE$), dissolved $^{\bullet}NO$ ($E^o(^{\bullet}NO/NO_2^{\bullet}) = 1.59\,V/SHE$), nitrates ($E^o(NO_3^-/NO_2^-) = 0.84\,V/SHE$) and nitrites ($E^o(NO_3^-/{}^{\bullet}NO) = 1.20\,V/SHE$ 1.20) formed by the reaction of $NO_2^{\bullet}$ with water. However, this reaction must be fast enough to occur quantitatively during the measurement period. The principle and procedure are described in Appendix II-1.

4.2.2.2 Measurement of nitrite and nitrate ions in solution

The determination of nitrate and nitrite ions during non-thermal plasma treatment was monitored by UV-Visible spectroscopy using a spectrophotometer at wavelengths of 435 and 350 nm respectively. The concentration of NO_2^- and NO_3^- ions was determined by calibration curves, constructed from $NaNO_2$ and KNO_3 standards respectively.

The calibration curves thus obtained are given in Appendix II.3 & 4.

4.2.3 Spectrophotometry UV-Visible analysis

Double BeamOPTIZEN 2021 takes UV/VIS spectrophotometry to a whole new level in terms of design, performance and functionality with new band features. This Spectrophotometer features a photometric single-beam system using tungsten-halogen and energy-saving deuterium lamps and operates from 200 to 700 nm.

This technique has been used primarily to determine the concentrations of nitrite, nitrate and decolorization rate (DEC) dyes and total oxidants in plasma-Glidarc-treated solutions. Equation 2.1 calculates the decolorization rate (DEC):

$$DEC(\%) = \frac{Abs_0^{\lambda} - Abs_t^{\lambda}}{Abs_0^{\lambda}} \times 100 \qquad \textbf{(Eq.7)}$$

Where:

Abs_0^{λ} : absorbance measured at wavelength λ at time t=0 (untreated sample);

Abs_0^{λ} : absorbance measured at wavelength λ at time t (sample treated for time t).

4.3 Quantification of phenol and its by-products

Concentrations of phenol and its derivatives were measured by liquid chromatography (YL9100, HPLC System YOUNGLIN); and the total organic carbon was measured using an Analytikjena multi-N/C 2100S TOC meter (Appendix II-5 & 6).

4.3.1 HPLC analysis

High-Performance Liquid Chromatography (HPLC) is a qualitative and quantitative analysis technique for discriminating between the various UV- and visible-absorbing molecules (mainly organic) in the same phase (mainly aqueous). Figure 18 shows the schematic diagram of liquid chromatography. The separation of products depends on their affinity for the stationary and mobile phases. This affinity is a function of the polarity of the products to be analyzed and of the two phases.

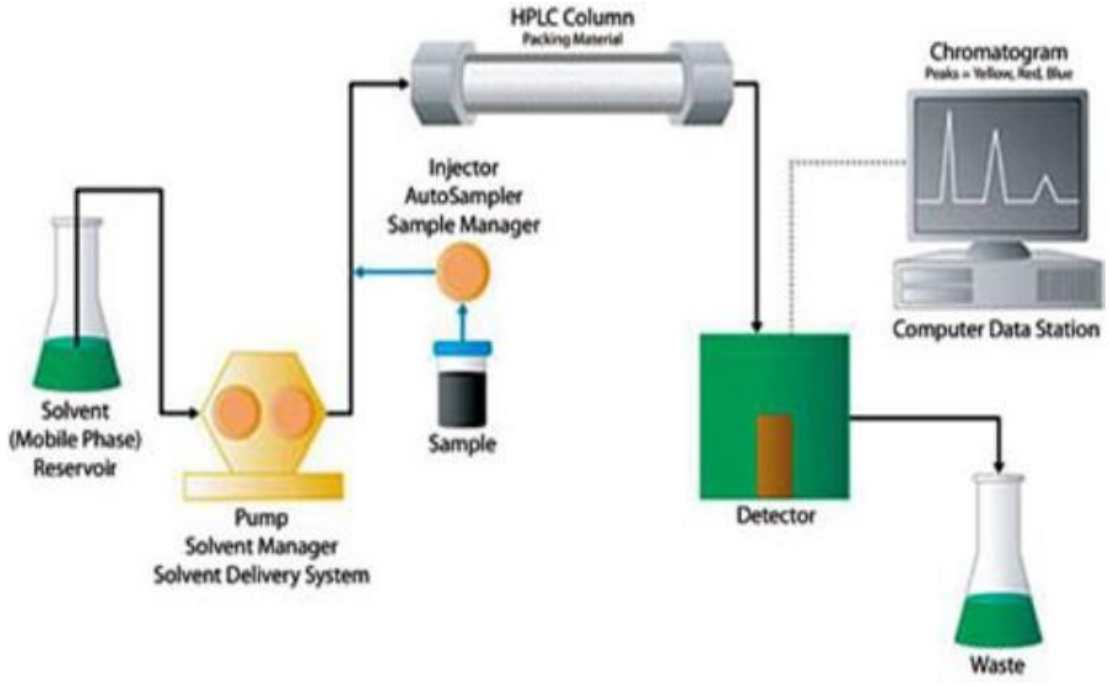

Figure 18. Schematic diagram of liquid chromatography (source: Comsol)

The stationary phase

The column is a polar stationary phase. The most widely used is based on silica gel, which is acidic due to the presence of silanol (-OH) groups on its surface. This phase represents the normal mode of analysis. In our study, we used the reverse mode, where the column of a normal phase is grafted with 18-carbon alkyl chains at the silanol (-OH) groups, which can generate spurious hydrophilic interactions. This makes the results non-reproducible. With the addition of a methyl function to the silica surface, the silanol functions are no longer free but in (Si-O-

CH_3) form. This phase is apolar and, therefore, requires a polar eluent (ACN, MeOH, H_2O). In this case, the more apolar compounds will have a greater affinity with the column. Their retention time will, therefore, be longer, and they will emerge at the end of the chromatogram. So, by switching from the normal phase to the reverse phase, the phase has changed from polar and hydrophilic (without the grafts) to apolar and hydrophobic. HPLC is sensitive to product concentrations of 1 to 10 µg mL^{-1}.

Mobile phase:

It can be polar or apolar, depending on the type of column used. By convention, an apolar column is used with a polar mobile phase, and vice versa. Some HPLCs are equipped with two or three pumps, enabling eluent mixtures to be prepared, or elution gradients to be applied during analysis. The aim here is to modify the more or less polar nature of the mobile phase and play on the retention times of the various constituents.

In our study, the solvent is a mixture of acetonitrile 40%, water 60%. The liquid sample is injected via a manual autosampler (sample volume = 20 µL).

Detector:

Once the molecules have been separated, they need to be identified. Identification is generally carried out indirectly, using a UV-Vis detector or diode array. This type of detector emits a light signal at a certain wavelength (typically between 190 and 350 nm for UV detectors). The difference between a UV-Vis lamp detector and a diode array detector lies in the wavelength range. A diode array will emit light at all wavelengths, and the detector will collect a signal corresponding to each of these wavelengths "in real time". A UV lamp detector, on the other hand, will only perform the analysis at a pre-defined wavelength. It is, therefore, necessary to identify in advance the maximum wavelength of the molecule you wish to study. The main advantage of this type of detector is that the intensity of the signal (i.e., the air of the peak) is directly proportional to the concentration of the molecule in the solution. After proper calibration, it is possible to precisely determine the concentration of the compound in the solution.

It is important to point out that the signal and the limit of quantification are directly linked to the molecule and its absorption coefficient at the wavelength under consideration (typically, aromatics absorb around 254 nm). To obtain the most accurate signal possible, it is essential to use eluents that do not absorb at the compound's wavelength.

In our laboratory, we have a YL9100, HPLC System YOUNGLIN HPLC instrument comprising a Ø 4.6 × 150 mm, 5 µm apolar stationary phase column and a UV/Vis/ PDA (photodiode

array) 190-900 nm detector. The mobile phase flow rate is isocratic (1 mL min^{-1}). The system is connected to a data acquisition and processing unit using YL-CLARITY.

4.3.2 Total organic carbon (TOC) analysis

Total organic carbon is a global parameter for estimating mineralization efficiency. In fact, this measurement gives the quantity of carbon (milligrams of carbon per liter of solution) present in organic form in an aqueous solution.

The theoretical TOC of a solution of a compound of the $C_xH_yO_z$ type is calculated according to equation II.4 [12, 30].

$$COT = x.M_C\ [C_XH_YO_Z] \qquad \textbf{(Eq.8)}$$

Where, M_C is the molar mass of carbon in g mol^{-1}, $[C_xH_yO_z]$ the concentration in mmol L^{-1} and TOC is given in mg of carbon per liter.

The principle of determining a sample's total organic carbon is based on the complete conversion of the organic compound's carbon atoms into carbon dioxide (CO_2). The measurement of total organic carbon is carried out in a combustion chamber at 680°C under a flow of pure oxygen. The total combustion of organic and inorganic materials produces a quantity of carbon dioxide, which is measured by IR spectroscopy at the furnace outlet.

During this work, TOC levels were measured using an analyzer equipped with a manual injector, using the total carbon (TC) method. The schema diagram of the TOC analysis method is presented in Figure 19. The samples, acidified to 1% with chlorophyll acid, are first bubbled with carbon dioxide-free nitrogen to eliminate any trace of CO_2.

Fifty µL are then automatically taken for analysis. The instrument performs each measurement three times, and the result is the average of the two best (closest) values obtained. Analyses were carried out by external calibration.

Calibrations were carried out using initial solutions of organic compounds or standard potassium hydrogen phthalate solutions.

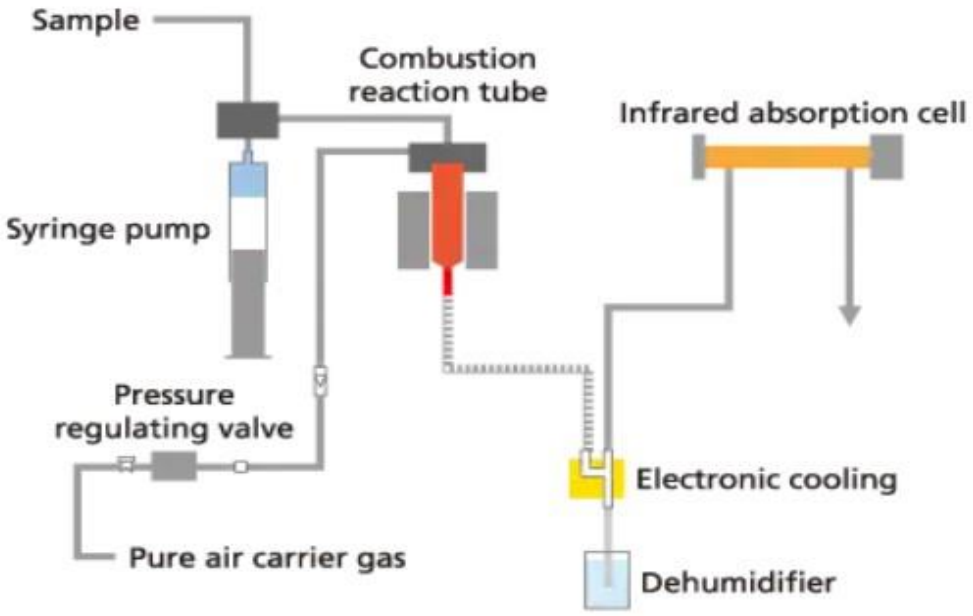

Figure 19. Schema diagram of TOC analysis [126]

Our liquid samples were analyzed by a multi N/C 2100S TOC meter from Analytikjena. The instrument gives us direct TOC values for our samples in mg L^{-1}. The degradation rate (DEG) of a molecule is calculated by equation (9).

$$DEG(\%) = \frac{TOC_0 - TOC_t}{TOC_0} \times 100 \quad \textbf{(Eq.9)}$$

Where,

TOC_0: TOC measured at time t=0 (untreated sample);

TOC_t: TOC measured at time t (sample treated for time t).

CHAPITRE III. Classification of plasma GAD reactors

CHAPTRE III. Classification of plasma GAD reactors

Introduction

Non-thermal plasma reactors represent a versatile and energy-efficient technology with a wide range of applications. Their capacity to generate reactive species at low temperatures opens up possibilities for innovative solutions in environmental protection, material science, chemical synthesis, and medicine. Non-thermal plasma technology is expected to play an increasingly important role in addressing global challenges and driving technological progress.

The gliding arc discharge is one of the most powerful plasma technologies, enabling a considerable flow of reactive species to be generated at a moderate temperature (around 50°C) and under atmospheric pressure. It is easy to adapt to the treatment of various aqueous solutions and can also be used to treat solid surfaces and gases. These characteristics make it safer, more beneficial, and easier to operate. It is particularly interesting from a technical and industrial point of view. It allows it to be proposed as a process or part of a process, whether for wastewater treatment or chemical synthesis.

The integration of plasma reactors into industrial processes represents a significant advancement in manufacturing and environmental technologies. Particularly, plasma gliding arc reactors offer unique advantages due to their ability to generate continuous flow of reactive species at low temperatures and with high energy efficiency. This capability makes them suitable for a wide range of industrial applications, including pollution control, materials processing, and chemical synthesis.

Despite the numerous advantages, the integration of plasma GAD reactors in industrial processes faces several challenges. These include the requirement for robust and scalable reactor designs, the optimization of process parameters for different applications, and the development of cost-effective power supplies. To overcome these obstacles, industry and academic staff must continue research and collaboration work to advance the technology and demonstrate its economic viability in real-world applications.

In this chapter, we present in detail the chemical and safety assessments for the four glidarc plasma configurations we have in mind in our STEVA laboratory. The chemical evaluation of these configurations is conducted based on the measure of the conversion rate and by-product selectivity for the chemical synthesis processes and both discoloration and demineralization rates for water depollution applications. While the safety evaluation is performed based on the proposed scenarios. The obtained results were explained based on the distinct physical-chemical characteristics present by the four prototypes, such as mass transfer properties, medium acidity, and plasma dose.

1. Plasma GAD configurations

In the previous chapter, we presented different plasma GAD configurations available in our laboratory, STEVA. These configurations are driven by air gas under atmospheric pressure and are used for water treatment. They have an identical principle of plasma production. In general, plasma Gliding arc reactors are classified as biphasic reactors, where reactive absorption is the characteristic phenomenon in which the produced plasma species passes from the gas to the liquid phases, where it reacts with the target molecules diluted in the aqueous solution.

Here in figure 01, we present the 04 plasma GAD generations developed in STEVA laboratory.

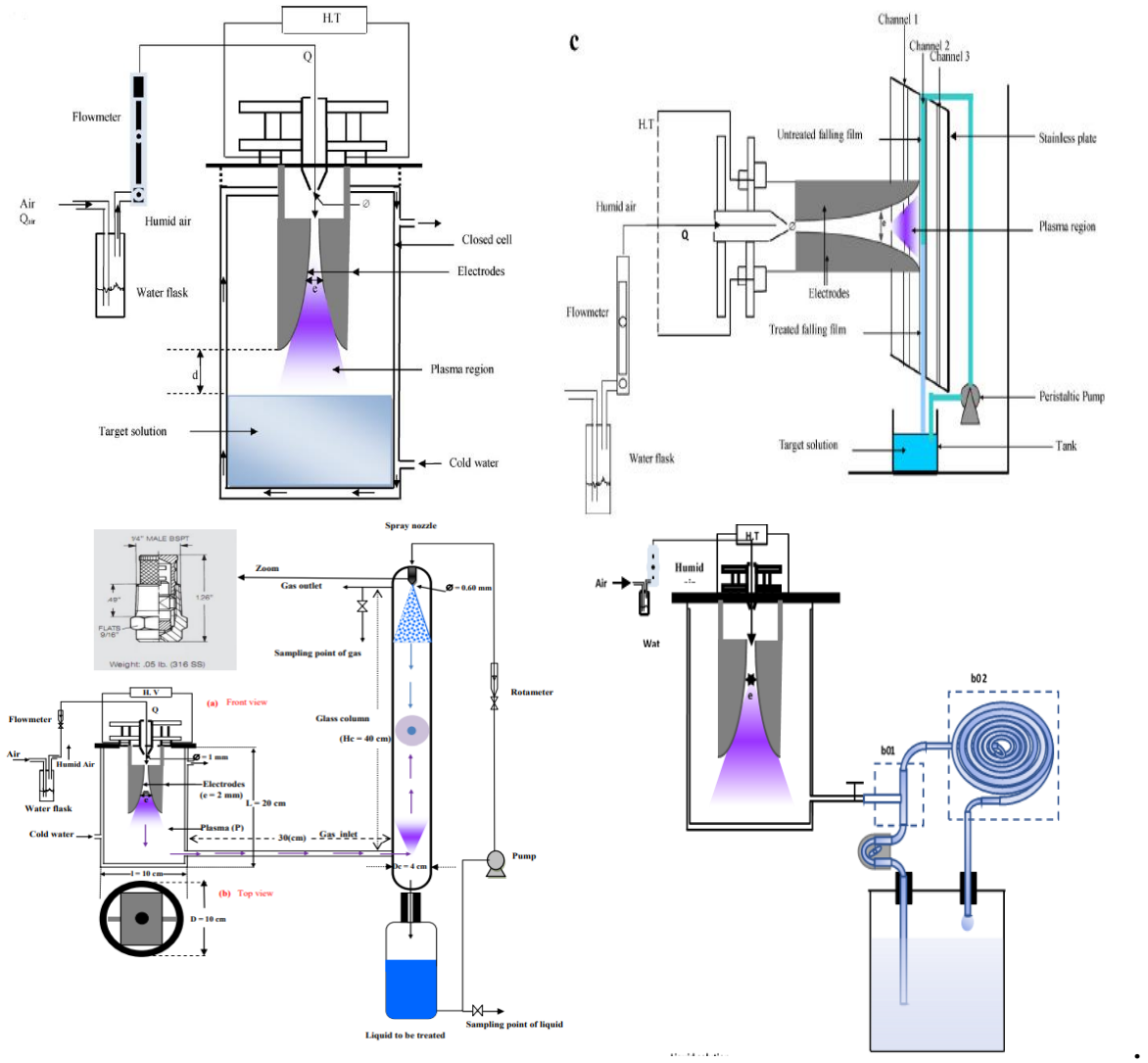

Figure 20. Plasma GAD configurations: (a) GAD-Batch [123], (b) GAD-Failing Film [90], (c) GAD-Spray Tower [105], (d) GAD-Venturi

1.1 Operating mode

The presented configurations were designed to optimize the specific requirements of different applications for liquid treatments. GAD-Batch is the first version; it is a batch reactor accompanied by a stirring system to ensure a homogenized mixture. This prototype was developed for the treatment of a limited liquid quantity, and it is suitable for the pharmaceutical industry and a small chemical synthesis [123]. For industrial uses, more suitable configurations have been developed, like GAD-Failing film, spray tower, and venturi [90, 105]. These reactors involve the same functioning principle, which revolves around a continuous liquid flow treatment in order to ensure a massive treated quantity and reach some industrial requirements. However, they show a different performance in terms of conversion rate and mass transfer; this disparity can be explained by the different chemical and physical properties presented by the GAD prototypes and will be deeply discussed in the coming sections.

2. Plasma GAD properties

Plasma gliding arc discharge (GAD) used for liquid treatment presents unique physical and chemical properties that make it a promising solution to the most difficult problems in environmental remediation and water purification and a powerful reactive technology for chemical synthesis [21, 22, 25, 127-129]. Its capacity to function effectively, safely, and sustainably highlights its potential as a cutting-edge liquid treatment technology, providing a viable way to improve water quality, safeguard public health, and produce eco-friendly chemicals.

2.1 Physical properties

The physical properties of GAD are defined by its ability to create and maintain an ambient temperature and atmospheric pressure plasma state, which eliminates the need for high-pressure rooms or vacuum systems. This not only makes the necessary equipment simpler, but it also lowers operating costs and boosts security. This remains the same for all described configurations, but they have unequal transferred quantities and reactivity. Therefore, in this study, a mass transfer coefficient for the plasma GAD prototypes is determined, and a chemical reaction mechanism is discussed in the following sections.

2.1.1 Mass transfer (Stripping, a, K_L)

The overall mass transfer coefficients K_L and K_G are determined using the solute stripping method [25], which consists of conducting simple phenol stripping experiments carried out

under the same conditions as its plasma treatment. The experiments are followed by a modeling and simulation study to fix K_L and K_G coefficients.

The current study uses Whitman's model [130] to model the mass transfer phenomena and explain the obtained experimental results. This model represents all biphasic systems by four zones; it summarizes all the resistance to the transfer of matter in two stagnant films adjacent to the gas-liquid interface; the latter represents a thermodynamic equilibrium expressed by Henry's law. This model considers that material transfer from the liquid side occurs only by molecular diffusion through a thin film between gas and liquid. The liquid and gas bulks are considered a perfectly agitated zone.

a) GAD-Batch system

Assuming the gaseous and liquid phases perfectly homogenized at constant volume (figure.21), it is possible to write the material balances in each of the two phases as below:

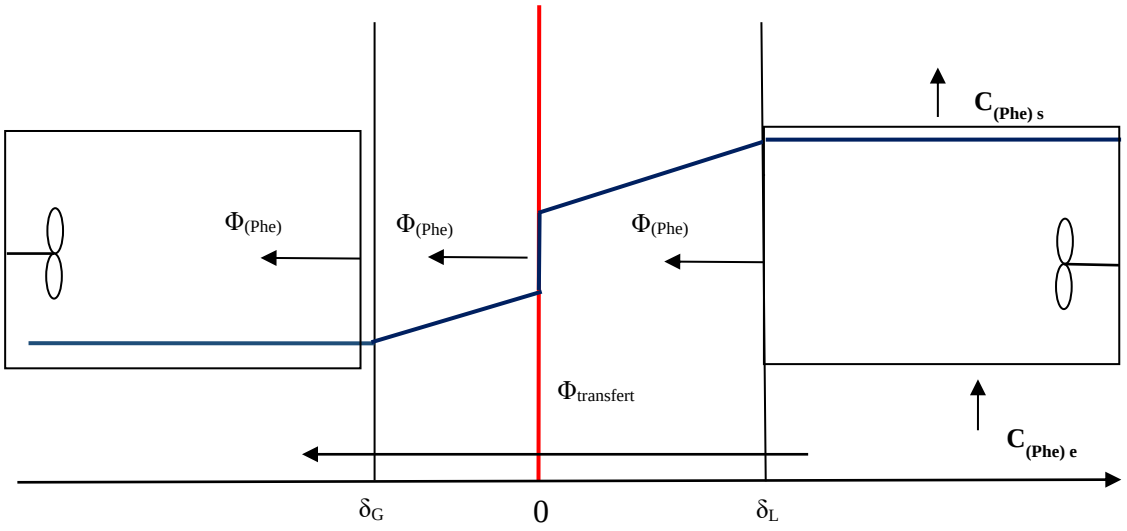

Figure 21. Phenol stripping for batch reactor

Liquid mass balance:

$$\frac{dC_{liquid}^{Phe}}{dt} * V_{liquid} = -\Phi_{transfert} \qquad \textbf{(Eq.10)}$$

Gas mass balance:

$$\frac{dC_{gaz}^{Phe}}{dt} * V_{gaz} = -\Phi_{transfert} - Q_{gaz} * C_{gaz}^{Phe}(s) \qquad \textbf{(Eq.11)}$$

With,

$$\Phi_{transfert} = K_L * S * \left(C_{liquid}^{Phe} - He * C_{gaz}^{Phe}\right) \quad \textbf{(Eq.12)}$$

$$\Phi_{transfert} = K_G * S * \left(\frac{C_{liquid}^{Phe}}{He} - C_{gaz}^{Phe}\right) \quad \textbf{(Eq.13)}$$

$$e_{liquid} = \frac{D_{liquid}}{K_L}, \quad e_{gas} = \frac{D_{gas}}{K_G} \quad \textbf{(Eq.14)}$$

The obtained mathematical system is solved using Simulink-MATLAB software, the simulation flowsheet is presented in figure 22.

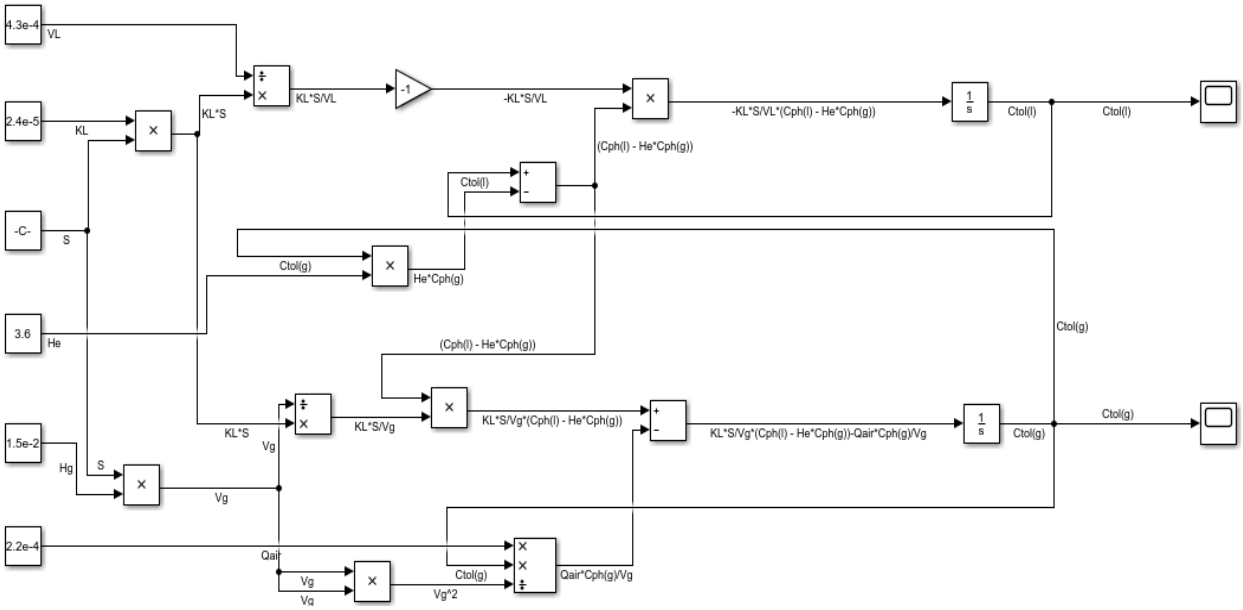

Figure 22. Simulation flowsheet of phenol stripping

This resolution was carried out with the Simulink software using a ranjkuta-4 integration method of equations (Eq.10 &11). It was able to plot the theoretical evolution of the concentration of phenol in the liquid phase over time. Hence, the methodology consisted of varying K_L (or K_G) until an elimination percentage identical to the experiment was obtained.

Figure 23 presents the final feting simulation plot of the evolution of phenol concentration. K_L was fixed at 1.56×10^{-6} m s^{-1}, where the theoretical plot perfectly matches the experimental results of the phenol stripping experiment.

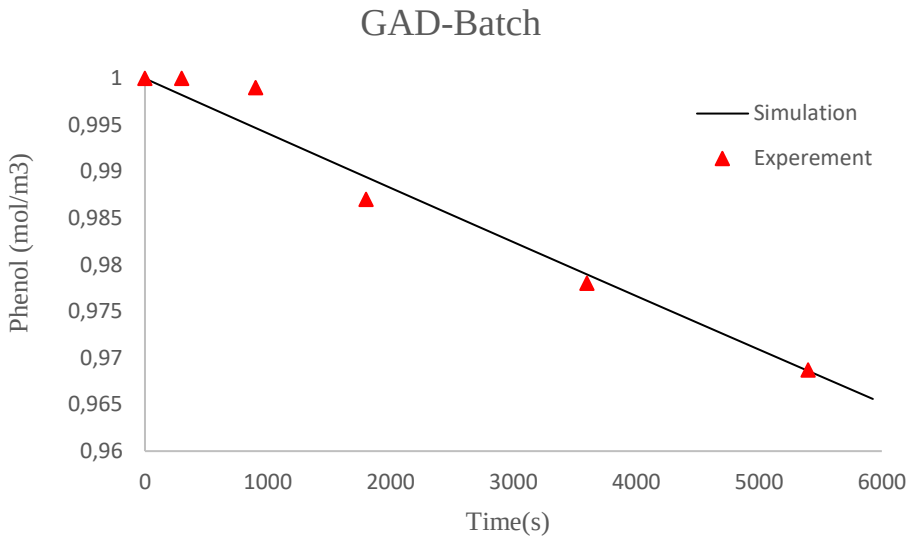

Figure 23. Phenol stripping, predicted and experimental results for GAD-Batch reactor

b) GAD-Continuous systems

For the GAD reactors functioning in continuous mode like failing film, spray tower and Venturi configurations, the model has been kept the same as the batch one with a slight difference on the mathematical model by taking into account the continuous flow for the liquid region.

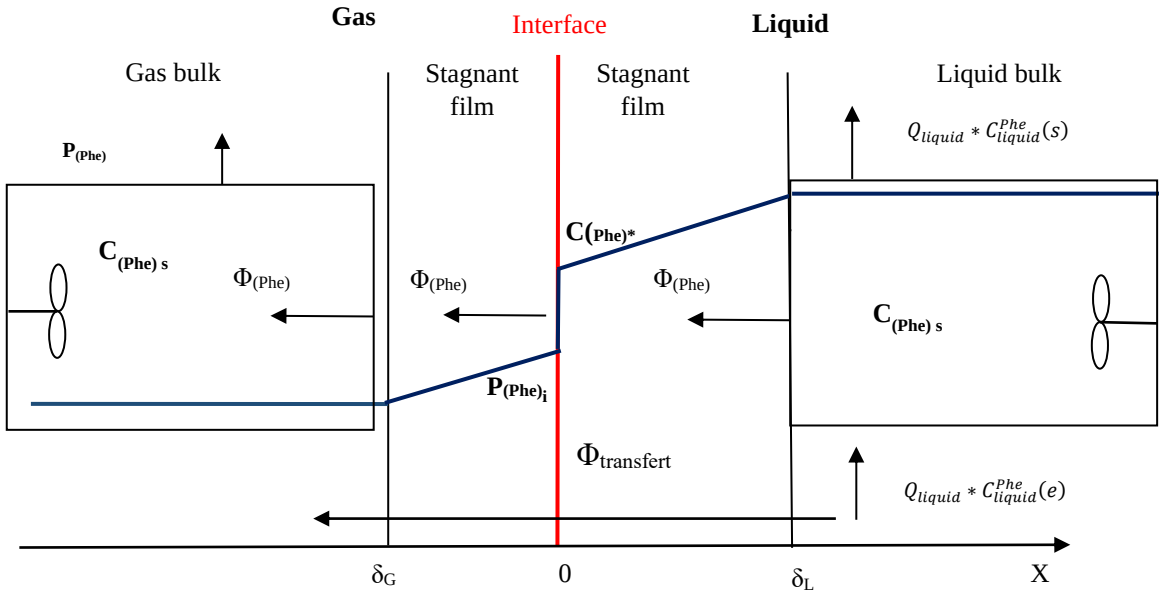

Figure 24. Phenol stripping for GAD continuous systems

The mass balance in such as configuration led to the following equations:

Liquid mass balance:

$$\frac{dC_{liquid}^{Phe}}{dt} * V_{liquid} = -\Phi_{transfert} + Q_{liquid} * (C_{liquid}^{Phe}(e) - C_{liquid}^{Phe}(s)) \quad \textbf{(Eq.15)}$$

Gas mass balance:

$$\frac{dC_{gaz}^{Phe}}{dt} * V_{gaz} = -\Phi_{transfert} - Q_{gaz} * C_{gaz}^{Phe}(s) \quad \textbf{(Eq.16)}$$

Figure 25 presents the simulation flowsheet on Simulink software of the obtained mathematical system of phenol stripping for continuous systems.

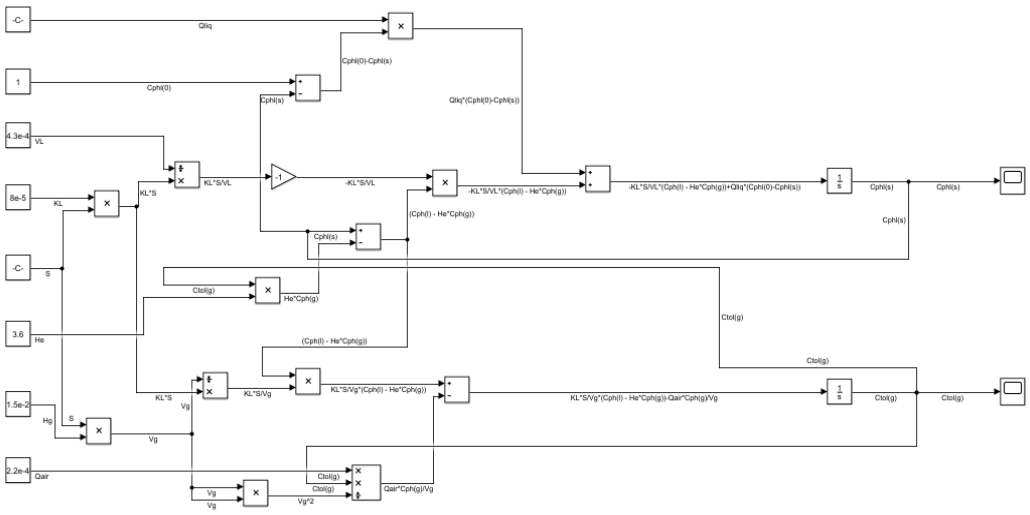

Figure 25. Simulation flowsheet of phenol stripping for continuous systems

After a fetching study of the mass transfer coefficient in liquid film, we obtained, as presented in Figure 26, a good coherence between phenol stripping experimental results and the predicted one obtained by the numerical resolution of the mathematical equations (Eq.15&16). This coherence was reached for K_L of 8×10^{-7} m s^{-1}, 6×10^{-6} and 9.5×10^{-7} m s^{-1} of the spray tower, Venturi, and failing film configurations, respectively.

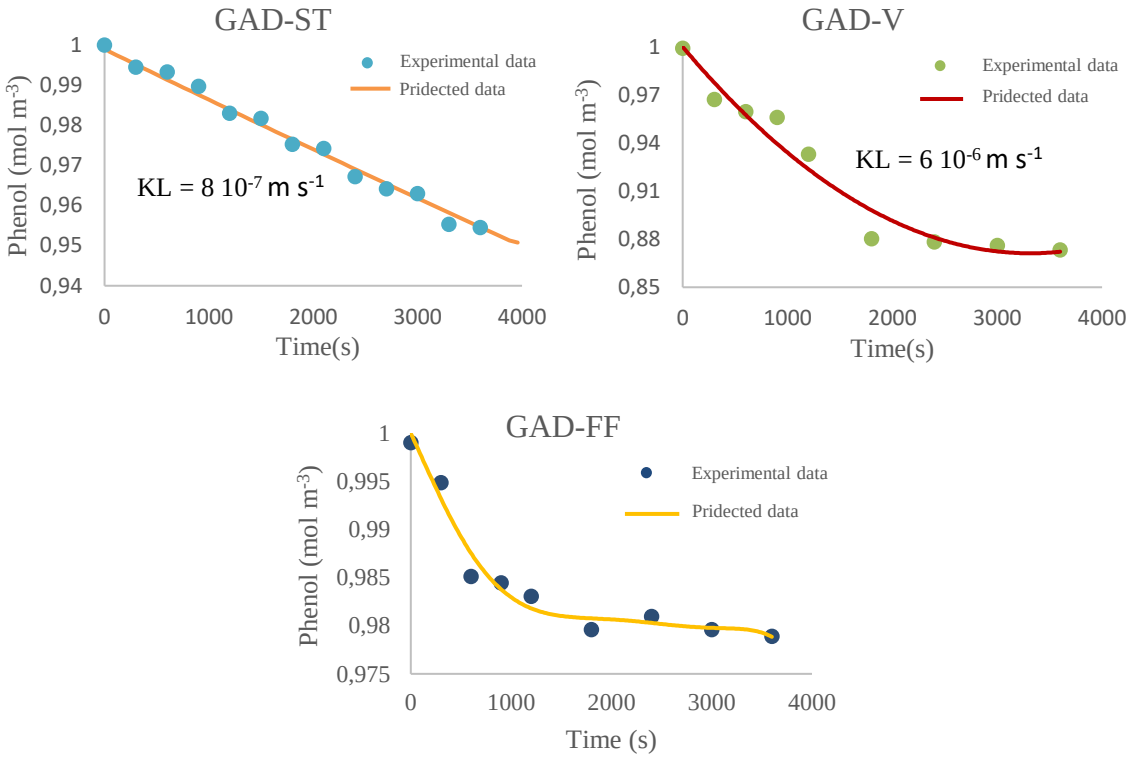

Figure 26. Phenol stripping, predicted and experimental results for GAD continuous

Table 5 summarizes phenol striping parameters and the simulation results for the four GAD configurations. The analysis of liquid mass transfer and gas flow coefficients in four different GAD (Gas-Assisted Deposition) configurations—Batch, Falling Film, Spray Tower, and Venturi reveals different performance characteristics. Due to its large surface area and efficient mixture, the Venturi reactor stands out for its high mass transfer coefficients for both liquid and gas (40 m s^{-1} and 0.0306 m s^{-1}, respectively). With its large volume and surface area, the Batch reactor exhibits strong mass transfer rates but a moderate elimination rate (3.1%). The reactor Falling Film has the lowest elimination rate (2.1%) and moderate mass transfer coefficients due to its smaller volume and comparatively smaller surface. Despite having lower mass transfer coefficients than the reactor Batch and Falling Film, the Spray Tower reactor achieves a higher elimination rate (4.5%) due to an improved liquid-gas contact and higher transferred flow. These results highlight the importance of selecting the proper reactor configuration based on the particular requirements of the liquid treatment process.

Table 5. K_L and K_G for all GAD configurations

GAD-Configuration	V (Cm^3)	S (m^2) 10^{-3}	Q (m^3s^{-1}) 10^{-7}	He (US*)	Stripping time (min)	Elimination rate (%)	K_L ($m\ s^{-1}$) 10^{-7}	K_G ($m\ s^{-1}$)
Batch	430	6.35	/	7644	60	3.13	15.6	0.0119
Failing film	180	3.23	9.7	7644	60	2.12	9.5	0.0073
Spray tower	300	1.91	9.7	7644	60	4.55	8	0.0061
Venturi	300	9.91	9.7	7644	60	12.68	40	0.0306

2.1.2 Discharge type

In plasma GAD reactors, three distinct discharge mechanisms are utilized to optimize liquid solution treatment: direct discharge, post-discharge, and spatiotemporal post-discharge. In direct one-involved batch and failing film reactors [33, 90, 123], the plasma plume is two to three centimetres from the liquid's surface, allowing immediate and intense interaction between the plasma-generated reactive species and the liquid interface area. This proximity ensures a massive reactive species and energy transfer, leading to an efficient reactivity and a high conversion rate. Post-discharge involves a continuing reaction of transferred plasma species after the plasma plume exposure has ended. This process benefits from the sustained activity of reactive species in the liquid, enhancing treatment efficacy over time without plasma exposure [30]. Meanwhile, spray tower and venturi configurations are characterized by spatiotemporal post-discharge methods that involve the transfer of plasma gas for more than 70 centimetres from a plasma tank reactor to a liquid solution [122]. This extended distance allows for the controlled transport and interaction of reactive species with no heating and UV light processes, which can be beneficial for treating more significant volumes of liquid or achieving more uniform treatment under a normal condition (TPN) and avoiding parasitic reactions caused by UV lights.

The three discharge types exhibit distinct populations of plasma species, leading to different chemical mechanisms. In direct discharge, a high concentration of short-lived entities such as electrons, reactive radicals, and UV photons since the plasma plume is too close to the liquid interface, which in turn provides a powerful chemical reaction and can act as a photocatalytic process known by plasma catalysis. Table 5 presents a plasma reaction mechanism proposed by Djakaou and his colleagues [26].

Table 6. Plasma direct discharge mechanism [26]

Plasma-chemical reactions		Constant rates at 298 K	
Distilled water	$^{\bullet}OH^{(g)} \xrightarrow{He_1} {}^{\bullet}OH^{(l)}$	**(R 49)**	$He_1 = 760$
	$^{\bullet}OH^{(l)} + {}^{\bullet}OH^{(l)} \xrightarrow{k_2} H_2O_2$	**(R 50)**	$k_2 = 10^7\ m^3\ mol^{-1}\ s^{-1}$
	$NO_2^{(g)} + NO_2^{(g)} \xleftrightarrow{k_3,k_{-3}} N_2O_4^{(g)}$	**(R 51)**	$k_3 = 6.02 \times 10^6\ m^3\ mol^{-1}\ s^{-1}$ $k_{-3} = 4.4 \times 10^6\ m^3\ mol^{-1}\ s^{-1}$
	$N_2O_4^{(g)} \xleftrightarrow{He_4} N_2O_4^{(l)}$	**(R 52)**	$He_4 = 39$
	$N_2O_4^{(l)} \xleftrightarrow{k_5,k_{-5}} NO_2^{\bullet} + {}^{\bullet}NO_2$	**(R 53)**	$k_5 = 7 \times 10^3\ s^{-1}$ $k_{-5} = 4.5 \times 10^5\ m^3\ mol^{-1}\ s^{-1}$
	$N_2O_4^{(l)} + H_2O \xrightarrow{k_6} NO_2^{-(l)} + 2H^+ + NO_3^-$	**(R 54)**	$k_6 = 10^6\ s^{-1}$
	$NO_2^{-(l)} + {}^{\bullet}OH^{(l)} \xrightarrow{k_7} NO_2^{\bullet(l)} + OH^-$	**(R 55)**	$k_7 = 10^7\ m^3\ mol^{-1}\ s^{-1}$
	$O_3^{(g)} \xrightarrow{He_8} O_3^{(l)}$	**(R 56)**	$He_8 = 0.3$
	$NO_2^{-(l)} + O_3^{(l)} \xrightarrow{k_9} NO_3^{-(l)} + O_2$	**(R 57)**	$k_9 = 5.8 \times 10^2\ m^3\ mol^{-1}\ s^{-1}$
	$NO_2^{\bullet} + {}^{\bullet}OH \xrightarrow{k_{10}} HOONO$	**(R 58)**	$k_{10} = 1.2 \times 10^7\ m^3\ mol^{-1}\ s^{-1}$
	$HOONO + H_2O \xrightarrow{k_{11}} NO_3^- + H^+$	**(R 59)**	$k_{11} = 1.1\ s^{-1}$
Phenol	$C_7H_{16}O^{(l)} \xrightarrow{He_{13}} C_7H_{16}O^{(g)}$	**(R 60)**	$He_{13} = 584640$
	$C_7H_{16}O^{(g)} + {}^{\bullet}OH^{(g)} \xrightarrow{k_{14}} Products$	**(R 61)**	$k_{14} = 5.1{\times}10^6\ m^3\ mol^{-1}s^{-1}$
	$C_7H_{16}O^{(l)} + {}^{\bullet}OH^{(l)} \xrightarrow{k_{15}} Products$	**(R 62)**	$k_{15} = 7.4{\times}10^6\ m^3\ mol^{-1}s^{-1}$

For indirect discharge, Fouad et al. have proposed a novel mechanism where long-lived species like ozone (HONOO) are the main components of this discharge type, as presented in Table 03 [131]. These species can maintain chemical interactions for longer periods, allowing for slower but more persistent oxidative processes. Chemical reactions depend on the oxidative potential of long-lived species since there are no photolytic effects ensured by the absence of UV lights.

Table 7. Plasma indirect discharge mechanism [131]

Plasma-chemical reactions		Constant rates at 298 K	
Distilled water	$HONOO^{(g)} \xrightarrow{He_1} HONOO^{(l)}$	**(R 63)**	$He_1 = 5.1{\times}10^6$
	$HONOO^{(l)} \xrightarrow{k_1} NO_2^{\bullet(l)} + {}^{\bullet}OH^{(l)}$	**(R 64)**	$k_1 = 6 \times 10^4\ s^{-1}$
	$NO_2^{(g)} + NO_2^{\bullet(g)} \xleftrightarrow{k_2,k_{-2}} N_2O_4^{(g)}$	**(R 51)**	$k_2 = 6.02{\times}\ 10^6\ m^3\ mol^{-1}\ s^{-1}$ $k_{-2} = 4.4{\times}\ 10^6\ m^3\ mol^{-1}\ s^{-1}$
	$N_2O_4^{(g)} \xleftrightarrow{He_2} N_2O_4^{(l)}$	**(R 52)**	$He_2 = 36.67$
	$N_2O_4^{(l)} \xleftrightarrow{k_3,k_{-3}} NO_2^{\bullet(l)} + NO_2^{\bullet(l)}$	**(R 53)**	$k_3 = 7 \times 10^3\ s^{-1}$ $k_{-3} = 4.5 \times 10^5\ m^3\ mol^{-1}\ s^{-1}$
	$N_2O_4^{(l)} + H_2O \xrightarrow{k_4} NO_2^{-(l)} + 2H^+ + NO_3^{-(l)}$	**(R 54)**	$k_4 = 10^6\ s^{-1}$
	$NO_2^{\bullet(l)} \xrightarrow{k_7} NO_2^{-(l)}$	**(R 65)**	$k_7 = 1.3\ 10^8\ s^{-1}$
AG25	$AG25 + {}^{\bullet}OH^{(l)} \xrightarrow{k_8} P1$	**(R 66)**	$K_8 = 10^9\ m^3\ mol^{-1}\ s^{-1}$

In summary, direct discharge relies on fast, UV-driven reactions with short-lived species, while post discharge and spatiotemporal post discharge focus on slower, sustained oxidative reactions with long-lived species.

2.1.3 Plasma reaction-absorption competition

Plasma GAD reactors are biphasic systems characterized by reactive absorption, where the mass transfer and the chemical reaction mechanism play a crucial role. The previously discussed results of mass transfer coefficients highlight the ability of the operated plasma GAD configurations, such as Batch, Falling Film, Spray Tower, and Venturi, to facilitate the transfer of reactive species into the liquid region. The type of discharge explains the nature and lifetime of these reactive species, which in turn define the plasma reaction mechanism.

Mass transfer and chemical reaction phenomena have an important and distinct impact on such reactors' performance. Therefore, understanding and optimizing the duality between these phenomena is a pivotal study to enhance the treatment capabilities of each GAD configuration. In this context, the double film model explains well the outlined competition by plotting the concentration profiles of the absorbed plasma reactive species and the treated molecules or by calculating some dimensionless numbers like Hatta, Z, R, and Da [100, 130]. Figure 27 presents the principle participating phenomena in plasma GAD reactive absorption.

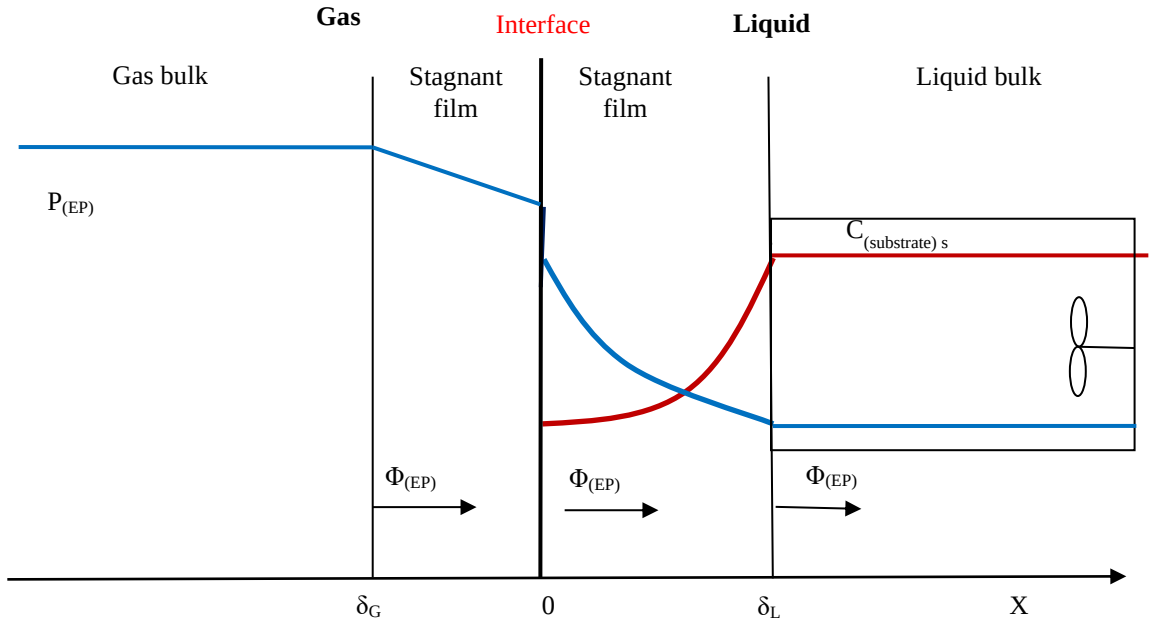

Figure 27. Plasma GAD reactive absorption

Plasma species react with treated substrate following this reaction:

$$EP^{(l)} + \vartheta\ Substrate^{(l)} \xrightarrow{K} \text{Products} \qquad \textbf{(R 67)}$$

Assuming the reaction is first order with respect to the treated substrate and plasma (EP) species. The expressions of reaction rates r(Phenol) and r(EP) are then the following:

$$r_{(\text{Substrate})} = K \cdot C_{(\text{Substrate})} \cdot C_{(EP)} \qquad \textbf{(Eq.17)}$$

$$r_{(EP)} = \vartheta \cdot K \cdot C_{(\text{Substrate})} \cdot C_{(EP)} \qquad \textbf{(Eq.18)}$$

In the framework of the Whitman double film model, the mass balance in the liquid film (figure 27) was conducted in order to reflect the diffusion-chemical reactions competition of Plasma bodies and the target substrate; these balances lead to the following differential equations [100]:

$$D_{(EP)} \frac{d^{2}C_{(EP)}}{dx^{2}} = k \cdot C_{(EP)} \cdot C_{(\text{Phenol})} \qquad \textbf{(Eq.19)}$$

$$D_{(\text{Phenol})} \frac{d^{2}C_{(\text{Phenol})}}{dx^{2}} = \vartheta \cdot k \cdot C_{(EP)} \cdot C_{(\text{Phenol})} \qquad \textbf{(Eq.20)}$$

Boundary conditions,

Interface gas/liquid (x = 0)

$$C_{(EP)} = C_{(EP)^{*}} \qquad \textbf{(Eq.21)}$$

$$\frac{dC_{(\text{Phenol})}}{dx} = 0 \qquad \textbf{(Eq.22)}$$

Boundary film/bulk ($x = \delta_L$),

The boundary conditions are given by the material balances in the core of the liquid, considering the chemical reaction and the fluxes transferred from the film by diffusion towards the core of the liquid in a batch configuration and circulating convective flux in continuous systems like spray tower, failing film and venturi.

For discontinuing systems:

$$C_{(EP)} = C_{(EP)s} \quad \textbf{(Eq.23)}$$

$$-D_{(EP)} \cdot S \cdot \left(\frac{dc_{(EP)}}{dx}\right)_{x=\delta L} = V_L \cdot r_{(EP)} \quad \textbf{(Eq.24)}$$

$$-D_{(Phenol)} \cdot S \cdot \left(\frac{dc_{(Phenol)}}{dx}\right)_{x=\delta L} = V_L \cdot r_{(Phenol)} \quad \textbf{(Eq.25)}$$

For continuing systems:

$$C_{(EP)} = C_{(EP)s} \quad \textbf{(Eq.26)}$$

$$-D_{(EP)} \cdot S \cdot \left(\frac{dc_{(EP)}}{dx}\right)_{x=\delta L} = V_L \cdot r_{(EP)} \quad \textbf{(Eq.27)}$$

$$-D_{(Phenol)} \cdot S \cdot \left(\frac{dc_{(Phenol)}}{dx}\right)_{x=\delta L} = Q \cdot C_{(NO_2^-)_s} + V_L \cdot r_{(Phenol)} \quad \textbf{(Eq.28)}$$

Putting equations (21), (22), (23), (24), (25) and (26) in dimensionless form makes it possible to define the characteristic dimensionless numbers of this system. For this, the chosen variables are:

$$X = \frac{x}{\delta L}, \quad EP = \frac{C_{(EP)}}{C_{(EP)^*}}, \; Phe = \frac{C_{(Phenol)}}{C_{(Phenol)_S}}, \; EPs = \frac{C_{(EP)s}}{C_{(EP)^*}} \quad \textbf{(Eq.29)}$$

The mathematical model for discontinuing systems become as following:

$$\frac{d^2EP}{dX^2} = Ha^2\ EP\ Phe \quad \textbf{(Eq.30)}$$

$$\frac{d^2PHE}{dX^2} = \frac{Ha^2}{Z} EP\ Phe \quad \textbf{(Eq.31)}$$

X=0

$$EP = 1$$

$$\frac{dPhe}{dX} = 0 \quad \textbf{(Eq.32)}$$

X=1

$$Phe = 1$$

$$\left(\frac{dEP}{dX}\right)_{X=1} = -EP_S \cdot R \quad \textbf{(Eq.33)}$$

The mathematical model for continuing systems become as following:

$$\frac{d^2EP}{dX^2} = Ha^2\ EP\ Phe \quad \textbf{(Eq.30)}$$

$$\frac{d^2Phe}{dX^2} = \frac{Ha^2}{Z} EP\ Phe \quad \textbf{(Eq.31)}$$

X=0

$$EP = 1$$

$$\frac{dPhe}{dX} = 0 \quad \textbf{(Eq.33)}$$

X=1

Phe =1

$$\left(\frac{dEP}{dX}\right)_{X=1} = -EP_S \cdot \left(R + \frac{1}{D_a}\right) \quad \textbf{(Eq.34)}$$

With [100],

$H_a = \frac{\sqrt{k \cdot C_{(Phe)_S} \cdot D_{(EP)}}}{K_L}$: Hatta number

$z = \frac{D_{(Phe)} \cdot C_{(Phe)S}}{\nu \cdot D_{(EP)} \cdot C_{(EP)^*}}$ In our case, ν = 1

$R = \frac{K_2 \cdot C_{(Phe)S} \cdot \varepsilon_L}{K_L \cdot a} = \frac{K_2 \cdot C_{(Phe)S}}{K_L \cdot a'}$

$D_a = K_L \cdot a \cdot \tau = K_L \cdot a \cdot \frac{V_R}{Q}$: Damköhler number

Phenol was chosen as a target substrate in our study because of its moderate solubility, high affinity, and reactivity with plasma species. In order to facilitate the calculations, A new kinetic model was proposed to describe plasma phenol interaction based on the phenol by-products produced during phenol exposure to the plasma plume. The plasma phenol product was hydroquinone, resorcinol from hydroxyl radicals interaction with phenol molecules, and Nitrophenol from phenol reaction; these radicals are the main reactive plasma species which are directly produced in the plasma plum and have a short living time due to their high reactivity they react between each other in liquid phases to produce HONOO which is responsible for the post-discharge treatment. However, in the spatiotemporal post-discharge, the peroxynitrite is produced in the gas phases due to the long time spent during the transportation of the plasma gas to the spray tower, which in turn reproduce the •OH and radicals after migration to the liquid region, where the hydroxyl radicals produced from the HONOO present the main role of phenol degradation. The variety of the plasma species led to a complex kinetic model according to the presence of parallel and successive reactions simultaneously, as presented in Table 8.

Table 8. A simplified kinetic mechanism

Plasma-Phenol reactions		Constant rates at 298 K	Ref
DD	$^{\bullet}OH^{(g)} \xrightarrow{He_1} {}^{\bullet}OH^{(l)}$	He_1= 760	**(R 49)**
	$NO_2{}^{\bullet(g)} \xrightarrow{He_2} NO_2{}^{\bullet(l)}$	He_2= 0.3	**(R 68)**
	$C_6H_6O^{(g)} \xrightarrow{He_4} C_6H_6O^{(l)}$	He_4= 70,644	**(R 60)**
	$C_6H_6O^{(l)} + {}^{\bullet}OH^{(l)} \xrightarrow{k_5}$ Products	$K_5 = 10^7$ m^3 mol^{-1} s^{-1}	**(R 61)**
	$C_6H_6O^{(l)} + NO_2{}^{\bullet(l)} \xrightarrow{k_6}$ Products	$K_6 = 10^6$ m^3 mol^{-1} s^{-1}	**(R 62)**
STPD	$HONOO^{(g)} \xrightarrow{He_8} HONOO^{(l)}$	He_8= 2.1 10^3 mol^1 m^{-3} Pas^{-1}	**(R 63)**
	$HONOO^{(l)} \xrightarrow{k_9} NO_2^{\bullet(l)} + {}^{\bullet}OH^{(l)}$	$K_9 = 1.2\ 10^4$ m^3 mol^{-1} s^{-1}	**(R 64)**
	$C_6H_6O^{(g)} \xrightarrow{He_4} C_6H_6O^{(l)}$	He_4= 70644	**(R 60)**
	$C_6H_6O^{(l)} + {}^{\bullet}OH^{(l)} \xrightarrow{k_5}$ Products	$K_5 = 10^7$ m^3 mol^{-1} s^{-1}	**(R 61)**

Considering the mass transfer and the chemical reaction mechanism, the mathematical model of each plasma GAD configuration becomes as follows:

a) Direct discharge systems

$$\begin{cases} \dfrac{d^2\,{}^{\bullet}OH}{dX^2} = Ha^2_{({}^{\bullet}OH/Phe)}\ {}^{\bullet}OH\ Phe + Ha^2_{({}^{\bullet}OH/NO_2^{\bullet})}\ {}^{\bullet}OH\ NO_2^{\bullet} & \textbf{(Eq.35)} \\ \dfrac{d^2NO_2^{\bullet}}{dX^2} = Ha^2_{(NO_2^{\bullet}/Phe)}\ NO_2^{\bullet}\ Phe + \dfrac{Ha^2_{({}^{\bullet}OH/NO_2^{\bullet})}}{Z_{({}^{\bullet}OH/NO_2^{\bullet})}}\ {}^{\bullet}OH\ NO_2^{\bullet} & \textbf{(Eq.36)} \\ \dfrac{d^2HONOO}{dX^2} = -\dfrac{Ha^2_{({}^{\bullet}OH/NO_2^{\bullet})}}{Z_{({}^{\bullet}OH/HONOO)}}\ {}^{\bullet}OH\ NO_2^{\bullet} + Ha^2_{\left(\frac{HOONO}{Phe}\right)} HONOO\ Phe & \textbf{(Eq.37)} \\ \dfrac{d^2PHE}{dX^2} = \dfrac{Ha^2_{({}^{\bullet}OH/Phe)}}{Z_{({}^{\bullet}OH/Phe)}}\ {}^{\bullet}OH\ Phe + \dfrac{Ha^2_{(NO_2^{\bullet}/Phe)}}{Z_{(NO_2^{\bullet}/Phe)}} NO_2^{\bullet}\ Phe + \dfrac{Ha^2_{(HONOO/Phe)}}{Z_{(HONOO/Phe)}} HONOO\ Phe & \textbf{(Eq.38)} \end{cases}$$

Batch

X=0

$${}^{\bullet}OH = 1 \qquad NO_2^{\bullet} = 1 \qquad \frac{dPhe}{dX} = 0 \qquad HONOO = 0$$

X=1

$$Phe = 1 \qquad HONOO = 1$$

$$\left(\frac{d\,{}^{\bullet}OH}{dX}\right)_{X=1} = -\,{}^{\bullet}OH_S \cdot \left(R_{({}^{\bullet}OH/Phe)} + R_{({}^{\bullet}OH/NO_2^{\bullet})}\right) \qquad \textbf{(Eq.39)}$$

$$\left(\frac{dNO_2^{\bullet}}{dX}\right)_{X=1} = -NO_{2\,S}^{\bullet} \cdot \left(R_{(NO_2^{\bullet}/Phe)} + R_{(NO_2^{\bullet}/\,{}^{\bullet}OH)}\right) \qquad \textbf{(Eq.40)}$$

Failing film

X=0

$${}^{\bullet}OH = 1 \qquad NO_2^{\bullet} = 1 \qquad \frac{dPhe}{dX} = 0 \qquad HONOO = 0$$

X=1

$$Phe = 1 \qquad HONOO^{\cdot} = 1$$

$$\left(\frac{d\,{}^{\bullet}OH}{dX}\right)_{X=1} = -\,{}^{\bullet}OH_S \cdot \left(R_{({}^{\bullet}OH/Phe)} + R_{({}^{\bullet}OH/NO_2^{\bullet})} + \frac{1}{Da_{({}^{\bullet}OH)}}\right) \qquad \textbf{(Eq.41)}$$

$$\left(\frac{dNO_2^{\cdot}}{dX}\right)_{X=1} = -NO_{2\,S}^{\bullet} \cdot \left(R_{(NO_2^{\bullet}/Phe)} + R_{(NO_2^{\bullet}/\,{}^{\bullet}OH)} + \frac{1}{Da_{(NO_2^{\bullet})}}\right) \qquad \textbf{(Eq.42)}$$

Direct discharge systems like batch and failing film have the same participants' spices and the exact chemical reaction mechanism but a different circulating system. There they have an identical mathematical model in the liquid film but different boundary expression.

b) Spatiotemporal post discharge systems

Spatiotemporal post-discharge systems like Spray Tower and Venturi have the same participants' spices and mass transfer systems. There, they have an identical mathematical model in both liquid film and bulk.

$$\begin{cases} \dfrac{d^2\,{}^{\bullet}OH}{dX^2} = Ha^2_{({}^{\bullet}OH/Phe)}\ {}^{\bullet}OH\ Phe - \dfrac{Ha^2_{(HONOO)}}{Z_{(HONOO)}}\ HONOO & \textbf{(Eq.43)} \\ \dfrac{d^2 NO_2^{\bullet}}{dX^2} = -\dfrac{Ha^2_{(HONOO)}}{Z_{(NO_2^{\bullet})}}\ HONOO^{\cdot} & \textbf{(Eq.44)} \\ \dfrac{d^2 HONOO}{dX^2} = \dfrac{Ha^2_{(HONOO)}}{Z_{(HONOO)}}\ HONOO & \textbf{(Eq.45)} \\ \dfrac{d^2 PHE}{dX^2} = \dfrac{Ha^2_{({}^{\bullet}OH/Phe)}}{Z_{({}^{\bullet}OH/Phe)}}\ {}^{\bullet}OH\ Phe & \textbf{(Eq.46)} \end{cases}$$

	X=0	**X=1**	
Spray Tower & Venturi Systems	${}^{\bullet}OH = 0$	${}^{\bullet}OH = 1 \quad NO_2^{\bullet} = 1 \quad Phe = 1$	
	$NO_2^{\bullet} = 0$		
	$\dfrac{dPhe}{dX} = 0$	$\left(\dfrac{dHONOO}{dX}\right)_{X=1} = \dfrac{1}{HONOO^{*}} \cdot \left(R_{(HONOO)} + \dfrac{1}{D_{a(HONOO)}}\right)$	**(Eq.47)**
	$HONOO = 1$		

With,

$$Ha_{({}^{\bullet}OH/Phe)} = \frac{\sqrt{K_5 \cdot C_{(Phe)_S} \cdot D_{({}^{\bullet}OH)}}}{K_{L({}^{\bullet}OH)}},\ Ha_{({}^{\bullet}OH/NO_2^{\bullet})} = \frac{\sqrt{K_3 \cdot C_{(NO_2^{\bullet})^{*}} \cdot D_{({}^{\bullet}OH)}}}{K_{L({}^{\bullet}OH)}},\ Ha_{(NO_2/Phe)} = \frac{\sqrt{K_6 \cdot C_{(Phe)_S} \cdot D_{(NO_2^{\bullet})}}}{K_{L(NO_2^{\bullet})}}$$

$$Ha_{(HONOO/Phe)} = \frac{\sqrt{K_7 \cdot C_{(Phe)_S} \cdot D_{(HOONO)}}}{K_{L(HONOO)}},\ Ha_{(HONOO^{\cdot})} = \frac{\sqrt{K_9 \cdot (HONOO)^{*} \cdot D_{(HOONO)}}}{K_{L(HONOO)}}$$

$$z_{({}^{\bullet}OH/Phe)} = \frac{D_{(Phe)} \cdot C_{(Phe)s}}{\nu \cdot D_{({}^{\bullet}OH)} \cdot C_{({}^{\bullet}OH)^{*}}},\ z_{(NO_2^{\bullet}/Phe)} = \frac{D_{(Phe)} \cdot C_{(Phe)s}}{\nu \cdot D_{(NO_2^{\bullet})} \cdot C_{(NO_2^{\bullet})^{*}}},\ z_{(HONOO/Phe)} = \frac{D_{(Phe)} \cdot C_{(Phe)s}}{\nu \cdot D_{(HONOO)} \cdot C_{(HONOO)^{*}}}$$

$$z_{({}^{\bullet}OH/NO_2^{\bullet})} = \frac{D_{(NO_2^{\bullet})} \cdot C_{(NO_2^{\bullet})^{*}}}{\nu \cdot D_{({}^{\bullet}OH)} \cdot C_{({}^{\bullet}OH)^{*}}},\ z_{({}^{\bullet}OH/HOONO)} = \frac{D_{(HONOO)} \cdot C_{(HOONO)S}}{\nu \cdot D_{({}^{\bullet}OH)} \cdot C_{({}^{\bullet}OH)^{*}}},\ z_{({}^{\bullet}OH/NO_2^{\bullet})} = \frac{D_{(NO_2^{\bullet})} \cdot C_{(NO_2^{\bullet})^{*}}}{\nu \cdot D_{({}^{\bullet}OH)} \cdot C_{({}^{\bullet}OH)^{*}}}$$

$$z_{(HOONO)} = \frac{D_{({}^{\bullet}OH)}}{\nu \cdot D_{(HONOO)} \cdot C_{({}^{\bullet}OH)s}},\ z_{(NO_2^{\bullet})} = \frac{D_{(NO_2^{\bullet})} \cdot C_{(HONOO)s}}{\nu \cdot D_{(HONOO)} \cdot C_{(NO_2^{\bullet})s}}$$

$$R_{(^{\bullet}OH/Phe)} = \frac{K_5 \cdot C_{(Phe)s} \cdot \varepsilon_L}{K_{L(^{\bullet}OH)} \cdot a} = \frac{K_1 \cdot C_{(Phe)s}}{K_{L(^{\bullet}OH)} \cdot a'},\ R_{(OH\cdot/NO_2^{\bullet})} = \frac{K_3 \cdot C_{(NO_2^{\bullet})s} \cdot \varepsilon_L}{K_{L(^{\bullet}OH)} \cdot a} = \frac{K_3 \cdot C_{(NO_2^{\bullet})s}}{K_{L(^{\bullet}OH)} \cdot a'}$$

$$R_{(NO_2^{\bullet}/Phe)} = \frac{K_6 \cdot C_{(Phe)s} \cdot \varepsilon_L}{K_{L(NO_2^{\bullet})} \cdot a} = \frac{K_6 \cdot C_{(Phe)s}}{K_{L(NO_2^{\bullet})} \cdot a'},\ R_{(NO_2^{\bullet}/{}^{\bullet}OH)} = \frac{K_3 \cdot C_{(^{\bullet}OH)s} \cdot \varepsilon_L}{K_{L(NO_2^{\bullet})} \cdot a} = \frac{K_3 \cdot C_{(^{\bullet}OH)s}}{K_{L(NO_2^{\bullet})} \cdot a'}$$

$$R_{(HONOO)} = \frac{K_9 \cdot C_{(HOONO)s} \cdot \varepsilon_L}{K_{L(HONOO)} \cdot a} = \frac{K_9 \cdot C_{(HONOO)s}}{K_{L(HONOO)} \cdot a'}$$

$$D_{a(HONOO)} = K_{L(HONOO)} \cdot a \cdot \tau = K_{L(HOONO)} \cdot a \cdot \frac{V_R}{Q}$$

$$D_{a(^{\bullet}OH)} = K_{L(^{\bullet}OH)} \cdot a \cdot \tau = K_{L(^{\bullet}OH)} \cdot a \cdot \frac{V_R}{Q}$$

$$D_{a(NO_2^{\bullet})} = K_{L(NO_2^{\bullet})} \cdot a \cdot \tau = K_{L(NO_2^{\bullet})} \cdot a \cdot \frac{V_R}{Q}$$

Table 9. Plasma GAD reactive absorption parameters

Parameters	Reactor configuration				Units
	GAD-Batch	GAD-FF	GAD-ST	GAD-Venturi	
$C_{(^{\bullet}OH)^*}$	1.412	1.412	-	-	mol m^{-3}
$C_{(NO_2^{\bullet})^*}$	5.13×10^{-2}	5.13×10^{-2}	-	-	mol m^{-3}
$C_{(^{\bullet}OH)s}$	1.86×10^{-1}	8.86×10^{-2}	1×10^{-1}	1.42×10^{-1}	mol m^{-3}
$C_{(NO_2^{\bullet})s}$	1.1×10^{-5}	6×10^{-6}	9.09×10^{-5}	9.09×10^{-6}	mol m^{-3}
$C_{(HOONO)s}$	4.28×10^{-5}	1.26×10^{-5}	1.44×10^{-4}	1.44×10^{-5}	mol m^{-3}
$C_{(HOONO)^*}$			5×10^{-3}	5×10^{-3}	mol m^{-3}
$C_{(Phe)s}$	1	1	1	1	mol m^{-3}
$D_{(^{\bullet}OH)}$	2×10^{-9}				m^2 s^{-1}
$D_{(NO_2^{\bullet})}$	1.85×10^{-9}				m^2 s^{-1}
$D_{(HOONO)}$	2.6×10^{-9}				m^2 s^{-1}
$D_{(Phe)}$	1×10^{-9}				m^2 s^{-1}
K_L	1.56×10^{-6}	9.5×10^{-7}	8×10^{-7}	6×10^{-6}	m^2 s^{-1}
S	63.5×10^{-3}	1×10^{-3}	1.91×10^{-3}	9.91×10^{-3}	m^2
V_R	1.8×10^{-4}	1.8×10^{-4}	2.5×10^{-4}	2.5×10^{-4}	m^3
a	14.8	5.56	6.36	33	m^{-1}
Q	-	1.94×10^{-4}	2.5×10^{-4}	1.94×10^{-4}	m^3 s^{-1}
τ	-	1.078	30.9	30.9	s^{-1}

A calculation study was performed on key dimensional numbers like Hatta (Ha), Z, R, Ei, and damkoler (Da) obtained in the above mathematical models for each reactor prototype. Table 09 below summarizes the parameters used for the calculation study.

The dimensionless numbers explain the competition between the mass transfer and the chemical reaction processes in biphasic reactors. The Hatta number (Ha) measures the maximum

reaction rate relative to the maximum quantity passing through the film by diffusion. This dimensionless number indicates where the chemical reaction takes place. When Ha2 << 1, the rate of conversion in the film is negligible, and the reaction takes place in the volume of the liquid, which is therefore decisive; on the other hand, if Ha >> 1, the reaction takes place entirely in the film, and the interfacial area is predominant. In that case, the reaction regime is fast for Hatta greater than three (Ha > 3) and instantaneous when Hatta is more than ten times the accelerator factor more significant than (Ha > 10 Ei) [100]. The Z criterion contains the ratios of diffusivities and concentrations; the R ratio compares the maximum flow of A that could be consumed by the reaction within the liquid with the maximum flow of A that can be physically absorbed. A small value of R corresponds to a slow reaction rate of A within the reactor compared with the potential input by absorption. Ei is the instantaneous reaction acceleration factor. Da is the specific Damköhler number of the reactor; it compares the characteristic transfer time to the passage time τ defined as the ratio of the reactor volume VR to the liquid flow rate Q through it. A small value of Da means that the transfer of matter from A is slower than the passage of liquid in the reactor. Table 10 summarizes the calculated dimensionless numbers.

Table 10. Plasma GAD reactive absorption dimensionless numbers

Plasma-Phenol reactions		Ha	z	Ei	R	Da
Batch-reactor	$^{\bullet}OH/Phe$	9.07×10^{4}	3.54×10^{-1}	1.15	-	-
	$NO_2^{\bullet}/Phe$	2.76×10^{4}	1.05	2.05	-	-
	$^{\bullet}OH/NO_2^{\bullet}$	6.84×10^{4}	3.36×10^{-1}	1.34	-	-
	$HONOO/Phe$	3.65×10^{1}	9.03×10^{3}	9.03×10^{3}	-	-
	$^{\bullet}OH/HONOO$	-	3.92×10^{-5}	1.00	-	-
Failing-Film	$^{\bullet}OH/Phe$	1.49×10^{5}	3.54×10^{-1}	1.15	1.89×10^{9}	5.69×10^{-6}
	$NO_2^{\bullet}/Phe$	4.53×10^{4}	1.05	2.05	1.89×10^{8}	5.69×10^{-6}
	$^{\bullet}OH/NO_2^{\bullet}$	3.87×10^{2}	3.36×10^{-1}	1.34	1.39×10^{4}	5.69×10^{-6}
	$HONOO/Phe$	6.00×10^{1}	3.05×10^{4}	3.05×10^{4}	2.37×10^{2}	5.69×10^{-6}
	$^{\bullet}OH/HONOO$	1.49×10^{5}	1.16×10^{-5}	1.00	2.01×10^{8}	-
Spray Tower - reactor	$HONOO$	1.37×10^{4}	1.54×10^{1}	1.64×10^{1}	3.40×10^{6}	1.57×10^{-3}
	$^{\bullet}OH/Phe$	1.25×10^{5}	1.29×10^{-2}	1.01	1.58×10^{6}	1.57×10^{-3}
	$NO_2^{\bullet}$	-	7.69×10^{1}	7.79×10^{1}	-	-
Venturi	$HONOO$	1.83×10^{3}	2.18×10^{1}	2.28×10^{1}	3.03×10^{6}	1.18×10^{-2}
	$^{\bullet}OH/Phe$	1.67×10^{4}	1.29×10^{-3}	1.00	7.27×10^{3}	1.18×10^{-2}
	$NO_2^{\bullet}$	-	3.52	4.52	-	-

The calculated results shown in Table 10 are significantly higher than ordinary. Hatta numbers of each plasma reaction were found to be greater than 10 Ei for each configuration; this reflects that the chemical reactions are super instantaneous and take place in the liquid film. However, it is difficult to distinguish between the chemical reaction dualities in each configuration since there is no specific abacus for such super instantaneous processes. Therefore, plotting the concentration profiles of the chemical species participating in this process is highly recommended. The obtained mathematical system is of second-order ordinary differential equations with a lack of data on the boundary conditions, referring to practically impossible concentration measurements at liquid film boundaries. A boundary values problem method is used to solve the proposed model using MATLAB bvp4c function, where the utilization of this software of programming was necessary to perform such ODEs system with particular limit conditions as it was demonstrated in equations (iii)

A simulation algorithm used to describe the absorption reaction competition in liquid film is presented in Figure 28. The simulations were conducted to plot phenol and plasma species concentration profiles in liquid film in order to characterize the plasma phenol reaction regime.

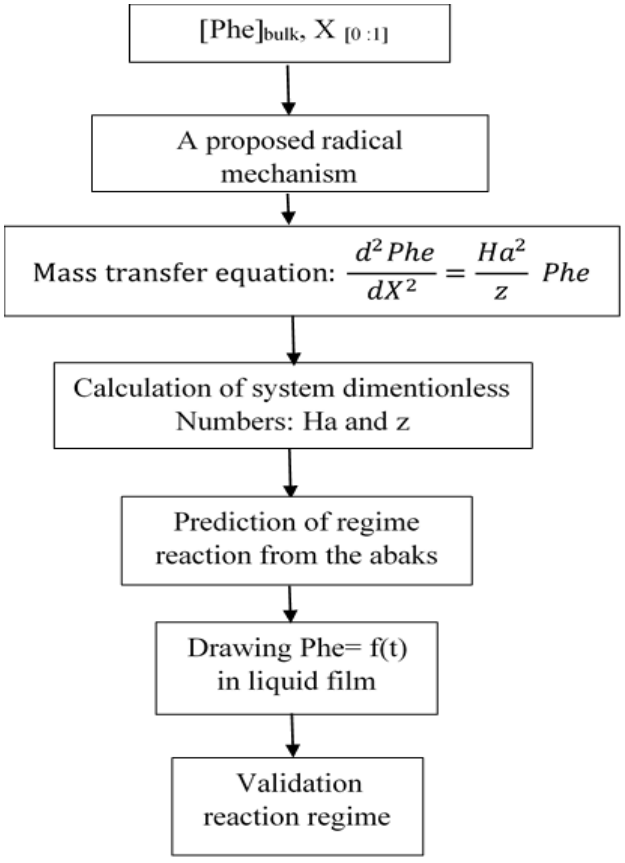

Figure 28. Simulation algorithm of plasma species concentration profiles in liquid film

The plotted concentration profiles of the process reactive entities in liquid film are presented in figure 29.

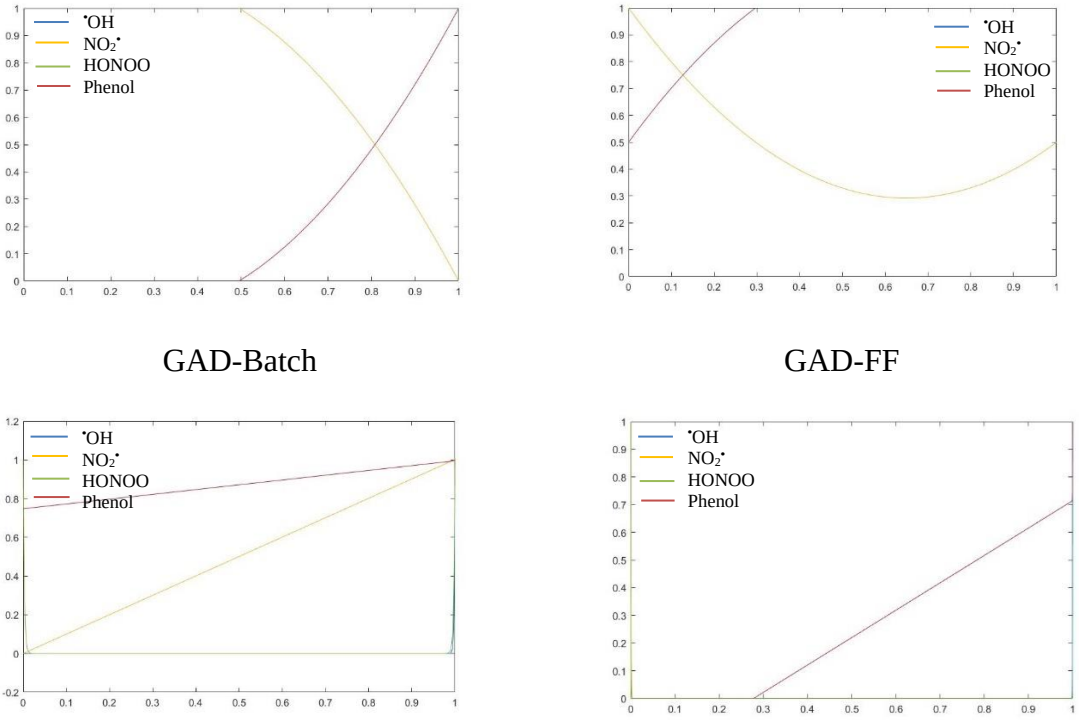

Figure 29. Reagents concentration plot in liquid film

In conventional reactions, the liquid reagent is not consumed in the film. Hence, its concentration is constant and equal to that of the liquid; the gas profile is a straight line. The process as a whole can be considered a physical absorption followed by a chemical reaction within the liquid.

In this case, the reaction is fast enough for a significant part of the absorbed gas to react in the diffusional film; the concentration profiles are no longer straight lines and are curved. The four dimensionless numbers R, Da, Ha, and Z play a role; there is no simple solution. We can see that the dissolved gas concentration in the liquid CAS depends on the hydrodynamics and the liquid retention in the reactor. In this domain, the influence of the interfacial area on the conversion rate begins to outweigh that of the liquid retention.

2.2 Chemical properties

Atmospheric GAD configurations such as Batch, Falling Film, Spray Tower, and Venturi exhibit different chemical properties in the treated liquid, including pH, conductivity, nitrite and nitrate concentrations, and plasma (RONS). These variations arise due to differences in the physical setup operational mechanisms and to the distinct populations of reactive species generated in each configuration.

2.2.1 pH

The acidity of the reactive medium plays a crucial role in term of homogenous catalysis especially for oxidative reactions. Therefore, a pH analysis is conducted in the four plasma GAD prototypes. Figure 30 present the obtained results.

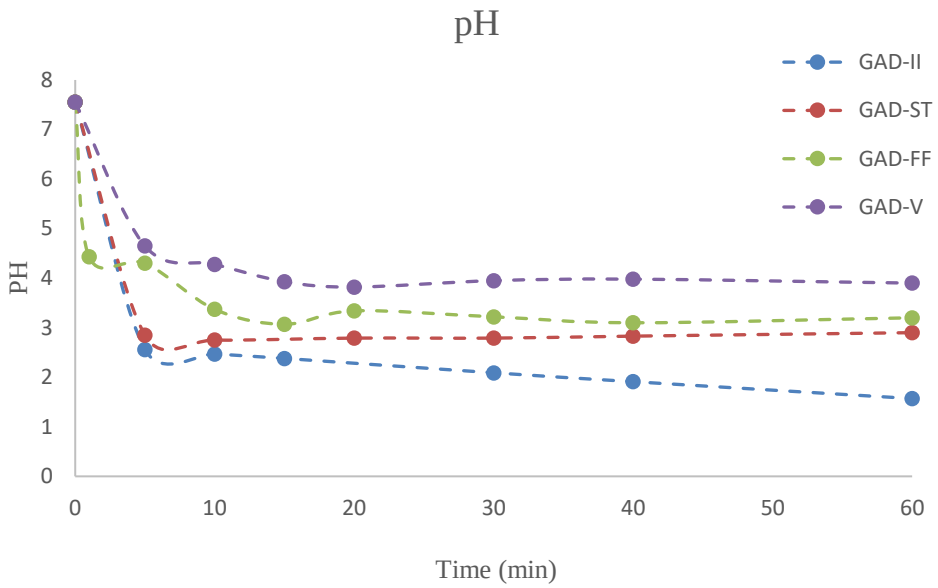

Figure 30. pH evolution in plasma GAD reactors

The acidity in such reactors varies due to the distinct gas-liquid interaction way for each configuration and absorbed reactive species. The pH analysis shows that the outlined reactors offer an acidic medium with uneven pH. The Batch one presents the highest acidity with a PH around 2 degrees due to direct and intense interaction with short-lived reactive species. Whereas GAD-VNT presents an acidic medium with a pH of 4 degrees and around 3 degrees acidic medium for both the spray tower and the failing film reactors. Which refers to the diffusion of long-lived species and the gas-liquid transferred flow.

Generally, the mass-transferred properties influence the acidity of the treated water. Therefore, each GAD prototype offered different acidity levels. The batch reactor medium remains the most acidic according to its effective plasma-liquid interaction.

2.2.2 Plasma dose

Plasma dose remains a crucial factor in evaluating plasma reactors; it measures the amount of reactive species generated and their impact on the treated liquid. It can be effectively evaluated through measurements of conductivity and total oxidative species (RONS).

2.2.2.1 Conductivity

The conductivity is directly related to the concentration of ions in aqueous solution. Therefore, it can be a significant indirect method to evaluate the plasma dose in the treated solution, such as the higher measured conductivity, the more absorbed plasma species. Figure 31 presents the evolution of the conductivity in plasma GAD reactors.

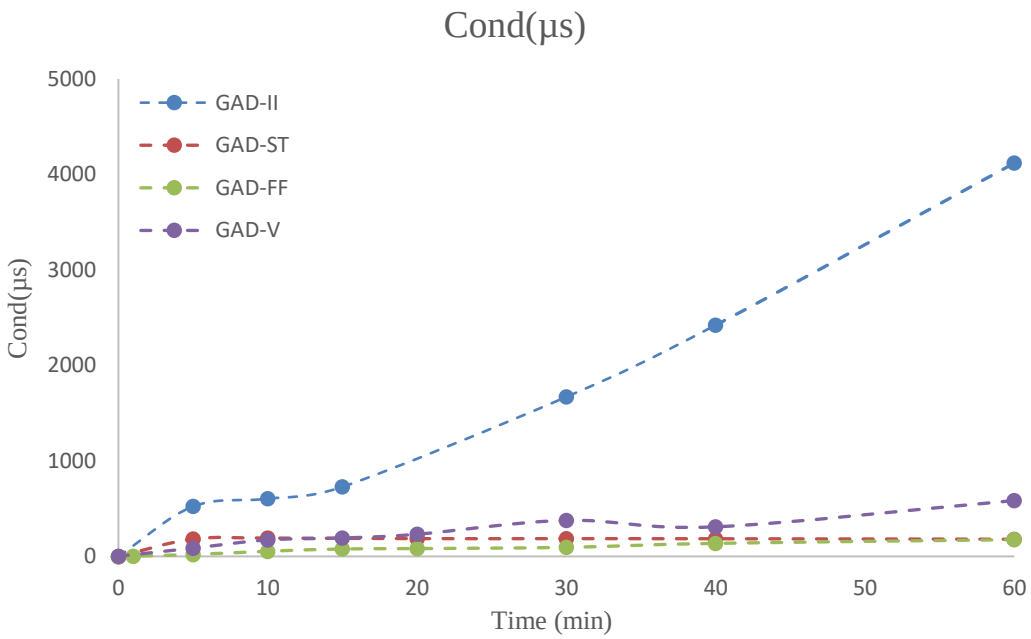

Figure 31. Conductivity evolution in plasma GAD reactors

Conductivity notices that GAD-ST and VNT present the same final conductivity after 60 min exposure time. However, the GAD-ST shows a rapid conductivity increase compared to the situation in facility ng film. This can be explained by an improved liquid-gas contact, which facilitates the transfer flow. The GAD-VNT and Batch show higher conductivity due to their high gas-liquid surface areas. The batch reactor presents the highest conductivity with a considerable difference.

2.2.2.2 Total oxidative species (RONS)

Total oxidative species measurement is more credible method for the evaluation of plasma dose since plasma reactions are oxidative processes. Non thermal plasma generates reactive oxygen and nitrogen species such as ozone (O_3), hydrogen peroxide (H_2O_2), hydroxyl radicals ($^{\bullet}OH$), azote dioxide ($^{\bullet}NO_2$) and peroxynitrite (HONOO) directly assess the oxidative capacity of the plasma.

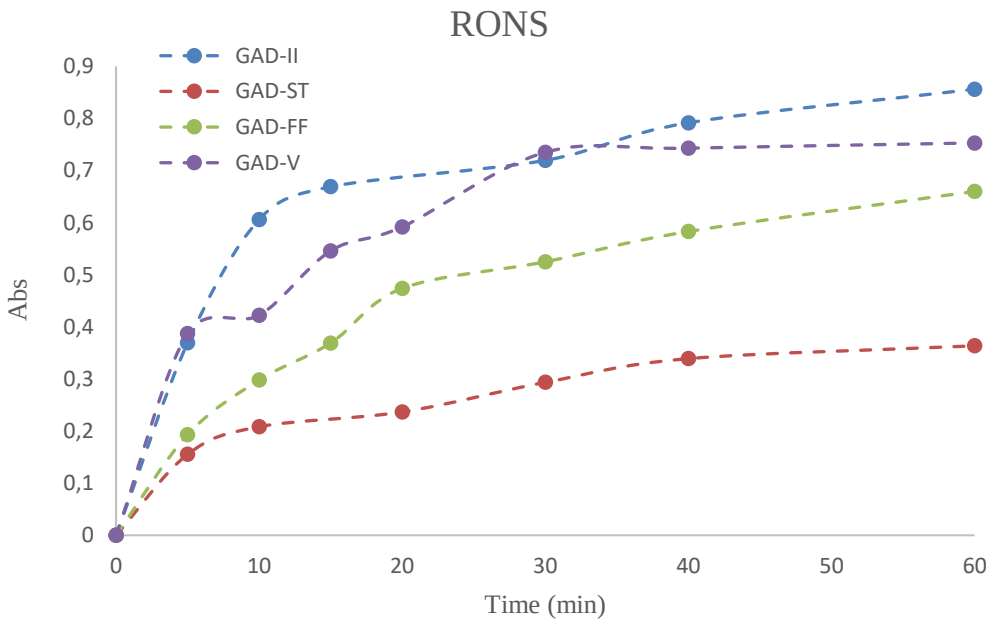

Figure 32. The evolution of total oxidative species in plasma GAD reactors

According to Figure 32, which represents the evolution of total oxidative species as a function of time in the four configurations of plasma gliding arc discharge, the batch reactor presents the highest quantity of the total oxidative species due to the intense mass transfer of highly reactive species. The venturi, characterized by high-speed gas flow and intense turbulence, promotes vigorous mixing and efficient mass transfer, resulting in high concentrations of oxidative molecules relatively close to those presented by the batch reactor. The GAD-Failing Film shows a moderate result, whereas the spray tower configuration shows less transferred oxidative species quantity.

In summary, by evaluating both conductivity and total oxidative species analysis, we conclude that the batch reactor has the highest plasma transferred dose flowed by venturi, failing film, and spray tower reactors. This uneven dose is responsible for the plasma GAD efficiency regarding reactivity and conversion rate. Remarkably, the batch and venturi configurations slightly differ in the measured RONS. In contrast, the batch reactor presents an enormously

high conductivity due to more charged species but less reactive ones. Contrary to the previous feature, the failing film shows an equal conductivity of the spray tower at 60 min of functioning time but a higher total oxidative power; this later goes back to the difference in plasma transferred population, such as the filing film presents a more reactive entity called short-lived species, while the spray tower presents more stable molecules known as long-lived species.

2.2.3 Nitrites and nitrates analysis

Atmospheric GAD plasma using air as the driven gas led to the formation of reactive nitrogen species which in liquid region convert to nitrite and nitrate ions as more stable molecules. Figure 33 present the evolution of both nitrite and nitrates concentrations in plasma GAD reactors.

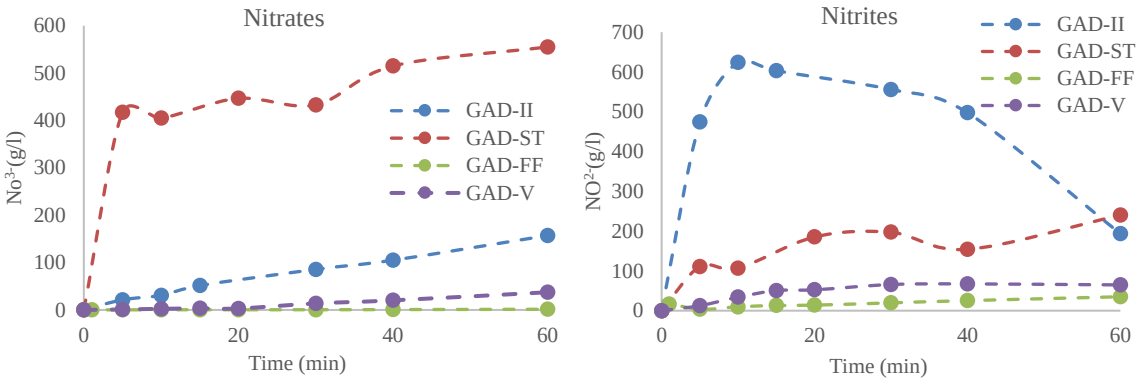

Figure 33. Nitrite and nitrates evolution concentrations in plasma GAD reactors

The plotted results in Figure 33 show that the batch configuration presents a high and fast increase in nitrite concentration of about 624 g L^{-1} for the first 10 min and starts to decrease to 193 g L^{-1} at 60 min treatment time; this is followed by a linear increase of nitrate concentration which reached 157 g L^{-1} in 60 min that can be explained by the continuous conversion of nitrites on nitrates as a more stable molecule. The GAD-ST shows a moderate nitrite concentration but an enormous higher nitrate concentration that reached 555.14 g L^{-1} even though it presents a low concentration of total oxidative species; this is explained by the fact that the spatiotemporal post-discharge presents more stable molecules than the direct discharge. The venturi and failing film show slight quantities of nitrite and nitrate ions according to their specific mass transfer and chemical conditions.

The unique chemical properties of each plasma GAD configuration for aqueous solution treatment, such as Batch, Falling Film, Spray Tower, and Venturi, vary significantly according to their unique interaction dynamics and reactive species.

In summary, all of the outlined configurations offer an acidic medium with a relatively uneven pH degree that refers to the uneven absorbed plasma species population and quantity. The Batch and Venturi configurations typically produce the highest plasma dose, showing a high conductivity and RONS concentration reflecting their high mass transfer coefficient and gas-liquid interface area. Meanwhile, the spray tower and failing film configurations provide moderate to significant plasma dose and acidity values. The lowest measured plasma dose for GAD-ST, followed by the highest concentration of nitrate ions, explains the fact that spatiotemporal post-discharge offers more stable molecules than direct discharge. For GAD-VNT, the efficient mixing in a high-speed flow environment allows a substantial transfer of reactive species when compared to the GAD-ST, where the spraying system allows only the molecules having the strong Henry's constant to be absorbed. It is important to notice that peroxynitrite has a higher Henry constant than the short-lived spices; this later converts easily in water to nitrate ions [26, 131].

3. Plasma GAD performances

The physicochemical properties discussed in the previous section exhibit unique performances for each plasma gliding arc reactor, such as conversion rates, selectivity, pollutant degradation, and dye decolorization. The analysis of the outlined performances remains a significant tool for the choice of the right configuration for the right process operation.

3.1 Depollution

In this part, an evaluation of depollution efficiency is conducted in order to select the appropriate configuration for a pollutant removal process. Phenol and Acid Green 25 (AG25) were chosen as a typical pollutant due to their distinct properties; where phenol is uncolor and partially dissolved in water, while AG25 is highly soluble and has a visible colored.

3.1.1 Decolorizarion

Green Acid 25 (AG25) is an anthraquinonic dye (Figure 34) called Toluennesulfonic acid, 6, 6'-(1, 4-Anthraquinonylenemino) disodium salt [132]. This class of dyes is characterized by a C-O binding and remains the second class of dyes used in the industry after azoic dyes. The basic formula derived from anthracene shows that the chromophore is a quinone ring to which hydroxyl or amine groups can be attached. It has a maximum wave length at 643 nm.

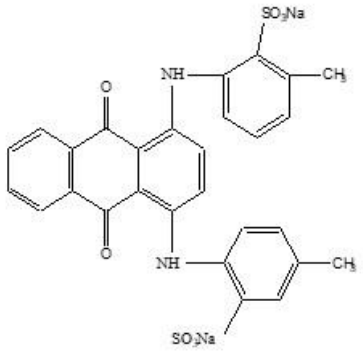

Figure 34. A semi-developed structure of the AG25

The discoloration process of AG25 (C= 80µM) using plasma GAD reactors involves breaking down the coloring functional groups through interactions with reactive plasma species dissolved in the treated aqueous solution.

The general degradation mechanism of green acid 25 was proposed by Ferhat et al. (2021). This mechanism is initiated by a discoloration process presented in Figure 35, where the hydroxyl radicals directly transferred from the plasma plum to the AG25 solution in direct discharge or being produced from the decomposition of peroxynitrite in indirect discharge, attack the unsaturated bonds in AG25 structure like C-N bound which connect the chromophore groups to the main molecule (anthracene 9.10 dione). The cleavage of this bound incorporates the detachment of the methyl benzene sulphonic acid molecule followed by the detachment of SO3-, demethylation of the benzenic ring, and insertion of hydroxyl radicals responsible for the color changing to a dark brown, then uncolored AG25 treated solution.

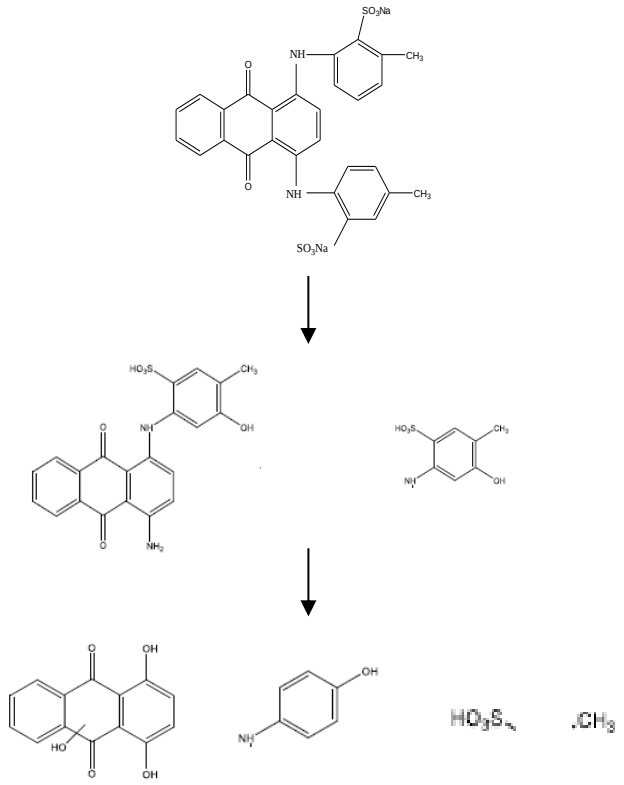

Figure 35. A semi-developed structure of the AG25

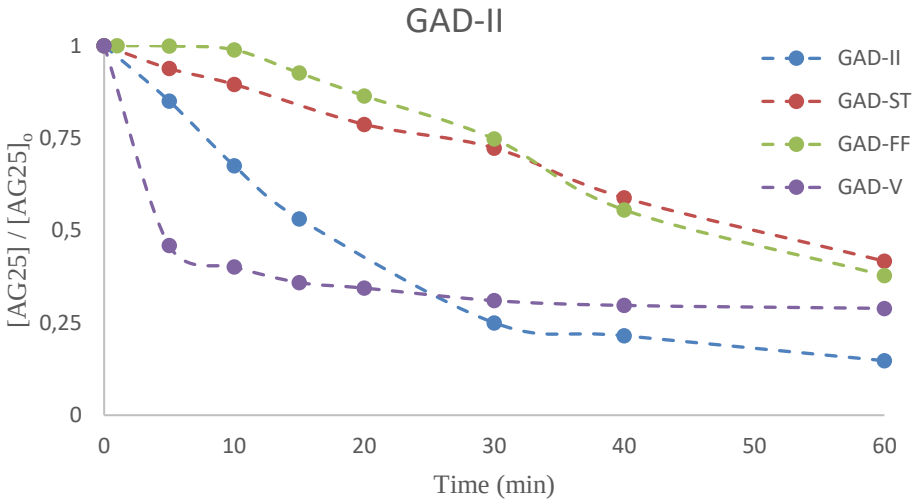

Figure 36. A semi-developed structure of the AG25

Figure 36 shows different discoloration patterns of the AG25 in different configurations. The GAD-VNT presents a faster discoloration process in the first 25 min, even if it does not have the highest plasma amount, which is explained by a fast and efficient plasma species interaction with the treated dye. This is ensured by the high-speed flow of plasma reactive species and the high affinity to the AG25 coloring functional groups. After 25 min treatment time, it shows a

discoloration steady state, and the Batch system remains the most intense decolorating process by the presence of more short-lived species, while its rapidity compared to the venturi process refers to the lower mass transfer properties and the presence of parasite reactions ensured by electrons and UV lights. This is confirmed by discussing the AG25 discoloration patterns in both spray tower and failing film configurations, which present lower plasma transferred flows. The failing film system presents a slower decolorating process, but it becomes more effective than the spray tower after 35 min plasma exposition time for the same reason of transferred plasma population.

3.1.2 Mineralization

Most of waste water pollutants are a phenolic compound with different chemical structure association. Therefore, phenol (C=1Mm) was chosen as the pollutant model in order to determine the effectiveness of plasma GAD reactors to demineralize uncolor and non-biodegradable pollutants, COT analyzer is used to determine the final demineralization rate.

Figure 37 presents the proposed demineralization mechanism inspired by Ferhat's announced process for spatiotemporal discharge [105]. The demineralization mechanism of phenol in plasma GAD reactors involves complex mechanisms driven by interactions with reactive plasma species. This process ultimately converts organic phenol molecules into inorganic carbon (CO_2) and water (H_2O). It starts with a simple oxidation of phenol interacting with hydroxyl and nitrogen dioxide radicals. This action led to the formation of less toxic phenolic derivatives that are easily demineralized. The continuous interaction of plasma reactive species on the formed phenolic derivatives leads to the breakdown of the aromatic ring of phenol and the forming of simple, intermediate compounds. Breaking down the aromatic ring of phenol and forming intermediate compounds. These intermediates are further oxidized into organic carbon (CO_2) and water (H_2O).

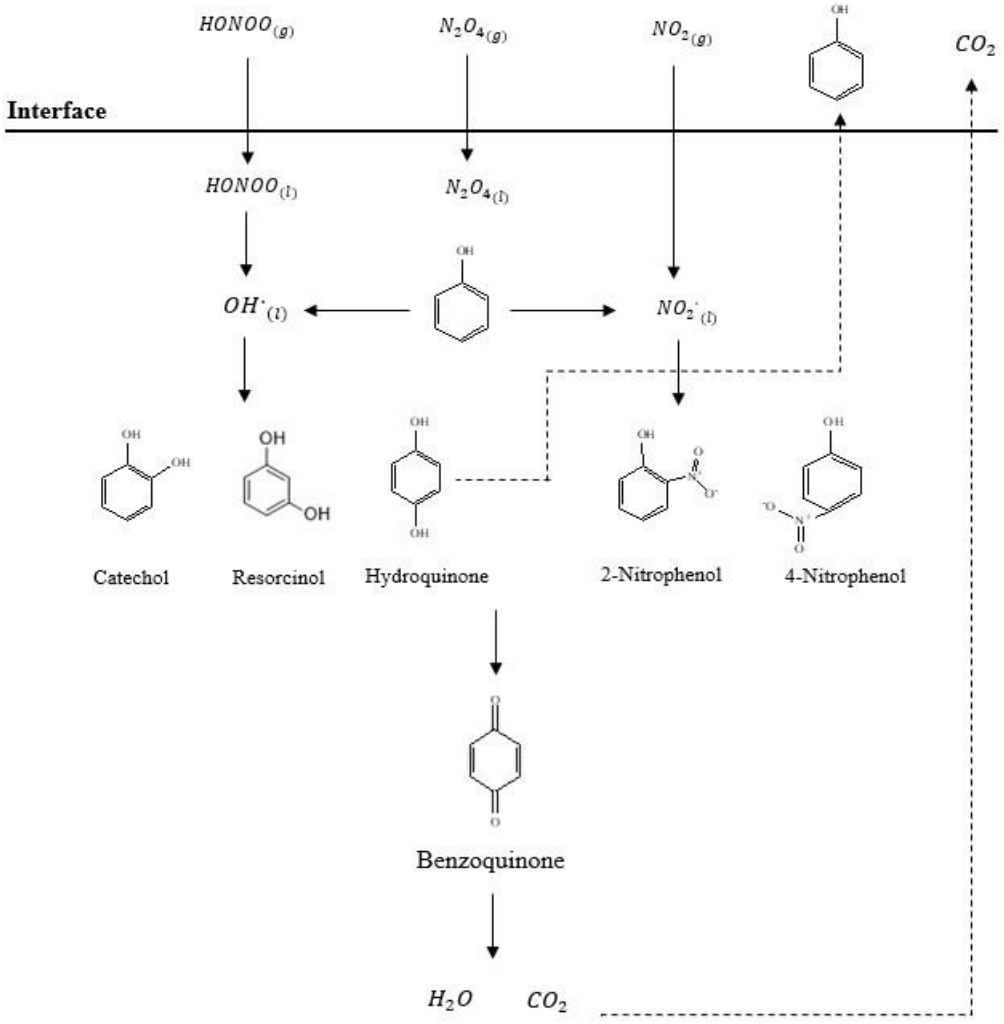

Figure 37. Phenol demineralization mechanism in STPD plasma treatment

Table 11 present the total organic carbon of the treated phenol solutions using different plasma GAD reactors. The initial phenol concentration was 0.001 mol L^{-1}, and the treatment time was consistently set at 60 minutes for all configurations. The initial TOC value for all configurations was 60.80 mg L^{-1}.

Table 11. Demineralization rate of phenol in plasma GAD reactors

GAD-Configuration	V (Cm^3)	Phenol concentration (M)	Treatment time (min)	Initial COT	Final COT	Deminiralization rate (%)
Batch	430	0.001	60	60.80	33.38	45.10
Failing film	180	0.001	60	60.80	51.54	15.23
Spray tower	300	0.001	60	60.80	53.84	11.45
Venturi	300	0.001	60	60.80	48.96	17.83

The unique characteristics of each configuration, such as mass transfer, acidity, and oxidizing power, determine the overall effectiveness of the phenol demineralization process. The batch reactor demonstrates the highest effectiveness of phenol breaking down into inorganic molecules with a demineralization rate of 45.10%, which refers to the direct and intense interaction of plasma reactive species with phenol molecules. The Venturi configuration achieved a demineralization rate of 17.83%, higher than those obtained by failing film and spray tower configurations of 15.23% and 11.45%, respectively. The high-speed gas flow and turbulence in the Venturi arrangement enhance reactive species mixing and mass transfer, which leads to the effective breaking down of phenol molecules. The less intense interaction in failing film and the low reactive species absorbed in spray tower configurations lead to less effective demineralization processes with a final total organic carbon of 53.84 and 51.54 g L^{-1}, respectively.
In such reactor processes, the overall efficiency of the demineralization process is mainly dependent on the strength of the interaction between the liquid and plasma species as well as configuration-specific dynamics. These findings emphasize how crucial it is to choose the best GAD design according to the particular objectives and expected effects of the treatment.

3.2 Chemical synthesis

Chemical synthesis using nonthermal plasma reactors is an advanced field, where plasma is an innovative solution to some synthesis process limitations such as conversion rates, Eco-friendship, and operational costs. The first instances of organic synthesis using plasma were carried out by introducing organic compounds in the gas phase into the discharge [133-136]. Remaining in the gas phase has limited the material involved in the conversions. Therefore, recent works have used biphasic plasma reactors for liquid chemical synthesis to provide better operational conditions and process performances [46, 67, 68, 128].
The unique properties of the nonthermal plasma reactors allow them to facilitate some complex synthesis processes without adding chemical products. The use of electricity and air gas as the principal raw materials for plasma production and the process sureness ensured by the high reactivity shown in these reactors could, therefore, be a step toward "green" chemistry [67, 137-139]. The operational conditions of such reactors, like atmospheric pressure and ambient temperature, reduce the need for costly installations or energy for heating, which in turn makes it economically beneficial. Many applications combine plasma and catalysis processes due to the UV lights generated from the plasma plum; this combination is known as the plasma catalysis process. However, in some cases, plasma can act as a catalyst, where the generated plasma species initiate some conventional processes [30, 91]. In addition, the high acidity offered by

such reactors plays a role in the homogenized catalysis process of the oxidative reactions. These advantages involve new reaction pathways and simplify conventional complex synthesis protocols.

In the study, phenol was chosen as an aqueous substrate model to evaluate the hydroxylation process in different plasma GAD configurations. This reaction is also industrially important for the manufacturing processes of synthetic catechol and pharmaceutical compounds. The evaluation is based on phenol conversion rate and catechol production selectivity.

3.2.1 Conversion

The conversion rate is a critical parameter in evaluating the chemical reactor's efficiency. Thereby, the phenol conversion rate in different plasma GAD reactors is measured using high-performance liquid chromatography analysis.

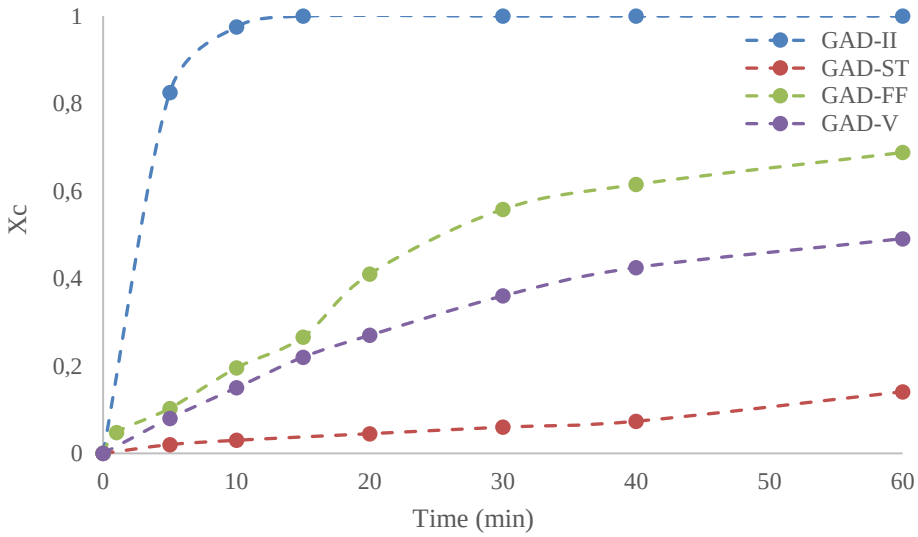

Figure 38. The evolution of phenol conversion rate in different plasma GAD configurations

Figure 38 shows the kinetic evolution of the phenol conversion rate in Batch, Falling Film, Spray Tower, and Venturi prototypes. The conversion rate varies significantly from one configuration to another.

The Batch configuration (GAD-II) has the highest efficiency, with fast and complete phenol conversion in the first ten minutes due to intensive contact with plasma reactive species. The Falling Film configuration (GAD-FF) also achieves complete conversion, although it takes approximately 30 minutes, indicating a regular and prolonged engagement with reactive species. The Spray Tower (GAD-ST) arrangement is the least effective, achieving a conversion rate of 20% after 60 minutes, most likely because of the dispersed droplets that reduce the intensity of engagement and the participant's lower reactive species. In contrast, the Venturi configuration

(GAD-V) presents a moderate efficiency, increasing on a regular basis to achieve a conversion rate of 60% in 60 minutes, thanks to improved mixing and turbulence.

In summary, the Batch and Falling Film configurations are the most effective for a quick and complete conversion of phenol, while the Venturi configuration provides an even performance with a moderate level of effectiveness. Despite being less effective, the Spray Tower structure may nevertheless be useful in applications that call for more substantial volumes or gentler circumstances.

3.2.2 Phenol by-Product selectivity

The plasma reactive species are themselves competitive and react together with phenol substrate in a parallel reaction mechanism, which make it very important to determine the production selectivity in order to evaluate the chemical performances of such as reactors.

Table 12. Phenol by-products selectivity

GAD-configuration	Oxydation phenol by-Product selectivity				Nitration phenol by-Product selectivity	
	Catechol	Hydroquinone	Resorcin	p-Benzoquinone	2-nitrophenol	4-nitrophenol
Batch	51.84%	15.59%	8.71%	18.81%	2.98%	1.97%
Falling Film	65.21%	9.32%	6.82%	11.78%	2.61%	2.26%
Spray Tower	81.60%	9.82%	0.00%	0.00%	5.23%	3.35%
Venturi	97.60%	0.61%	0.03%	1.21%	0.11%	0.44%

Table 12 illustrates the selectivity production of phenol derivatives in different plasma GAD configurations. In the batch reactor, catechol emerged as the predominant byproduct, followed by hydroquinone, with a selectivity of 51.84% and 15.59%, respectively. The direct discharge presented by this configuration ensured high concentrations of hydroxyl radicals, favoring the formation of these dihydroxybenzenes. The formation of nitrophenols was comparatively lower in this configuration. The venturi reactor showed a high selectivity towards catechol production. The intense mixing of plasma reactive with phenol molecules in the absence of electrons and UV lights provides a consistent and controllable production of catechol with a minimal concentration of nitrophenols. Catechol was the major byproduct, accounting for approximately 97.60% of the total byproducts. However, the plasma Falling Film reactor demonstrated a balanced selectivity towards hydroquinone, resorcinol, and catechol. Catechol accounted for 65.21% of the byproducts, with hydroquinone and resorcinol following at 9.32% and 6.82%. Different reaction routes were limited by the absorption process of the participant plasma reagents. The spray tower reactor demonstrated a distinct selectivity profile. Catechol

is always the major byproduct. However, higher concentrations of nitrophenols were measured compared to the other configurations. Catechol represents 81.60% of the byproducts, while 2-nitrophenol makes up 5.23%. The droplet system controlled the absorption process of plasma reactive species, providing lower mass transfer resistances to nitrogen reactive species, proved by higher concentrations of nitrite and nitrates. This favor explains the formation of more nitrophenols.

In conclusion, the venturi configuration is the most effective for achieving high selectivity towards catechol synthesis, making it preferable to be proposed for chemical production processes. The failing film and the Batch configurations provide a balanced approach, while the Spray Tower configuration may be suitable for processes where nitrophenols are of equal importance to hydroxylating byproducts. Understanding these selectivity profiles helps optimize the use of Plasma GAD reactors for specific chemical industrial applications.

3.3 Security

With the aim of integrating plasma reactors into industrial processes, safety analysis is one of the most important aspects to be studied. Therefore, the Hazard Operability Method (HAZOP) and safety integrity level (SIL) are used respectively to identify and assess the risks present in the studied configurations. These studies are rigorous procedures where the HAZOP study is designed to determine how a process can deviate from its design intent [140], while the SIL study assesses the potential for malfunction of individual pieces of new or existing equipment and the indirect effects on the installation as a whole. Both HAZOP and SIL are teamwork studies conducted in meeting sessions and directed by the chairman. The team has to be multidisciplinary, and the members must have sufficient experience and knowledge of the process. The conduction of these methods consists of using guidelines (such as not, more, less, etc.) in conjunction with process parameters (such as temperature, debit, pressure, etc.) to identify deviations (such as a higher temperature or lower debit) from the intended course of the process or normal operation. Keyword + Parameter = Deviation [141], and 04th classification levels of the risk potential from the safer class to the risky one nominated from SIL1 to SIL4, respectively [142]. The procedure is applied in a particular node as a component of the system that is defined by a nominal intention of the operational parameters. Once the deviations have been determined, the professional team looks into all potential causes and their effects and comes out with a final classification of the identified risks and a recommendation list [143].

In this section, HAZOP and SIL studies are conducted using Hazop+ 7.0 software to assess the risks involved in the four plasma glider topologies. Since they are complementary studies,

Hazop+ 7.0 software provides a directly combined study called HAZOP-SIL to a fast and restricted study. This later converts directly the gravity and the probability of the identified risk to a safety classification level.

Table 123 presents the HAZOP-SIL study worksheet resuming the identified deviations, risk levels, and the agreed recommendations. The studied plasma GAD reactors work at atmospheric pressure; however, since they are powered by a continuous air gas flow, the probability of high-pressure Deviation increases with respect to the feeding gas flow, especially for the closed systems like the batch one and to a lesser extent the spray tower and Venturi systems in case of plasma gas pipeline obstruction of which were classified as SIL4, SIL1 and SIL2 respectively, while this Deviation have no possibility in totally open systems like the Failing film configuration. The higher pressure in the batch configuration promotes a reactor crack to a fatal explosion in the worst cases. Therefore, it is highly recommended that an automatic valve be installed to maintain constant pressure. This Deviation can be caused by a faulty gas flow valve and result in a high pressure and gas leak, which in turn can cause reactor explosion and occupational disease for the operator for a long exposure time.

The feeding gas passes through two electrodes connected by a 9000 volt and 30 mA electric arc; these electrical conditions are highly dangerous and can cause serious injury to death in case of touching uncovered electric wire as both human and operating risk, this Deviation has is classified as SIL4 in both batch and failing film reactors, while it is of a 2nd level (SIL2) for venturi and spray tower ones as the operating part of the reactor is far enough from the electrical part.

The contact between the air and the electric arc creates a plasma plum containing highly reactive, dangerous, and toxic free radicals. Since plasma reactions are of an exothermic behaviour, plasma GAD reactors are usually assisted by a cooling system to control the operating temperature; however, a faulty cooling system scenario promotes a high-temperature deviation that lowers the reactor performances by increasing striping phenomena and promotes reverse reactions, as well as inducing installation cracks and corrosion, this scenario has an acceptable safety level (SIL2) for the all configurations except the failing film which present a third safety integrity level (SIL3) according the absence of the cooling system.

Several studies have identified UV lights generated from plasma plum and proposed an interactive process known as plasma catalysis to provide a higher chemical performance of the plasma GAD reactors. However, from a safety point of view, these UV lights are harmful to the operator's health and cause occupational disease, as well as the inhalation of plasma gas

caused by the gas leak. The safety integrity level of these deviations differs from unacceptable (SIL3 & SIL4) for the batch and the failing film to an acceptable level (SIL2) for spray tower and venturi configurations, according to the fairness of the plasma source even though the HAZOP-SIL team recommends installing the plasma source in a closed dark room.

According to the user's experience, reverse flow deviation can take place only in the Venturi configuration even if it has an acceptable safety level and a low-cost ranking; it is caused by low pressure in the plasma tank and results in faulty operating conditions and lower performances. Furthermore, the use of highly volatile and dangerous compounds at a certain additional condition (contact with an electric arc, concentration, pressure, temperature) for chemical synthesis can lead to a fatal explosion, especially for direct treatment systems like the batch and the failing film configurations. There for it is preferable to use indirect systems like Venturi and ST as they present a sufficient distance between the electric arc and the treated solution. In conclusion, the venturi configuration is the most effective for achieving high selectivity towards catechol synthesis, making it preferable to be proposed for chemical production processes. The failing film and the Batch configurations provide a balanced approach, while the Spray Tower configuration may be suitable for processes where nitrophenols are of equal importance to hydroxylating by-products. Understanding these selectivity profiles helps optimize the use of Plasma GAD reactors for specific chemical industrial applications.

Table 13. HAZOP-SIL evaluation table

Hazop Description: Identification and classification of hazard risk in plasma GAD reactors.		Hazop Location: Abdelhamid Ibn Badis University		Comments:			
Session: GAD reactors		Node: 1. GAD-II / FF / ST / VNT		Deviation: 4. All			
Chairman: Bilal BELMEKKI PhD student at STEVA laboratory				Secretary:			
GAD- configuration	Deviations	Likelihood	SIL Level	Severity	Causes	Consequences	Cost Ranking	Actions Completion date: Sunday 7 juillet 2024, Priority: Medium Responsible person: STEVA laboratory - PhD student Bilal BELMEKKI
Batch	Higher Temperature	Occasional	SIL 2	High	1. Faulty cooling system	1. Increasing streeping phenomena of the target substrate. 2. Revers system for an exotermic reaction	High	3. Install a high temperature alarm
	Higher Pressure	Frequent	SIL 4	Critical	1. A closed operating reactor 2. High inlet gas flow	1. Explosion of GAD reactor 2. Gas leak	Unacceptable	2. Install an automatic valve to maintain a constant pressure
	Gas Leak	Probable	SIL 3	High	1. High pressur in GAD reactor 2. High inlet gas flow 3. The presence of cracks in reactor and pipe lines	1. Occupational disease 2. Low performances	High	4. Install an alarm assisted with shutdown system
	UV Lights	Frequent	SIL 4	High	1. Normal reactor operating conditions	1. Occupational disease	Unacceptable	6. Install the GAD reactor in a closed room
	High Voltage	Frequent	SIL 4	Critical	1. Normal reactor operating conditions	1. Serious injury to death	Unacceptable	7. Set a safe operating protocol
Failing Film	Higher Temperature	Probable	SIL 3	Moderate	1. Absence of cooling system	1. Increasing the stripping process 2. Reverse process in case of exothermic reaction	Medium	3. Install a cooling system

	Gas Leak	Frequent	SIL 4	High	1. Open system (Normal reactor operating conditions)	1. Occupational disease	Unacceptable	4. Install an alarm assisted with shutdown system
	UV Lights	Frequent	SIL 4	High	1. Normal reactor operating conditions	1. Occupational disease	Unacceptable	6. Install the GAD in a closed room
	High Voltage	Frequent	SIL 4	Critical	1. Normal reactor operating conditions	1. Serious injury to death	Unacceptable	7. Set a safe operating protocol
Spray Tower	Higher Temperature	Occasional	SIL 2	High	1. Faulty cooling system	1. Reactor glass crack	High	3. Install a high temperature alarm
	Higher Pressure	Remote	SIL 1	High	1. Gaz outlet obstruction	1. Explosion of GAD reactor	Medium	2. Install an automatic valve to maintain a constant pressure
	Gas Leak	Occasional	SIL 2	High	1. High pressure in GAD reactor 2. Hole in gas pipe line	1. Occupational disease	High	4. Install an alarm assisted with shutdown system
	Reverse Flow	Remote	SIL 1	Moderate	1. Low pressure in GAD reactor 2. Gas leak	1. Faulty operating conditions Low performances	Low	
	UV Lights	Probable	SIL 3	Moderate	1. Normal reactor operating conditions	1. Occupational disease	Medium	6. Install the GAD in a closed room
	High Voltage	Remote	SIL 2	Critical	1. Normal reactor operating conditions	1. Serious injury to death	High	7. Set a safe operating protocol
Venturi	Higher Temperature	Occasional	SIL 2	High	1. Faulty cooling system	1. Reactor glass crack	High	3. Install a high temperature alarm
	Higher Pressure	Occasional	SIL 2	High	1. Gaz outlet obstruction	1. Explosion of GAD reactor	High	2. Install an automatic valve to maintain a constant pressure
	Gas Leak	Occasional	SIL 2	High	1. High pressure in GAD reactor	1. Occupational disease	High	4. Install an alarm assisted with shutdown system
	Reverse Flow	Occasional	SIL 2	Moderate	3. Low pressure in GAD reactor 4. Gas leak	2. Faulty operating conditions 3. Low performances	Low	

	UV Lights	Probable	SIL 3	Moderate	1. Normal reactor operating conditions	1. Occupational disease	Medium	6. Install the GAD in a closed room
	High Voltage	Remote	SIL 2	Critical	1. Normal reactor operating conditions	1. Serious injury to death	High	7. Set a safe operating protocol

In conclusion, the findings of this HAZOP-SIL study emphasize the importance of rigorous safety assessments in plasma GAD reactors according to the risks identified in each configuration. In this study, it was found that the spatiotemporal post-discharge configurations like spray tower and Venturi systems present a safer operability condition with an average of SIL1.83 and SIL 2,17, respectively, according to the open flowrate and the isolating distance between the plasma source and the operable part of the reactor. The GAD-Batch shows a lower safety condition with an average of SIL3.4, referring to the closed system. At the same time, the failing film remains the most dangerous system with an unacceptable safety level of an average of SIL3.75 with respect to uncontrolled plasma gas, uncovered electrodes, no cooling system, and too close a plasma source to the operating side. The HAZOP-SIL team proposed several recommendations, including installing an automatic valve, alarm, and shutdown system for high pressure and gas leaks; installing the plasma tank in a closed room to eliminate the exposition to the plasma UV-lights and setting an operating protocol to avoid the high voltage electrical choc. The recommendations derived from this analysis are vital to minimize the identified operability hazards.

Conclusion

The classification of the batch, Failing Film, Spray Tower, and Venturi configurations highlights the versatility and adaptability of the oxidative processes in various applications. Each configuration presents unique advantages and challenges, influencing factors such as reaction kinetics, mass transfer, efficiency, environmental compatibility, and operational safety.

The Batch and Venturi configurations are especially noteworthy for producing the highest plasma dosages, which reflects their effective mixing system and indicates their high conductivity and concentration in reactive oxygen and azote species (RONS). This is mostly due to their favorable mass transfer coefficients and substantial gas-liquid interfacial zones. These characteristics make them especially useful for processes that call for quick conversions, such as pollutant degradation and catechol synthesis.

In contrast, the Spray Tower and Falling Film configurations yield moderate to significant levels of plasma dose and acidity, indicating their potential effectiveness in different scenarios. Notably, the GAD-Spray Tower configuration presents the lowest measured plasma dose, accompanied by the highest concentration of nitrate ions. This discrepancy is attributed to the more stable molecules formed via spatiotemporal post-discharge processes and the spraying mechanism that enables the absorption primarily of molecules with higher Henry's constants. This characteristic allows for effective treatment of larger volumes, albeit with reduced efficiency compared to the Batch and Venturi systems. The Falling Film configuration presents moderate efficiency and offers unique advantages in specific scenarios where controlled reactions are necessary.

On the other hand, the Spray Tower and Venturi configurations remain the safer prototypes, earning SIL1.83 and SIL2.17 ratings, respectively, because of their efficient flow control and separation between plasma sources and operational components. Meanwhile, the GAD-Batch and Falling Film configurations have a worse safety profile because of uncontrolled plasma gas and the proximity of the electrical part and plasma source to operational areas.

Ultimately, by analyzing the interplay between the efficiency and safety of each configuration, the Venturi configuration emerges as the best reactor option. Its design facilitates high plasma generation and effective mass transfer, resulting in outstanding conversion rate performance. Additionally, the Venturi systems operate in safer conditions, achieving a SIL2.17 safety rat-

ing. This balance of high efficiency and robust safety measures positions the Venturi configuration as a preferred choice for industrial applications. This ensures that operators can achieve optimal performance while minimizing risks associated with electrochemical reactions.

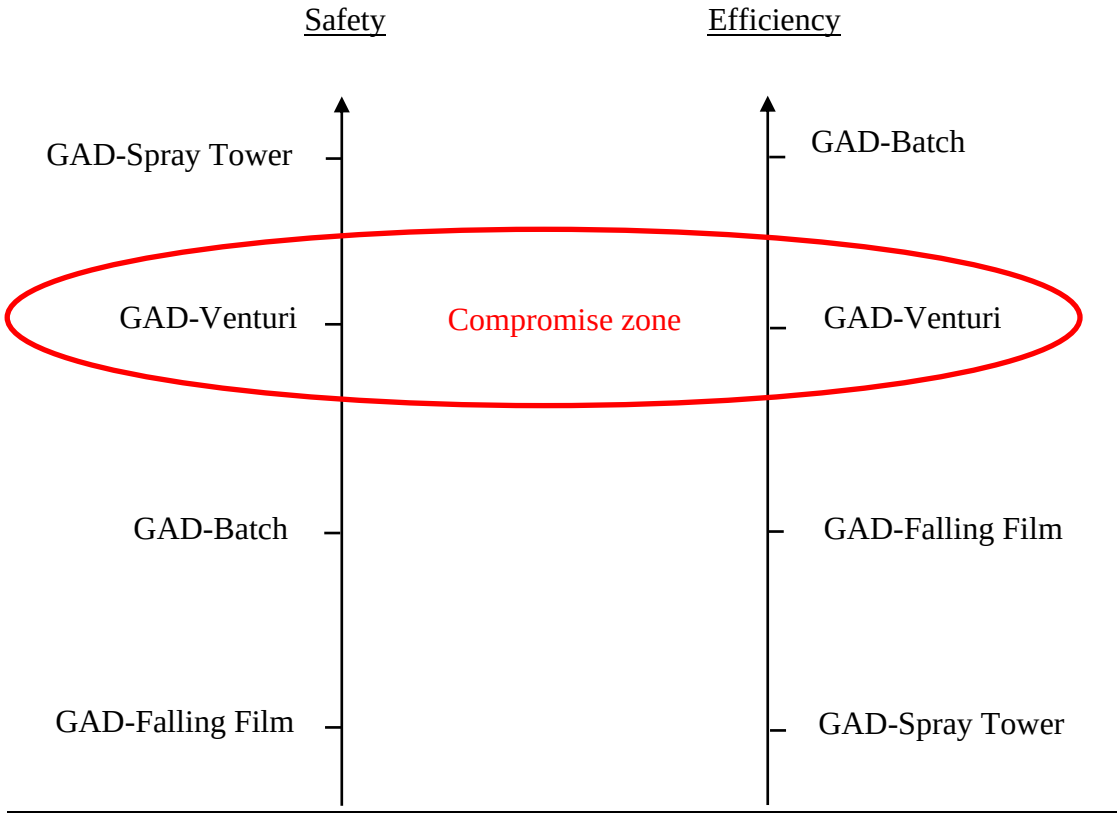

Figure 39. Plasma GAD reactor classification based on performance and safety levels

CHAPTRE IV. Catechol production process using plasma-reactor

Introduction

This chapter is a manuscript titled —" A novel approach of Catechol production assisted by plasma process: Lab-Scale experiment and modeling, Commercial-Scale Design and Economic Evaluation", recently published in the Journal of Chemical Engineering. No changes have been made to the original content, except for the layout, word editing, and presentation of more precise information.

This chapter presents the experimental results of phenol conversion into catechol and its mesomeric obtained by GAD-VNT and GAD-ST separately. Based on these results, a comparison study based on conversion rate and selectivity was carried out to propose the best configuration for an industrial-scale extrapolation for massive catechol production.

The experimental study was followed by a modelling work of the mass transfer and kinetic models of the GAD-VNT process. The aim is first to validate the proposed mechanisms for the conversion of phenol with a view to subsequent optimization of the process. Based on the experimental results, the model will then calculate phenol by-product constant rates using COMSOL software.

Thus, based on the previously conducted experimental and modelling results, we have chosen to use HYSYS software to design and present an industrial scale for catechol production. The simulation of this process was carried out in three complementary actions:

Firstly, the physicochemical properties of plasma species were estimated. This action was conducted using the HYSYS estimating function available for newly added components. The estimating results were used to predict the behavior of these species in the process simulation study and defined the plasma's reactivity under different process conditions.

The second step consisted of designing the proposed process in the HYSYS flowsheet window and defining the streams and equipment parameters. Then, a parametric study was conducted to study the dual influence of inlet flow rates and feeding phenol concentration on the process selectivity.

The third action was to determine the financial feasibility of the developed process. This later consisted of calculating the total capital, operating costs, and product sales using Aspen Process Economic Analyzer (APEA) software. The financial feasibility was determined by comparing the calculated costs and revenues. This study aims to propose a suitable process flowrate scale and phenol concentration that presents promising beneficial revenues.

CHAPTRE IV. Catechol production process using plasma reactor

Before embarking on the design and realization of this project, it is necessary to review the state of the art in terms of utilities, the limits of existing processes and the volume of the catechol market. This preliminary study provides a superficial overview of the technical and economic feasibility of the novel process.

1. State of the art of catechol production processes

1.1 Physicochemical properties

Catechol, also known as pyrocatechol or 1,2-dihydroxybenzene, is an organic compound made up of two hydroxyl groups attached to a benzene ring, making it a member of the phenolic family. This compound is of major interest to me because of its distinctive physicochemical properties. At room temperature, it appears as white to yellowish crystals, either crystalline or powder. Its solubility in polar solvents such as water, ethanol and ether make it a hydrophilic compound [144]. However, its reactivity with atmospheric oxygen can lead to the formation of brown pigments called melanins, a common phenomenon observed in fresh cut fruits known as enzymatic browning [145].

Furthermore, Mr Md Sohel Rana and her colleagues have identified a rapid oxidative browning of combustion and biomass burning substituted catechol pollutants at the air−water interface enabled by nitrate radicals [146]. This ability to form quinones by oxidation is often exploited in various applications. In addition, its oxidative potential of about 0.18 V ensures a specific chemical reactivity with oxidising agents, acids, bases, metals and reducing agents, making it a versatile and valuable compound in many fields, including organic chemistry for the synthesis of pharmaceutical and agrochemical compounds, as well as in the polymer, adhesive and dye industries. Its potential to form complexes with various transition metals also offers catalysis and coordination chemistry opportunities. The physicochemical properties of catechol make it a compound of great scientific and industrial importance, although its sensitivity to oxidation requires appropriate handling and storage to retain its desired properties.

1.2 Applications

Catechol is an organic compound of major interest in many industrial and scientific fields. Its intrinsic characteristics, including its solubility in various polar solvents such as water and ethanol, its distinctive melting and boiling points, its chemical reactivity and its ability to form complexes, make it a versatile element in organic chemistry, pharmacology, polymer industry, materials engineering, cosmetics industry, catalysis and many other fields.

1.2.1 Pharmacology and biomedical

Catechol has crucial participation in drug conception and medicinal chemistry, where it found that 78 of 8659 drugs of the Comprehensive Medicinal Chemistry (CMC) database and more than 19 agents between oral and injectable were approved by the U.S. Food and Drug Administration (FDA) database are Catholics, the identified catecholic drugs present different pharmacological effects such as antioxidant activity, bronchodilator, adrenergic, antiparkinsonian and antihypertensive [147]. The oxidative potential of catechol (about 0.18 V) makes it a great antioxidant agent that is attributed to the fact that the semiquinone radical derived from H-atom donation of catechol can be stabilized by an intramolecular hydrogen bond and the electron-donating properties of the ortho-OH [146-148]. Maria Koufaki and her colleagues have synthesized substituted chromans by catechol derivatives and studied their ability to protect cultured cells from H_2O_2 caused DNA damage [149]. Moreover, Hee Soon Shin and his coauthors found that the catechol group was responsible for the anti-inflammatory effect of Chlorogenic and caffeic acids by scavenging reactive oxygen species (ROS) [150]. Advanced neuro researchers found that catholic moieties can be an effective therapeutical agent for one of the most crucial social problems caused by senile diseases known as Alzheimer's Disease, where it found that a specific catholic derivative class invented by Pr. Fukazawa et al. serves to inhibit the progressive disease and promote the production and secretion of nerve growth factor that enable the degenerated nerves of central nervous system to recover their functions [151].

Another specific catholic class named catecholamines plays a crucial role in different physiological metabolism activities. Catecholamines like dopamine, epinephrine, and norepinephrine are neurotransmitters naturally produced in the adrenal medulla to control cardiological activities; they also regulate airway reactivity, blood pressure and other metabolic functions [152]. Catecholamines are highly described as either injected or drunk medicines to solve cardiological problems. However, the excess of catecholamines amount leads to the dysregulation of the outlined activities [153]. Elevated catecholamine levels after Traumatic brain injury (TBI) lead to peripheral vasoconstriction that results in arterial hypertension, an increase in cerebral blood flow and raised intracranial pressure. [154] It also increases oxygen demand by the heart and brain, causing cardiovascular dysfunction and possibly further brain damage. Recent research found that excess catecholamines have the same outcomes as COVID-19, which might be key mediators in COVID-19 [155]. Catecholamine drugs are usually produced via an extraction or chemical reaction processes; a recent work by Lin Dong and his mates developed three ways for the production of dopamine with different row materials such as vanillin, softwood lignin

and catechol that was converted into dopamine by a chemical process based on enzymatic reaction [148].

Catechol compounds have further biomedical applications, such as diabetic wound treatment, where catechol-functionalized hyaluronic acid (HA-CA) shows a promising result and is nominated to be the novel therapeutic strategy [156]. Furthermore, functionalizing drug molecules with catechol moieties allows for targeted delivery and control release; they have also shown an anti-microbial effect where the double hydroxyl function allows them to disrupt bacterial biofilms and inhibit viral attachment. Wei Zhang et al. l. Have developed an interesting review of the biomedical applications of a functionalized hydrogel by catechol groups [157].

1.2.2 Technical applications

Rather than biomedical and pharmacological uses, catechol derivatives and catechol functionalized polymers remain very useful for other fields, such as environment, surface adhesion, and energy storage. Many recent works have found that functionalized polymers with catechol moieties serve as a versatile solution for environmental problems and water treatment, such as metal chelation, organic contaminant removal, water filtration and liquid separation.

Water remediation

Polydopamine is one of the most common catechol-functionalized polymers. Specially nanoparticles of polydopamine, which are characterized by their high-level active sites, are used as a typical adsorbent; Farhadi et al. have used polydopamine nanoparticles for coper absorbance as a water purification process, where it reached in 4.5 hours an absorbance capacity of 34.4 mg g^{-1}, this low absorbance capacity is reported to the low surface area of the outlined materials. Thus, a combination synthesis process of nanoparticle polydopamine with a large surface area absorbent material is highly required; therefore, Gao's Groupe have synthesized a polydopamine-modified graphene hydrogel with a surface area of 310.6 m^2 g^{-1}, the resultant hydrogel has increased the absorbance capacity about 1.4 times for Cd (II) and 3 times for Pb (II) comparing to pristine graphene hydrogel, it was measured to be 145.48 and 336.2 mg g^{-1} respectively. [158]. Moreover, a fascinating work was developed by Mr P. Karthik and his colleagues and resulted in the synthesis of a catechol-TiO_2 carbonaceous polymer that is stimulated to be visible-light active with a band gap of 1.9 eV. The synthesized hybrid material enhanced the photocatalytic activity compared to pure TiO_2 for Cr (VI) reduction and solar light-driven H_2 production 5 to 10 times, respectively. [159]. Catechol-functionalized polymers can also serve for water/oil separation based on their surface hydrophobicity. Accordingly,

metal-catechol polymer films were prepared using Fe and Cu metals to study their water purification ability. The prepared polymers showed high textile dye removal, especially at lower concentrations. The metal-catechol polymers have presented a good water-oil separation, where it found that Fe-catechol polymer coated cotton is the best water/oil separation membrane with a separation ratio of more than 99%; the membrane has conserved the same ratio even for 50-cycle treatment.[160].

Coating

Catechol functionalization of solid material has become one of the most researched interest works; this action can be conducted either by direct graphing of catechol moieties on their surfaces or by applying a specific coating characterized by catechol functions; this functionalization directly affects the material properties, which can be very useful to ensure some required activities like anti-corrosion, adhesion, anti-fouling and much more others. For instance, applying metal-catechol coating on cotton has modified its hydrophilicity and wettability where water drops showed non-adhesion to the surface, the coated cotton is superhydrophobic with a contact angle of more than 160º instead of 0º for the pure cotton [160], further researchers have developed new copolymer coatings based on catechol and comonomers like PEG(meth)acrylates, long-alkyl chain (meth)acrylates and fluoroalkyl (meth)acrylates in order to control the hydrophilicity-hydrophobicity of the synthesized coatings where their contact angles go from 40º to 172º based on different substrates and coating conditions such as PH and composition [161].

Once more, catechol's anti-oxidant feature, due to its oxidative potential, has motivated scientists to develop a novel coating bearing catechol moieties to ensure the anti-corrosion function of the coated surface. Naito and his co-authors have taken advantage of the versatile and robust banding of catechol and free-layer polymers to form a firm and transparent coating in the presence of hydrophobic alkyls; the formed coating has shown an excellent anti-corrosion feature on copper, aluminium, iron, and Magnesium in different corrosive mediums such as acidic solution and salt-water mediums [162]. These metals have unique physicochemical characteristics. For instance, Magnesium is widely used in the electronic and automobile industries because of its lightweight and potent properties. However, it has a very low oxidative potential (E^o =-2.73 V), which makes it susceptible to fast and harmful corrosion. In this context, sol-gel has shown good Magnesium corrosion resistance, but only for a limited protection period of 3days in saline solution; therefore, the Jiao li group have developed a novel sol-gel coating

based on catechol/lysine copolymer, which in turn has extended the protection period of Magnesium alloys to 18 days in NaCl solution (C= 0.1M).[163]. Furthermore, catechol molecules have strong binding forces to a wide range of surfaces, which in turn offers strong adhesion properties; the cheng-yuan Feng group have taken this advantage for the metallization of the Polyphenylene Sulfide (PPS) surface with thin copper layers. The strategy consists of fixing the catechol/polyamine functional group on the polyphenylene sulfide that ensures a strong copper layer adhesion to the factionalized PPS; the deposed copper layers exhibit good corrosion resistance in acid, alkali and salt-corrosive mediums. [164]. Moreover, in order to prepare a bilayer piezoelectric composite, Vincent Bouad et al. have developed a novel approach to the use of a macromolecular coupling agent, where the method rivals the functionalization of poly methyl methacrylate (PMMA) by catechol moieties which offer a large interfacial surface and strong adhesion properties. This macromolecular coupling agent was first deposed on the piezoelectric ceramic surface. Then, the modified surface was coated by the piezoelectric copolymer P(VDF-co-TrFE) to form the desired bilayer piezoelectric composite.[165].

Energy

Due to its electrochemical properties, the functionalization of surface materials with catechol moieties can enhance their energy level and ensure photocatalytic activity and energy storage. For photocatalytic activity, it was found that catechol functions improve the visible light absorption and broaden the bandgap of the functionalized semiconductors. Accordingly, Sadman Sakib and his mates used catechol molecules as photo-absorption amplificants to enhance the photocatalytic activity of metal oxides. The study was started by the adsorption of catechol-type ligands on the metal oxide surface by forming complexes with metal atoms through adjacent phenolic —OH groups; the adsorbed catechol function has raised the visible light absorption yield, which ensures a safe, economical and effective photocatalysis, photoelectrochemical biosensing, and solar cell applications. [166]. Subsequently, P. Karthik et al. shifted the TiO_2 bandgap to the visible light region by the formation of catechol–TiO_2 carbonaceous polymer, where it found that 1.0 wt% of this later tailored the bandgap of the TiO_2 from 3.1 to 1.9 eV. The resultant material has shown 10 times solar light-driven H_2 generation yield toward sustainable energy production compared with pure TiO_2. [167]. More importantly, electrochemical energy storage (EES) systems are one of the modern solutions to solve the potential energy crisis. However, current EES storage systems could hardly satisfy the booming development of a safe, green and sustainable society. In this regard, researchers have conducted thousands

of studies that found that catechol polymers remain the most suitable solution for designing safe, low-cost, and sustainable next-generation EES devices. Catechol in the acidic medium can be easily converted to ortho-quinone by a tow-electron oxidation process; the produced form presents a strong aromaticity that increases redox potential and improves the reaction reversibility, appearing as strong energy density and long cycle life, respectively. Indeed, this catechol/ ortho-quinone redox reversibility has been extensively used in aqueous-based pseudo-capacitors and proton batteries. Moreover, as discussed in the previous section, catechol has shown a high metal chelating; this interesting catechol property has been used in metal ion batteries. This is highly desired in the design of catechol-based universal electrodes compatible with battery chemistries, including mono and multivalent cell configurations. [168] In addition, bioinspired redox-active (macro)molecules bearing catechol function like polydopamine that offer a high carbon yield, robust wetting and adhesion capabilities, as well as a reversible redox activity to store electrons/metal cations constitute a promising class for the design of a safe, economical and sustainable electrochemical energy storage devices (the next-generation energy storage devices) [169-171]. Furthermore, Choi et al. have modified the lithium-ion batterie separator with polydopamine moieties; this modification has increased the hydrophilicity of the separator with a contact angle of 39º instead of 108º, which in turn increased the uptake amount of the electrolyte by 30% that improved the batterie performances [172-174].

1.3 Production processes

1.3.1 Natural accurence and recuperating process

As discussed in the previous section, catechol shows a wide range of significance both in natural systems and industrial processes. In nature, plants are the most prominent occurrence of catechol [175-178], which serves as a precursor in the biosynthesis of plant hormones, particularly auxins. These hormones play pivotal roles in regulating plant growth and development, influencing cell elongation, root formation, and fruit development. Catechol also participates in plant defense mechanisms, acting as a signaling molecule in response to environmental stresses and pathogen attacks. For instance, a fresh cut remains harmful damage to the fruit defense system; at that time, the contained catechol on the cut surface reacts with the oxygen present in the air, forming a brown pigment on the cut surface as a signaling response to the harmful attack [145].

Indeed, catechol can be recovered from various plant sources using isolation methods, where liquid extraction remains the most useful technology. Link and Walker have reached out an analytically pure catechol production from a pigmented onion using an acetone extraction process; the process consists of using acetone as an organic solvent where catechol is highly dissolved, and the residue is washed by water in order to separate the water-soluble from the water-insoluble substances [178]. Catechol can also be synthesized from other natural biocomponents like lignin [179, 180]

1.3.2 Lab synthesis

The catechol produced from these processes has been found to meet market requirements. Therefore, researchers have developed a wide chemical synthesis route for this later. Le Yanga used mineral hydrochloric acid catalysis to convert guaiacol to catechol in high-temperature water; a conversion rate of 99% was achieved in specific pH, temperature and pressure conditions [181]. Subsequently, D. P. Ivanov proposed another catechol and hydroquinone production method by oxidizing phenol with nitrous oxide oxidant [182]. Both the dihydroxylation of benzene and a simple hydroxylation of phenol can produce catechol compounds [183, 184]. However, these synthesis routes present a lack of greens and environment compatibility, which encouraged K. Pamin and his mates to develop a green hydroxylation of phenol into catechol by using glycerol as a solvent medium with the presence of hetero-poly compounds, tungstophosphate ions have shown the best Catechol yielding rate [185].

Furthermore, advanced oxidation processes (AOPs) like photocatalysis, Fenton and non-thermal plasma have shown interesting results in converting phenolic compounds as water depollution processes. Azizi et al. have used the Fenton-Enzymatic process as a phenol chemical removal process; the process achieved a global conversion rate of 54%, where hydroquinone, benzoquinone and catechol were found as the major organic intermediates with maximal concentrations of 26.4, 8.54 and 36.63 mg L^{-1} respectively [186]. Besides, Huixian Shi et al. have used a photocatalytic process for the conversion of phenol to catechol and hydroquinone compounds with a conversion rate of up to 87.8% with a yield of 37.0% and 27.4% for CAT and HQ, respectively [187].

1.3.3 Industrial production

Catechol can be produced from natural biocomponents like glucose [188] and lignin, the most abundant biomass components and a major waste by-product from the pulp and paper plant,

wood and food industries. In such processes, lignin is converted into catechol by a direct hydrothermal cracking process with a low conversion rate. Therefore, catalytic cracking was performed to improve the production yield [189].

Traditionally, catechol is mainly produced in the industry by the alkaline hydrolysis of dichlorobenzene, 2,4-sulphonic-5-phenol or o-chlorophenol [190], or by oxidation of petroleum compounds like phenol, benzene and cyclohexene [191-193]. Indeed, James and Willingford have developed an interesting catechol manufacturing process [191], using KA-Oil as the main row material. Figue01 presents the block flow diagram of the outlined process, where it is clear that the process is mainly composed of 4 stages; hydrotreatment, dehydration, oxidation and dehydrogenation.

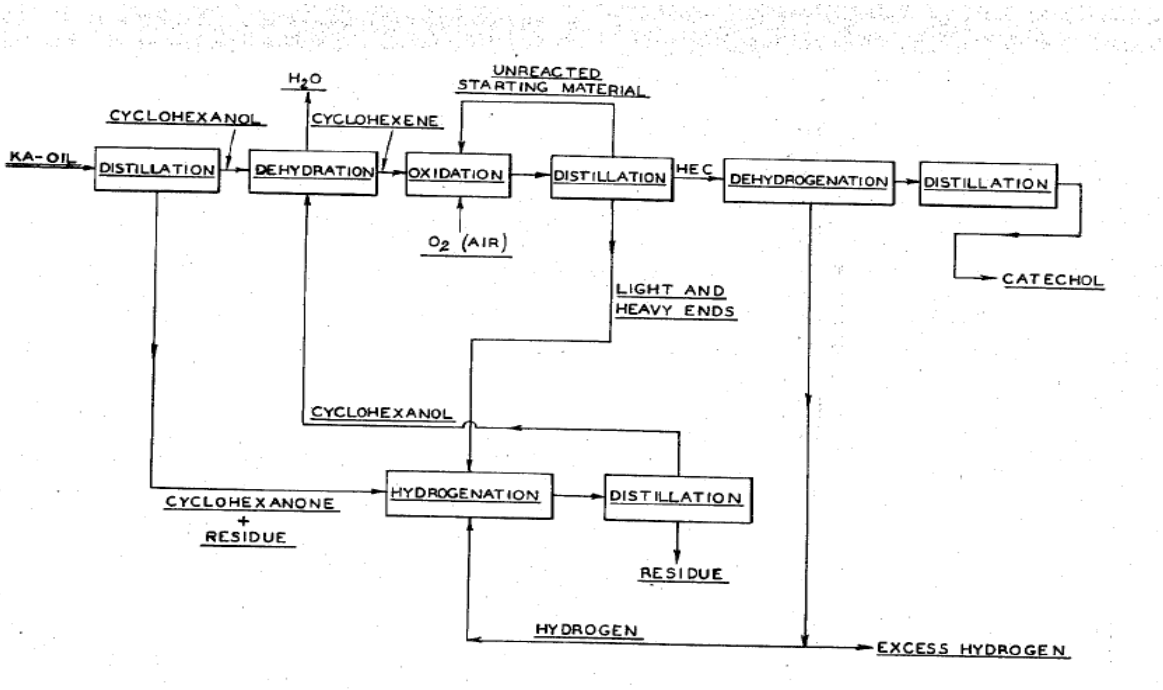

Figure 40. Conventional catechol production diagram [191]

According to the process, The KA oil, a mixture of 60-80% cyclohexanol with 40-20% cyclohexanone, is first distilled to separate the cyclohexanone from the cyclohexanol. Then, the separated cyclohexanone passed by a catalytic hydrogenation process using a divided catalytic bed of copper chromite at about 150 to 350°C and about 1500 psia H_2. The resulting product is subsequently distilled to form additional cyclohexanol and some residues; the formed cyclohexanol is added to the original. Hence, the cyclohexanol is dehydrated to cyclohexane on a fixed bed catalytic hydration process in the vapor phase at temperatures of about 300o, employing gamma alumina catalysts; this dehydration represents the second stage. Whereas the

third stage oxidation of cyclohexene to form 1,2-epoxy-3-hydroxycyclohexane (HEC), this oxidation is achieved by making cyclohexene in contact with air or oxygen in the presence of an ion-exchanged bimetallic catalyst like cobalt or copper
and vanadium-exchanged x-Zeolite. These reactions are generally carried out in the liquid phase at temperatures ranging from about 25 to 150°-200°C for periods of about 1 to 10-20 hours with a conversion rate of about 30%. The unconverted cyclohexane is separated from the material product by a distillation process and then recycled to the oxidizer unit, as shown in the flow diagram. The 1,2-epoxy-3-hydroxycyclohexane is the dominant oxidation product material with a 50-60% ratio. Whereas 35-40% of the material products represent the volatile by-products like cyclohexene oxide, 2-cyclohexene-1-ol and 2-cyclohexene-1-one and only 5% for residue that comprise heavy materials such as dimers and polymers of oxidized olefin. A distillation unit separates the product mixture; the volatile oxidation materials are recycled to the hydrotreater after being converted to cyclohexanol by a hydrogenation process.
The fourth stage consists of converting the HEC separated from the distillation unit to catechol by a dehydrogenation process in the presence of Group VIII transition metal like palladium, platinum, or ruthenium fixed on an inert support such as alumina as a dehydrogenation catalyst; the catalyst should be present in amounts of from about 1 to 10 weight per cent based on the weight of the starting material. The reaction can be carried out in either the liquid or vapour phase; for the liquid ones, it is desirably carried out at temperatures of from about 175° to 350°C using high boiling alkyl or aralkyl hydrocarbon solvents such as phenyl dodecane or dodecane.
The dehydrogenation products are then separated by a distillation unit, where catechol is recovered. The hydrogen generated is recycled to the hydrogenation unit, as shown in the accompanying diagram.
This method requires the installation and subsequent removal of the guide group in advance, which results in low atom economy and high synthesis costs. Therefore, a recent invention was patented to solve the outlined problem by providing a novel synthesis method of catechol compounds with simple conditions, low waste emissions, simple reaction equipment, and easy industrial production [192]. The invention consists of combining a cyclohexanone compound with sulfone or sulfoxide, which are mixed and reacted under a catalytic action; the catalyst is selected from any one of the iodine elements, bromine element, N-iodosuccinimide, N-bromosuccinimide, hydrogen iodide and hydrogen bromide, while it is preferably to be elemental iodine.

The molar ratio of the sulfone or sulfoxide and the cyclohexanone compounds is 1000:1 to 1:1, and the cyclohexanone compound to the catalyst is 1000:1 to 1:1. The solvent is preferably to be methanol, ethanol or acetonitrile with a dosage of 0.02 to 2 mol L^{-1}, and the reaction temperature is fixed to be 60°C. The synthesis route is as follows:

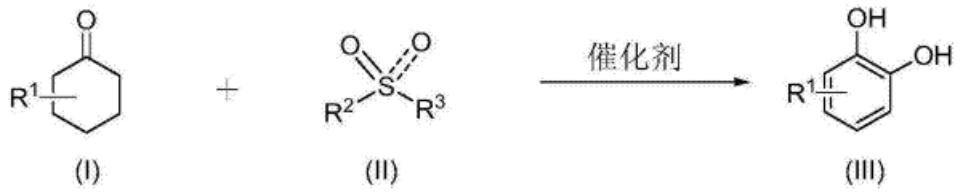

(R 69)

R^1, R^2 and R^3 are selected from hydrogen, alkyl group, alkoxy group, aryl group, substituted aryl group, aldehyde group, ester group, carboxyl group and amide group.

One of the most used processes for catechol production was the oxidation of phenol in the presence of iron compound as a catalyst [193]; the process was carried out on an industrial scale by adding hydrogen peroxide solution to a phenol solution with a mole ratio of phenol to hydrogen peroxide fixed preferably within the range of 1:0.05 to 1. The catalyst used should be below 1 mole per cent based on the phenol feed and preferably within the range of 0.0001 to 1 mole per cent, although carrying out the reaction within the range of 40 to 100° C is preferable. The oxidation of phenol to catechol was found to be accompanied by the production of hydroquinone. Therefore, any modification of the phenol/hydrogen peroxide molar ratio or catalyst amount will significantly affect the process selectivity. That is, the larger the ratio of hydrogen peroxide is, the more the conversion rate will increase, while it will be lower for a larger phenol ratio. Subsequently, if the conversion of phenol is too high, dihydroxybenzene will be further oxidized to produce higher oxides, and thereby the selectivity of the reaction will be reduced.

1.3.4 A novel catechol production process

The biggest limitation of these traditional synthesis methods is that they have low selectivity and generate a variety of products, which causes certain difficulties in the separation and purification of the target product; these processes also present further disadvantageous like the number of stages including numerous operations units accompanied by a high production cost and a lower environment compatibility. Therefore, a novel process for catechol production is proposed to overcome the conventional process limitations and ensure a high-level production; the process consists of using non-thermal plasma technology as a source of hydroxyl radicals

to react with phenol molecules without any catalyst material. The process comprises 05 operation units defining 03 operating stages, as follows:

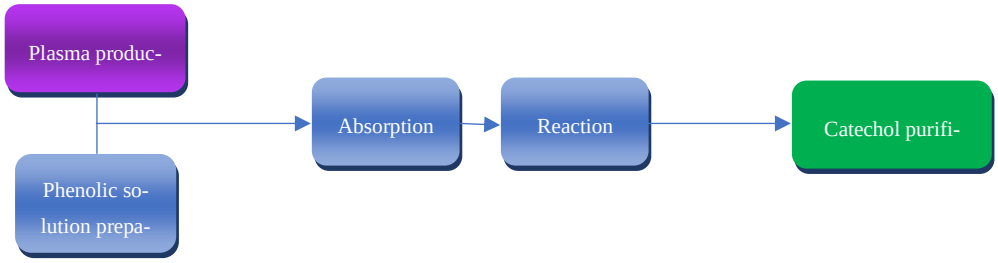

Figure 41. Principle operations in the proposed process

The first stage consists of preparing the reagent materials, where phenol ether in a solid or liquid form is mixed with ambient water using an agitated tank to ensure the homogeneity of the prepared solution. In contrast, plasma reagents are prepared in the gliding arc discharge reactor; this reactor consists of applying 9000 eV on a gas flow passing between two diverging electrodes. Argon, nitrogen, and oxygen can be used as inlet gas flow; however, from an industrial point of view, it is preferable to use air as the feeding gas according to its abundance, low cost and operability, even if it may affect the process selectivity for the desired product due to the varied produced plasma species.

The produced reagents are then driven to a biphasic reactor to ensure the desired reaction; this later comprises an absorption system and plug flow reactor. The venturi contactor was chosen as the absorption system for the conducting study according to the high offering interface area. However, other systems like pulverization, film, or bubble contactors can also be used. The mixture is then passed by a plug reactor where phenol is converted to catechol with a slight quantity of nitrophenol hydroquinone and resorcinol byproducts. This step represents the second stage. The last stage remains the purification of the produced catechol. That is conducted by a separating unit, preferably a distillation one, where the unreacted phenol and the byproduct are separated based on their volatility.

It is important to mention that the proposed process works in normal conditions such as temperature and pressure, which makes it easy and advantageous to carry out on an industrial scale. The use of air as feed gas and phenol as the primary reactive present an economic significance by ensuring a low row material cost as well as a green process feature, while the use of water as a medium solvent offers a safer operating level.

2. Experiments

This section focuses on determining the plasma phenol by-product and choosing the right plasma GAD configuration based on the hydroxylation rate, conversion rate and reactor selectivity to the desired by-product (catechol). For the Gliding arc discharge, there are three operating modes such as direct, post-discharge (PD) and spatiotemporal post-discharge (STPD) treatment; these modes present a different performance based on the produced plasma reagents and the operating conditions. The STPD was chosen for the study according to its continuity, easy implementation on industrial scale and safer operating condition.

2.1. GAD reactor

The STPD was chosen for the study due to its continuity, easy implementation on an industrial scale, and safer operating conditions. However, the conventional configuration (GAD-ST) presents an important limitation regarding hydroxylating power and conversion rate. Therefore, a new GAD configuration named GAD-Venturi (V) is proposed to offer better mass transfer and chemical reactivity performance. A comparative study was conducted with the conventional indirect treatment reactor (GAD-ST).

Figure 42 presents the GAD-Venturi (V) configuration; this later involves the same principle of plasma gas production as GAD-ST but a different gas-liquid contact system. For the conventional one, the liquid solution is sprayed on counter-current with the plasma gas; this system presents a low liquid gas interfacial area while the Venturi system presents a larger one that allows a better plasma transferred masses, the fluids (liquid and plasma) circulate in co-current for 100 cm into a spiral hose in order to increase the residence time that ensure better performance as well. Both GAD-ST and Venturi characteristics and parameters are detailed in Chapter II and kept the same in this section..

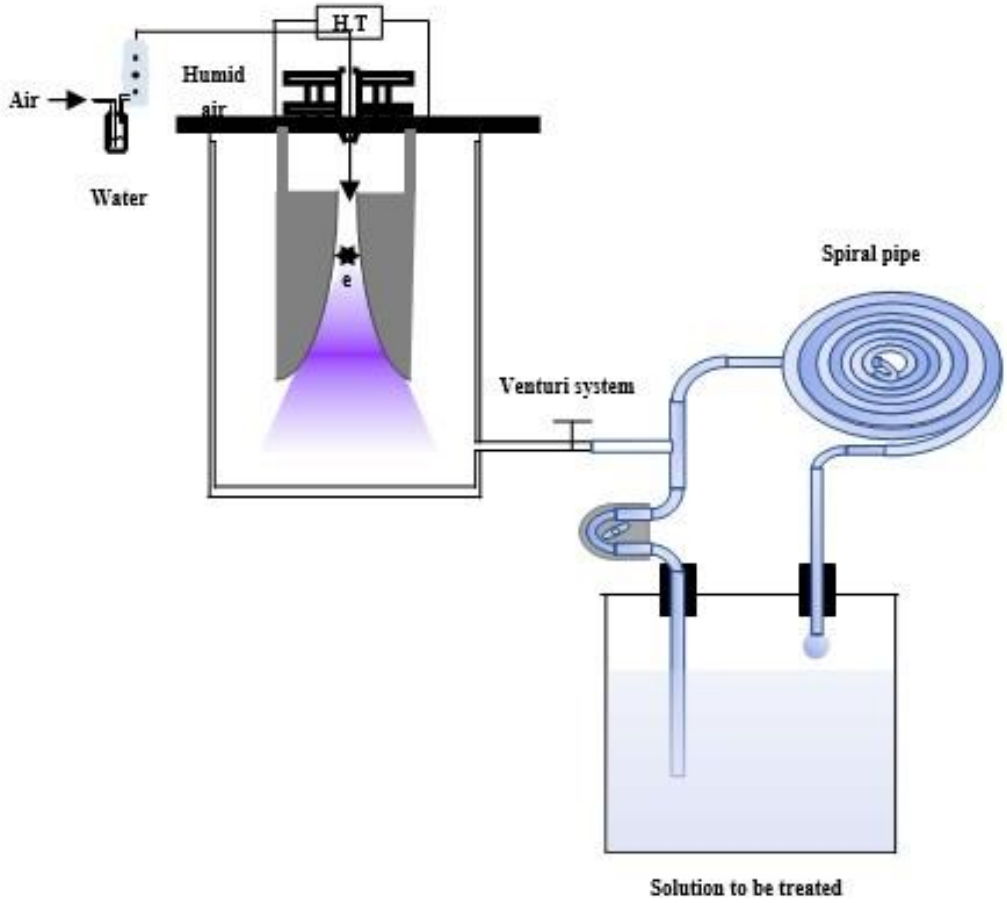

Figure 42. Schema of GAD-V reactor

2.1 Discharge characterization

Optical emission spectrophotometry (OES) was used to determine the various excited species present in the plasma phase during the discharge. The optical fibre was placed at the centre of the discharge, and the analysis was carried out at the 190 to 900 nm wavelength range.

Figure 43 presents the Optical emission spectrum of the atmospheric plasma plum; four distinct zones were identified. The first one extends from 230 to 305 nm and corresponds to the bands associated with NO-type nitrogen species. The second zone extends from 305 to 325 nm and is mainly the zone of $^{\bullet}$OH emission bands. The third extends from 325 to 340 nm and corresponds to nitrogen species. Finally, the last zone, around 760 nm, corresponds to the oxygen bands.

The analysis has shown a high intensity of hydroxyl radicals $^{\bullet}$OH that reflects their abundance compared to nitrogen and oxygen radicals. This abundance gives the possibility to classify plasma Gliding arc discharge as a promising source for hydroxylation applications.

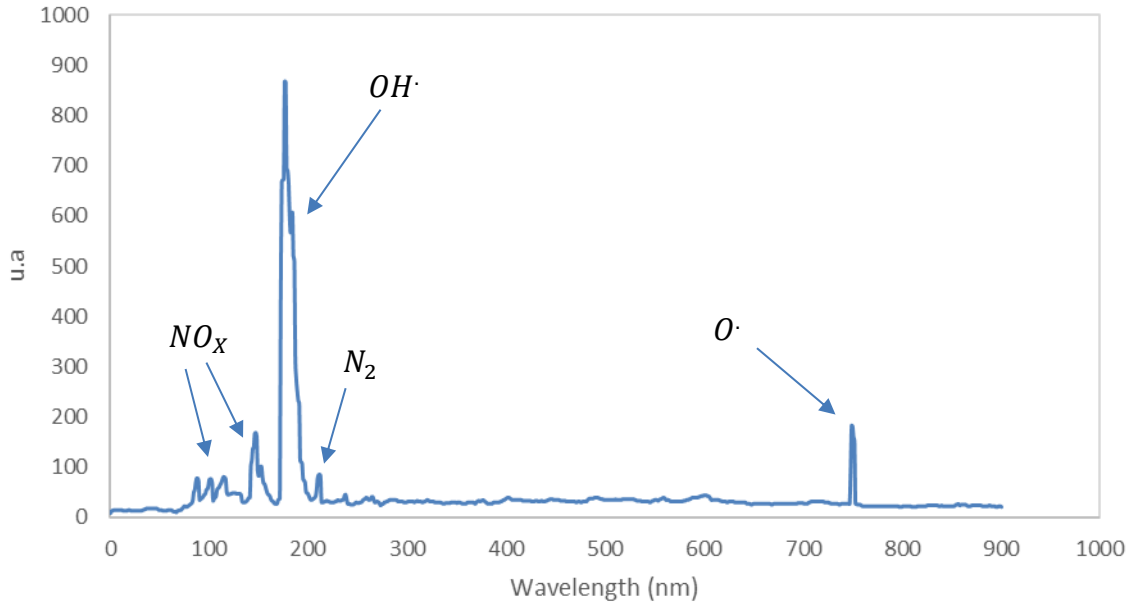

Figure 43. Optical emission spectrophotometry (OES) of the plasma GAD discharge

2.2 Plasma reactor performances

300 mL of Phenol solution (10^{-3} mol L^{-1}) was treated using GAD-V and ST reactors separately for different treatment times. Different analytical methods were employed to determine the outlined configurations' performances.

First, the total organic carbon (TOC) was measured using a multi-N/C 2100S TOC analyzer from Analytik- Jena. This study was carried out in order to compare the hydroxylating power of the outlined reactors on phenol substrate; the analysis was followed by a calculation study using the following equation:

$$COT = \sum_{i=1}^{n} \alpha_i \, M(C) \, C_i \qquad \textbf{(Eq.48)}$$

$$COT = \sum_{i=1}^{n} C_{i0} \, \alpha_i \, M(C) \, (1 - X_i) \qquad \textbf{(Eq.49)}$$

$C_{i0} = initial\ concentration\ of\ spiceis\ "i"\ (mol/l)$

$C_i = \ temporal\ concentration\ of\ spiceis\ "i"\ (mol/l)$

$X_i = temporal\ conversion\ rate\ of\ spiceis\ "i"$

$\alpha_i = number\ of\ organic\ carbon\ in\ \ spiceis\ "i"$

$M(C) = molecular\ wight\ of\ carbon\ (g/mol)$

Table 14 presents the measured and calculated COT of the initial and final phenol-treated solution. After 45 min plasma exposure time, the COT of phenol solution decreased from 60.8 to

55.21 mg L^{-1} for the GAD-ST, while it reached 52,87 mg L^{-1} for the GAD-V. For the non-treated (pure) sample, it is observed that the calculated COT matches ideally the measured one with values of 60 and 60.8 mg L^{-1}, respectively; this overlapping result validates the proposed equation (IV-2). According to the study on the GAD-ST by Ferhat et al., the hydroxylation process was the first conversion step [131]. The hydroxylation process remains the first mineralization step, according to the organic compound definition, which can be explained by converting one organic carbon from a benzene ring to a mineral one by replacing a carbon-hydrogen bond with a carbon-oxygen one. The hydroxylation rate was found to be 46% using formula 03, while 48% was measured as conversion rate in the next section; this compromise confirms that the reaction is of hydroxylation type. However, the slight difference can be explained by the presence the apparition of second-generation phenol by-products.

Table 14. Initial and final total organic carbon (COT) measured and calculated

	Non-Treated		**Treated**	
	Measured	Calculated	GAD-V	GAD-ST
CT (mg L^{-1})	60.96	-	52.96	55.38
CI (µg L^{-1})	154.3	-	233.5	172
COT (mg L^{-1})	60.80	60	52.96	55.21
X_i	0%		46%	5.5

Secondly, Young Lin high-performance liquid chromatography (HPLC) was used to determine the phenol conversion pathway and quantify the produced by-products. The analysis experiment was conducted using a C18 chromatography column under 1 mL min-1 of ultrapure water and acetonitrile mixture as mobile phases with 0.6 and 0.4 volume fractions, respectively.

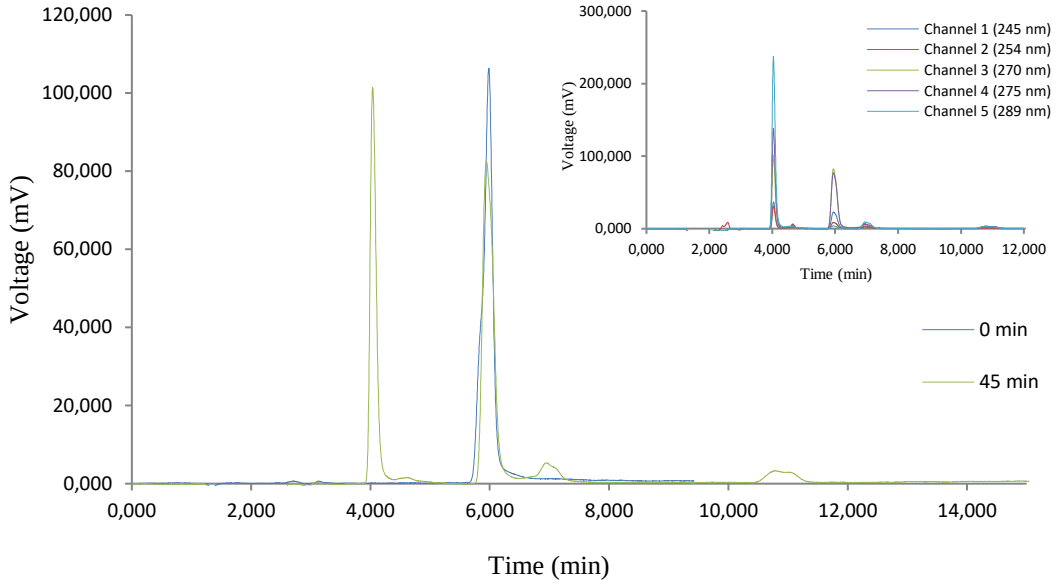

Figure 44. HPLC chromatograms of phenolic byproducts

Figure 44 presents the final by-product HPLC chromatograms. Accordingly, hydroquinone, resorcin, catechol, two and 4-nitrophenol were identified, which can explain that atmospheric plasma treatment of phenol can undergo both hydroxylation and nitration processes with unequal byproduct fractions. That is resumed as following:

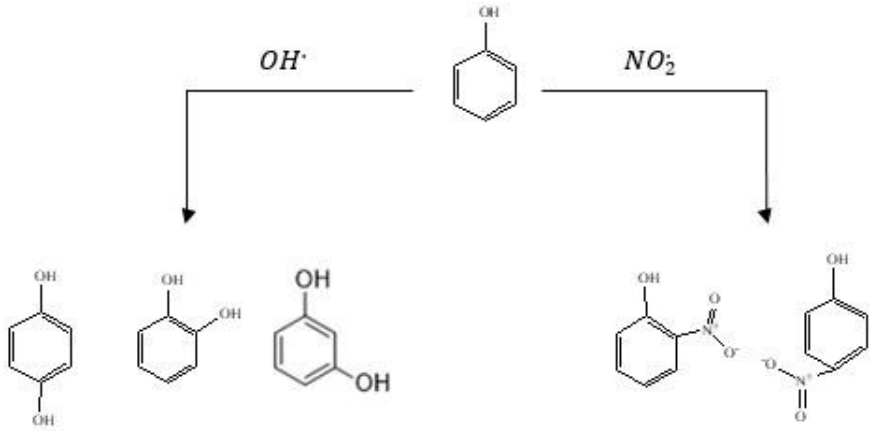

Figure 45. Shema of phenol conversion mechanism

The hydroxylation process is conducted by electrophilic attack of hydroxyl radicals on the phenol aromatic ring in the ortho meta and para positions relative to the OH group of the phenol to give hydroxyl compounds: catechol, resorcinol and hydroquinone. Meanwhile, nitrogen dioxide radicals formed in solution react rapidly with phenol molecules in the ortho and para positions relative to the phenol OH group, forming 2- and 4-nitrophenol.

Catechol was the most dominant byproduct, with uneven production quantity for the GAD-V and spray tower configuration. Such as, 46% of the phenol amount was converted after 45 min of plasma GAD-V treatment time instead of 8% using GAD-ST, and the consumed quantities were converted to 0.47 10×10^{-3} and 0.065 10×10^{-3} mol L^{-1} catechol compound, respectively. Table 15 presents phenolic byproducts mole fractions; the results show that the new configuration, in addition to sureness in terms of conversion rate, also presents a high catechol production selectivity, where it was found to be 97.6% and 81.6% for the spray tower configuration.

Table 15. Phenol by-product selectivity in spray tower and venturi plasma configurations

	Oxidation by-products				Nitration by-products	
GAD-configuration	Catechol	Hydroquinone	Resorcin	p-Benzoquinone	2-nitrophenol	4-nitrophenol
GAD-ST	81.60%	9.82%	0%	0.%	5.23%	3.35 %
GAD-V	97.60%	0.61%	0.0.32%	1.23%	0.11%	0.44%

Generally, in reactive absorption processes the duality between mass transfer and the chemical reaction phenomena determine the reactor performances and can be resumed in the following properties:

(i) interfacial properties, expressed by interfacial residence time and area;
(ii) solubility, expressed by Henry's law constant;
(ii) affinity, expressed by the rate constant.

Plasma biphasic reactors are characterized by their instantaneous chemical reaction processes, which delegate their mass transfer to the limiting step where plasma species have to pass all mass transfer conditions that differ from one reactor configuration to another,
According to the penetration model that will be detailed in the next section, the exposer time of liquid core elements at the interface level is calculated by the following equation [194]:

$$t_{\exp\,(i)} = \frac{4D_i}{\pi}\left(\frac{C_{i,I}^{(l)} - C_{i,0}^{(l)}}{\varphi_i}\right)^2 \qquad \textbf{(Eq.50)}$$

$C_{i,I}^{(l)}$: concentration of species "i"at the interface "I" within the liquid region (mol. l^{-1})

$C_{i,0}^{(l)}$: initial concentration of species "i" within the liquid (mol. l^{-1})

φ_i: The average material flow of species "i" fromthe gas to the liquid region (mol L^{-1}).

Table 16. Modelling and calculated plasma GAD reactor parameters

Parameters	GAD-ST	GAD-V
P(kW)	0,3	
t(min)	45	
V(L)	0,3	
D_{HONOO} (m^2s^{-1})	2.9×10^{-9}	
φ(mol $m^{-2}s^{-1}$)	28.935	
a (m^{-1})	5.56	33
[Phe]i (mol m^{-3})	1	1
[Phe]f (mol m^{-3})	0,9125	0,5416
[HONOO]g (mol m^{-3})	0,005	0,44
t_{exp}(s)	2.57×10^{3}	19.9

Table 16 resumes the calculated residence times in both reactor configurations. It was found that plasma gas species spend 7.74×10^{3} times on the interface region using GAD-V when compared to GAD-ST at the same operation conditions; this explains the fact that the conventional configuration presents a higher amount of the long-lived species such as nitrite, nitrate and other, these reagents are classified as the last plasma spices generation and characterized by a low reactivity, which explains the low conversion rate presented by this configuration. However, the new one has shown a smaller amount of long-lived spices but a better conversion rate; this can be explained by the presence of a higher amount of short-lived species that are characterized by their high reactivity and instability; these spices have an extremely exciting level which makes it difficult to be measured by a chemical method.

3. Modelling and simulating study

In the previous section, we presented the experimental results of plasma-phenol treatment, reactor performances and the identification of phenol derivatives after being converted by the plasma GAD-V process. In light of the results obtained, a mass transfer model coupling

A novel kinetic mechanism has been proposed, depending on the physical and chemical characteristics of the used reactor configuration.

To fully understand the subject and analyse the transfer, kinetic mechanisms, and the prediction of the production constant rates of the identified by-products, digital modelling using COMSOL multi-physics software was a necessary tool to meet these objectives. Secondly, the novel plasma catechol production process developed in section 01 is interesting to model to better understand the different aspects and parameters that play a key role in the efficiency of the

proposed process. HYSYS simulator software was used to simulate the proposed process of calculating the industrial catechol production scale. This study was followed by an economic simulation in order to predict the beneficial revenues of the proposed process.

3.1 Phenol byproduct constant rate prediction

Plasma Glow discharge is classified as a reactive absorption process where plasma reactive species are produced in the gas region and transferred to the liquid ones. In spatiotemporal post-discharge, STPD, the produced radical species react with each other in gas phases to produce a long-lived species like HONOO, N_2O_4, and H_2O_2, which in and after their transfer to the treated solution can dissociate to a more reactive species, allowing the conversion of the targeted molecules. This mechanism was developed by Ferhat and his colleagues for the degradation of AG25 dye [131] and will be used in the conducting study to predict the constant rate of phenol by-product production. Table 17 summarizes the outlined kinetic mechanism.

Table 17. kinetic reaction model

Plasma-chemical reactions		Constant rates at 298 K	
Distilled water	$HOONO^{(g)} \xrightarrow{He_1} HOONO^{(l)}$	**(R 63)**	$He_1 = 5.1\times10^6$
	$HOONO^{(l)} \xrightarrow{k_1} NO_2^{\bullet(l)} + {}^{\bullet}OH^{(l)}$	**(R 64)**	$k_1 = 6\times10^4\ s^{-1}$
	$NO_2^{(g)} + NO_2^{(g)} \xleftrightarrow{k_2,k_{-2}} N_2O_4^{(g)}$	**(R 51)**	$k_2 = 6.02\times10^6\ m^3\ mol^{-1}\ s^{-1}$ $k_{-2} = 4.4\times10^6\ m^3\ mol^{-1}\ s^{-1}$
	$N_2O_4^{(g)} \xleftrightarrow{He_2} N_2O_4^{(l)}$	**(R 52)**	$He_2 = 36.67$
	$N_2O_4^{(l)} \xleftrightarrow{k_3,k_{-3}} NO_2^{\bullet(l)} + NO_2^{\bullet(l)}$	**(R 53)**	$k_3 = 7\times10^3\ s^{-1}$ $k_{-3} = 4.5\times10^5\ m^3\ mol^{-1}\ s^{-1}$
	$N_2O_4^{(l)} + H_2O \xrightarrow{k_4} NO_2^{-(l)} + 2H^+ + NO_3^{-(l)}$	**(R 54)**	$k_4 = 10^6\ s^{-1}$
	$NO_2^{\bullet(l)} \xrightarrow{k_7} NO_2^{-(l)}$	**(R 65)**	$k_7 = 1.3\ 10^8\ s^{-1}$
Phenol	$\text{Phenol} + {}^{\bullet}OH^{(l)} \xrightarrow{k_8} P1$	**(R 61)**	$K_8 = 10^7\ m^3\ mol^{-1}\ s^{-1}$
	$\text{Phenol} + NO_2^{\bullet(l)} \xrightarrow{k_8} P2$	**(R 61)**	$K_8 = 10^6\ m^3\ mol^{-1}\ s^{-1}$

Accordingly, plasma reactions have extremely high constant rates compared to Henry's constant; this comparison classified plasma chemical reactions as an instantaneous process, making the mass transfer phenomena the limiting step determining such reactors' performance. These reactors are characterized by their gas-liquid interface areas that control the transferred plasma species; the proposed configuration "GAD-V" for spatiotemporal post-discharge based

on the Venturi system creates a fluidic mixture with 10 times the surface area when compared to the spray tower configuration. Spatiotemporal post-discharge allows only long-lived species to participate in the phenolic conversion process. However, it presents a bit of complexity in terms of modelling their transfer phenomena; penetration models have usually been used to modulate complex systems regarding their simplicity and curability with plasma biphasic reactors; figure 46 represent the plasma penetration model; this model presents a liquid and gas regions separated by an interface that represents a thermodynamic equilibrium, presented as following:

- Gas-phase: perfectly homogenized phase where diffusion and convection defined the mass transfer phenomena as following:

$$\frac{\partial C_i^{(g)}}{\partial t} - D_i \times \frac{\partial^2 C_i^{(g)}}{\partial x^2} + u_g \times \frac{\partial C_i^{(g)}}{\partial x} = R_i \qquad \textbf{(Eq.51)}$$

With : u_i : fluid velocity in the domain ($\mathrm{m}.s^{-1}$), D_i : fluid velocity in the domain ($\mathrm{m}.s^{-1}$), $C_i^{(g)}$: concentration of species "i" in gas region ($\mathrm{mol}.m^{-3}$), $C_i^{(l)}$: concentration of species "i" in liquid region ($\mathrm{mol}.m^{-3}$), R_i: production or consummation reaction rate of species "i" ($\mathrm{mol}\,m^{-3}.s^{-1}$).

The created turbulence sent plasma species to the gas/liquid interface

- Interface: at the interface a thermodynamic equilibrium is described by Henry's low:

$$\mathrm{C_i^{(l)}} = \mathrm{C_i^{(g)}} \times \mathrm{H_e} \qquad \textbf{(Eq.52)}$$

Liquid core elements are sent by convection to the interface, where they remain there for an identical interface exposition period "t_{exp}", during which they absorb plasma species from gas phases through a unidirectional molecular diffusion mechanism, the transfer is described by Fick's second law:

$$\frac{\partial \mathrm{C_i(t,x)}}{\partial \mathrm{t}} = \mathrm{D_i} \times \frac{\partial^2 \mathrm{C_i(t,x)}}{\partial \mathrm{x}^2} \qquad \textbf{(Eq.53)}$$

- Liquid-phase: Charged liquid core elements are returned to be perfectly homogenized with the core phase's achieved by flow discontinuity, where diffusion and convection defined the mass transfer phenomena.

Ones again, the equation (3) is used for liquid region regarding the compatible mass transfer phenomena to the gas one, with $C_i^{(l)}$ instead of $C_i^{(g)}$ such as: $C_i^{(l)}$: concentration of species "i" in liquid region (mol m^{-3})

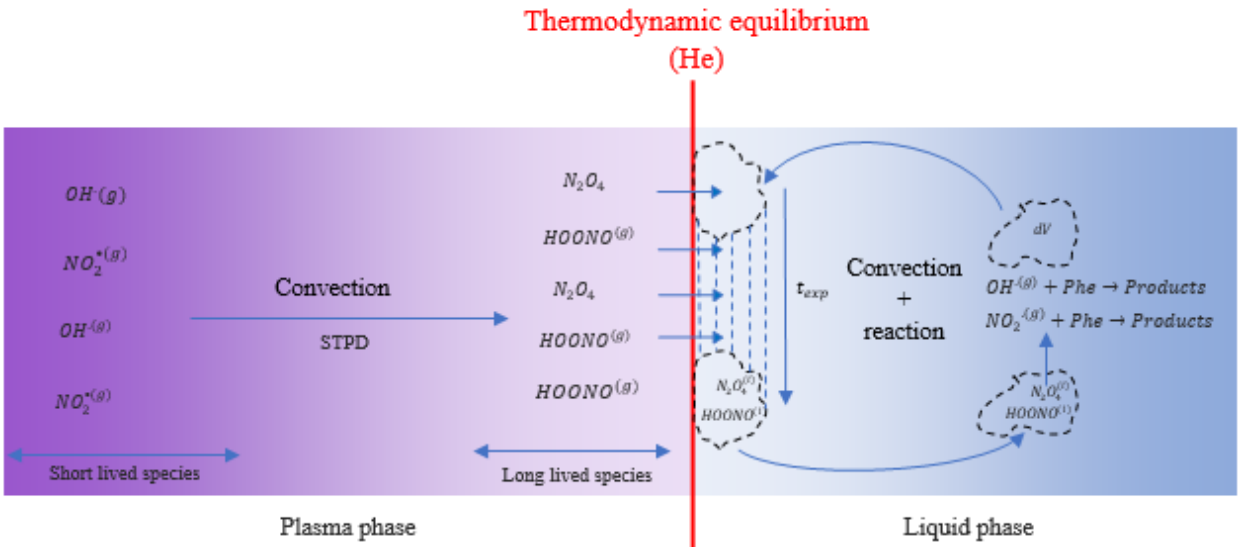

Figure 46. Mass transfer penetration model in plasma GAD-V reactor

At the first stage, a time dependent simulation of both proposed mass transfer and kinetic models using chemical reaction and diluted species transport modules in COMSOL Multiphysics 5.5 version was conducted to predict phenol concentration's evolution during plasma exposition process. The predicted results were fitted to the experimental one in order to validate the outlined models.

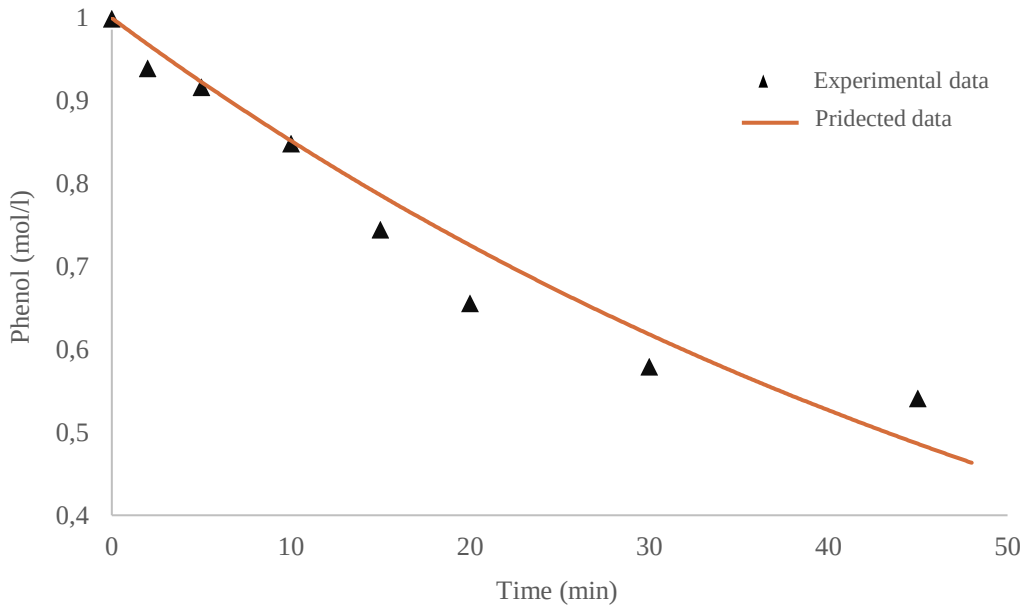

Figure 47. Evolution of phenol concentration during Plasma GAD-V treatment

Figure 46 presents the evolution of phenol concentration for both experimental and predicted data. The plotted results showed a high compromise, which confirms plasma species inlet concentrations and validates the proposed mass transfer and kinetic reaction models for the new GAD reactor. The inlet reagent flow rates were calculated to be 7.47×10^{-9} and 5×10^{-8} mol s^{-1} for $NO_2^{\bullet}$ and HONOO, respectively.

After the identification of plasma phenolic byproducts in the previous section, the parallel reaction system for such byproducts is presented as follows:

$$\text{Phenol} + {}^{\bullet}\text{OH}^{(l)} \xrightarrow{k_8} \text{Cathecol} \qquad \textbf{(R 70)}$$

$$\text{Phenol} + {}^{\bullet}\text{OH}^{(l)} \xrightarrow{k_9} \text{Hydroquinone} \qquad \textbf{(R 71)}$$

$$\text{Phenol} + {}^{\bullet}\text{OH}^{(l)} \xrightarrow{k_{10}} \text{Resorcine} \qquad \textbf{(R 72)}$$

$$\text{Phenol} + \text{NO}_2^{\bullet(l)} \xrightarrow{k_{11}} 2\text{Nitrophenol} \qquad \textbf{(R 73)}$$

$$\text{Phenol} + \text{NO}_2^{\bullet(l)} \xrightarrow{k_{12}} 4\text{Nitrophenol} \qquad \textbf{(R 74)}$$

Once again, the proposed model was simulated using COMSOL 5.5 software. The calculated concentrations were fitted to the measured ones in order to fix the byproduct's constant rates; the procedures algorithm is presented in Figure 48.

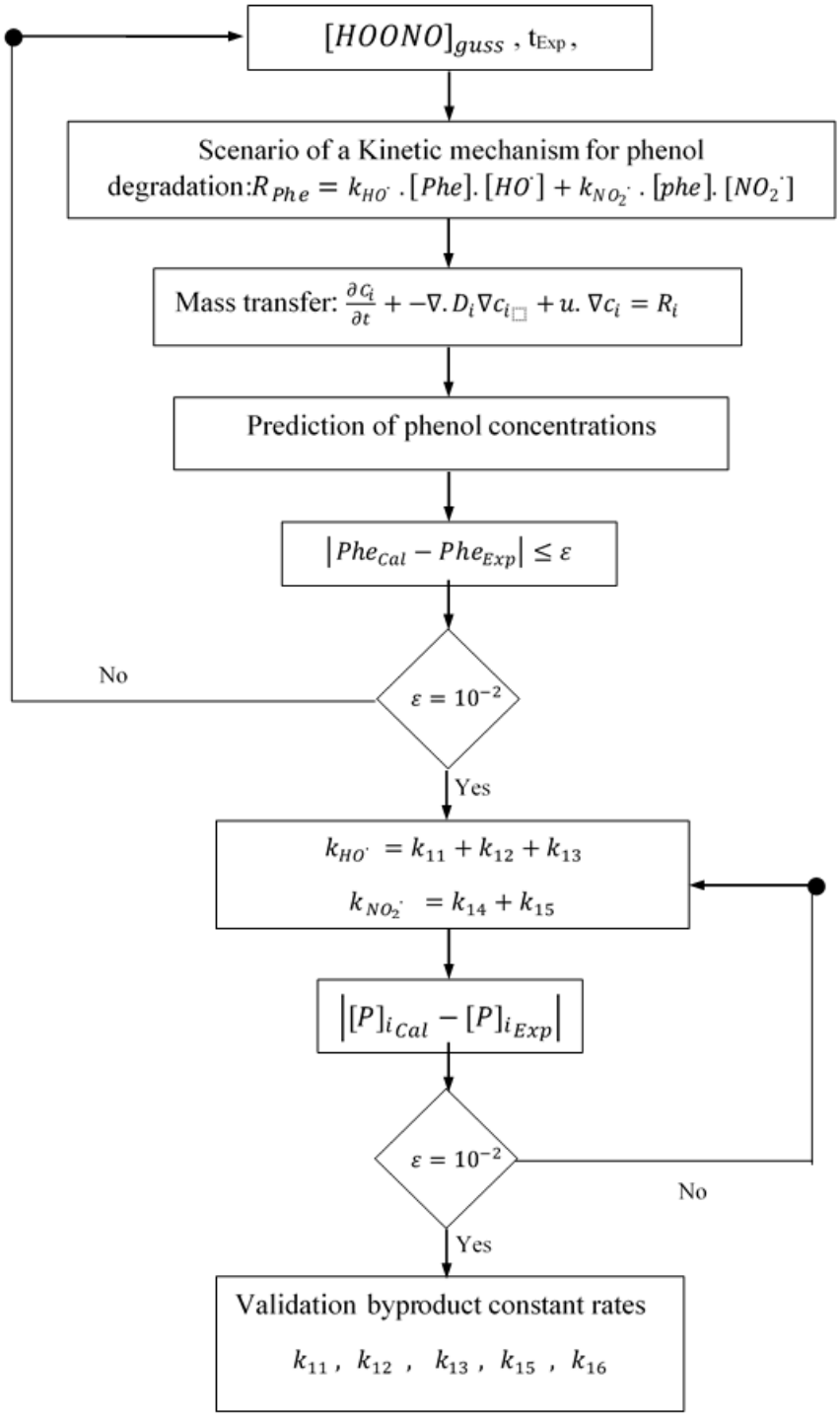

Figure 48. Simulation algorithm

Figure 48 presents the final fitted results showing a great match to the experimental ones for hydroxylation constant rates of about 9.81×10^6, 6.13×10^4 and 3.43×10^3 m^3 mol^{-1} s^{-1} for catechol, hydroquinone and resorcin, respectively. In contrast, the nitration ones are about 2×10^5 and 8×10^5 m^3 mol^{-1} s^{-1} for 2-nitrophenol and 4-nitrophenol, respectively. It is clear that catechol

has the highest production constant rate, which reflects the high affinity of the studied process to convert phenol to catechol and is shown by its production selectivity factor when compared to the other byproducts as discussed in the previous section. 2 and 4-nitrophenols have present a constant rate bit higher than hydroquinone and resorcin but a less production quantity than the subsequent ones, this can be explained by the minor quantity of nitrogen reactive species comparing to hydroxyl radicals. It is important to notice that plasma chemical reactions are superfast reactions, which can be preliminarily checked from their high reactivity presented by a constant rate of around 10^6 m^3 mol^{-1} s^{-1}. In this context, the calculated Hatta number was 2.11×10^5 for the phenol hydroxylation reaction and 6.67×10^4 for the nitration one. These Hatta values are extremely higher than those of the literature abacuses, which temporarily makes the distinction between regimes such as reaction impossible. A special abacus for such reactions is highly required and serves for the right process dimensioning.

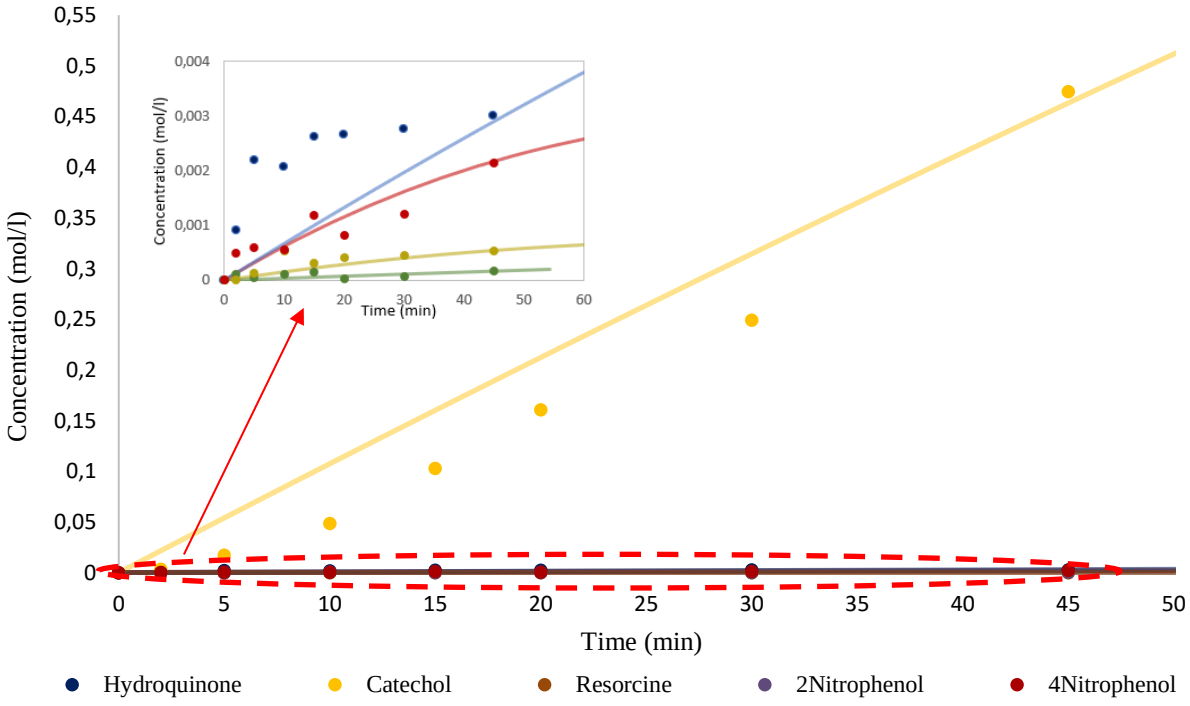

Figure 49. Evolution of phenol byproducts concentrations: measured and calculated

3.2 Process Simulation

This subsection focused on conceptualising and designing the novel catechol production process that combines several chemical and physical activities such as feed preparation, absorption, reaction and product purification. The simulation was conducted using Aspen HYSYS software (version 11) based on the experimentally fixed process parameters, such as mass

transfer and kinetic mechanisms, and the determined byproduct constant rates. HYSYS is one of the most used process simulators because of its interactable and simple interface. It provides numerous functionalities that address the process engineering challenges in several industries. The study was carried out in order to determine the physicochemical properties of plasma species, fixe an industrial parametric scale for the proposed process and estimate its economic revenues.

3.2.1 Thermodynamic model

In our simulation using HYSYS software, the NRTL (Non-Random Two Liquids [195]) model was used to simulate the conversion of phenol solution to catechol and estimate the physicochemical properties of the hypothetical components. The NRTL (Non-Random Two Liquids) model is a thermodynamic model that describes liquid-liquid equilibrium (LLE) in mixtures of two components. It is based on the concept of non-randomness in molecular interactions within the liquid phase. The NRTL model is particularly useful for systems where the components have different sizes and shapes, leading to non-ideal mixing behavior.

3.2.2 Component List

Table 02 presents all chemical components used in this simulation with all detailed properties that allow the thermodynamic model to predict their behavior in the simulation environment. Phenol, water, hydroquinone and N_2O_4 were directly added from the HYSYS pure component list. However, oxygen and nitrogen radicals and phenol byproducts are unlisted. The latter have been added as hypothetical components, and their physicochemical properties, such as the critical parameters properties, have been estimated based on the molecular weight, temperature boiling point, and density that have been directly added from the literature. Meanwhile, plasma chemical species like $^{\bullet}OH$, $NO_2^{\bullet}$ and HONOO were fully estimated based on experimental data of catechol and phenol byproduct mass fraction after simulation of the production process using COMSOL predicted constant rates and other parameters. The estimation study used a HYSYS function called “Estimate unknown”.

Phenol byproducts are classified as isomers with the same molecular weight. However, the position of the added hydroxyl function may show different properties like normal boiling point, absorbance wavelength, liquid density and critical parameters; this difference allows the separation of phenol by the product under specific conditions and special operation unit, like a component splitter which separates the mixture based on different standard boiling point as used in our simulation study. The simulation of the catechol production process fixed plasma

radicals properties, where it shows that $^{\bullet}OH$, $NO_2^{\bullet}$ and HONOO have a normal boiling point of 30,35,35 C, respectively and liquid densities of 925, 995 and 615.75 kg m^{-3}, respectively, too, the prediction study have shown different critical parameters of the outlined chemical species.

Table 18 summarized all predicted data.

Table 18. Physico-chemical properties of the participation compound

Reagents (name & formula)	Normal Boiling point [°C]	Masse molaire (g mol^{-1})	Liquid density [Kg m^{-3}]	Tc [°C]	Pc [KPa]	Vc [m^3 $Kmole^{-1}$]	
$^{\bullet}OH$	30	17	923	233,87	7545,23	0,1953	b
$NO_2^{\bullet}$	35	46	995	244,69	8428,57	0,1879	b
HONOO	35	63	615.75	190,98	3285,29	0,314	b
N2O4	29,07	92,01	1463,43	158.00	10132	8,25	a
Phenol (Acide phénique) (Acide carbolique) C_6H_6O	181,7	94,11	1070	421.1	6121	0.2290	a
1,2-Dihydroxybenzène (Catechol) $C_6H_6O_2$	245	110,11	1340	525.05	3561.81	0.2196	b
1,3-Dihydroxybenzène (Resorcin) $C_6H_6O_2$	277	110,11	1280	556.41	3436.12	0.4134	b
1,4-dihydroxybenzène (Hydroquinone) $C_6H_6O_2$	286,5	110,11	1358	548,85	7450,00	0,3000	a
1,4-Benzoquinone $C_6H_4O_2$ (p-Benzoquinone)	180	108.10	1320	448.03	4504.41	0.2923	b
2-Nitrophénol $C_6H_5NO_3$	216	139.10	1495	493.70	3732.93	0.1771	b
4-Nitrophénol $C_6H_5NO_3$	279	139.10	1480	565.15	3112.63	0.4074	b

a.From data **b**.Calculated.

3.2.3 Process description

Figure 4 represents the process flow diagram of the novel catechol production process. Our proposed process focused on using plasma GAD technology as a source of highly reactive species. This process provides a simple, green, and efficient catechol production method by directly hydroxylating the phenol substrate. This action can be resumed in three simple steps: feed preparation, reactive absorption, and product purification.

The process was first simulated on a laboratory scale range concerning the conducted experiment parameters to fix the process simulating parameters and conditions; then, an industrial scale range was proposed by studying the influence of both phenol solution and plasma gas flowrates on the catechol production masses.

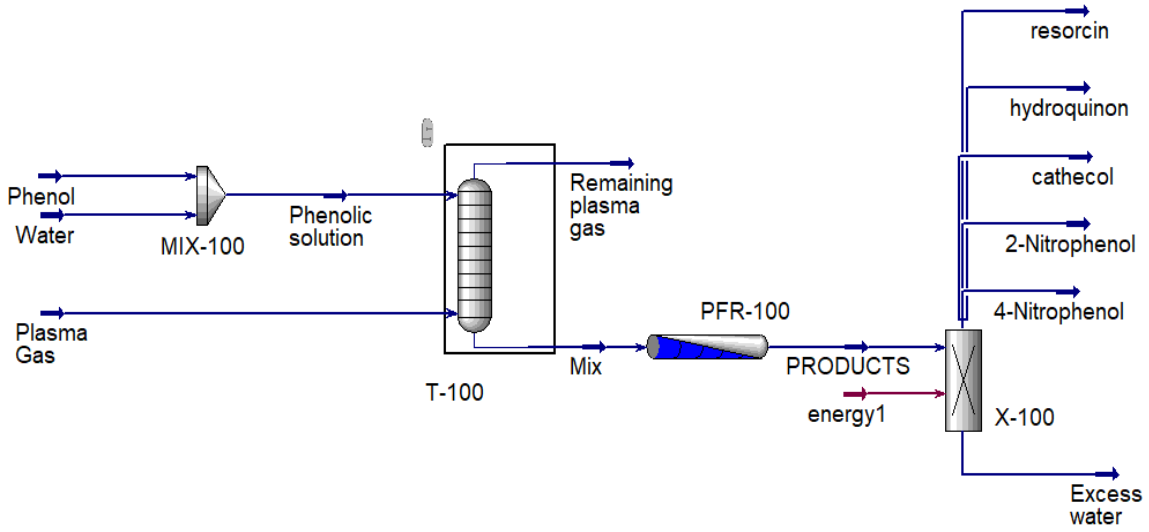

Figure 50. PFD of catechol production process using plasma reactor

3.2.3.1 Feeds preparation

Air, water, phenol and high-voltage electricity are the main raw materials for our proposed process. These impute present a low cost, Eco friendship and safe operability, which allow the novel process to be easily implemented on an industrial production scale. In our simulation study, plasma gas was directly added as an impute stream comprising the plasma spices defined in the component list as hypotheticals after estimating their physicochemical properties. Figure 1 presents the feed preparation section.

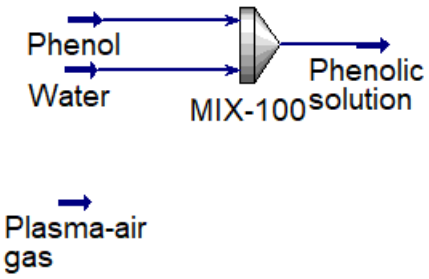

Figure 51. PFD of catechol production process using plasma reactor

Table 19. Input and outlet stream parameters for the feeds preparation section

Feeds preparation section					
	Parameters	Inlet			Outlet
		Phenol	Water	Plasma-air gas	Phenol solution
Stream	Vapour Phase Fraction	0.000	0.000	0.000	0.000
	Temperature [C°]	20.00	20.00	50.00	20.00
	Pressure [atm]	1.000	1.000	1.000	1.000
	Volume flowrate [m^3h^{-1}]	$9{,}451\times10^{-7}$	$9{,}999\times10^{-3}$	0.700	1.000×10^{-2}
	Composition (Mass fraction)	C_6H_5OH: 1.000	H_2O: 1.000	Air: 0.9082	C_6H_5OH: 0.9999
				HONOO: 0.0618	
				N_2O_4: 0.0301	H_2O: 0.0001
Mixter	Pipe diameter [m]	0.010			

Table 19 resumes all information parameters of the inlet and outlet streams of the outlined section. The plasma gas stream was fixed at 50 C°, 1 atm and 0.7 m^3 h^{-1} flowrate with a composition of 0.9082, 0.0618 and 0.0301 mass fractions of air, HONOO and N_2O_4, respectively; the composition was fixed concerning their concentrations in the previous COMSOL simulation study, phenol and water feeds were mixed to generate a phenol solution stream at 20 C°, 1 atm and 0.01 m^3 h^{-1} flowrate with 00.01% of phenol mass fraction that refers to a concentration of 1 mM.

3.2.3.2 Reactive absorption

Because of the plasma GAD nature, an absorption column was coupled with a plug reactor to simulate the reactive absorption conducted by the GAD-VNT for the proposed process. At first, the phenol solution passes in the counter current with the plasma gas flow in an absorption column of 10 stages and normal pressure and temperature conditions. Table 20 presents the highlighted streams and operation unit parameters.

Table 20. Input and outlet stream parameters for the Reactive absorption section

Reactive absorption section							
Stream	Parameters	Inlet		Intermediate		Outlet	
		Phenol solution	Plasma-air gas	Mixture	Remaining gas	Products	Energy01
	Vapour Phase Fraction	0.000	0.000	0.000	1.000	0.000	
	Temperature [C°]	20.00	50.00	27.31	38.45	30.00	
	Pressure [atm]	1.000	1.000	1.000	1.000	1.000	
	Volume flowrate [m^3h^{-1}]	1.000×10^{-2}	0.700	2.962×10^{-3}	0.7070	3.120×10^{-3}	
	Composition (Mass fraction)	C6H5OH : 0.9999	Air: 0.9082	Air: 0.0002	Air: 0.9398	Air: 0.0003	
				H_2O: 0.9301	H_2O: 0.0215	H_2O: 0.7760	
			HONOO: 0.0618	HONOO: 0.0544	HONOO : 0.0290	•OH: 0.0428	
			N_2O_4: 0.0301	N_2O_4: 0.0152	N_2O_4: 0.0097	HNO_3: 0.0233	
				C_6H_5OH: 0.0001		HNO_2: 0.1573	
						Catechol: 0.0003	
	Heat flow rate [KJ h^{-1}]						434.5

Absorber	Pipe diameter [m]	0.010
Plug reactor	Number of stages Volume (m^3) Mixture Temperature (°C) Mixture Pressure (kPa)	10 $3{,}927\times10^{-5}$ 27.73 101.3

The absorber volume was calculated to be $3{,}927\times10^{-5}$ m^3 in lab scale simulation and 0.8836 m^3 in industrial one. The lean gas is released into the atmosphere under normal pressure and temperature conditions. The mixture effluent exits the absorption column with a plasma species mass fraction of about 0.0618 of HONOO and 0.0301 of N_2O_4 with a total flow rate of 2.743 kg h^{-1}. The latter enters the plug reactor of 03 10^{-4} m^3, where the reaction conditions are ensured. Figure 52 presents the reactive absorption system. Firstly, the long-lived species dissociate to hydroxyl and nitrogen dioxide radicals, which react with phenol molecules to produce catechol and other byproducts, as discussed in the previous sections. This reaction system presents an exothermic behavior responsible for a thermic energy release of about 399.2 kg h^{-1}. The product stream effluent presents a catechol mass fraction of 0.0003 with 100% selectivity concerning catechol. However, the product stream contains undesirable species like nitrite and nitrate and may have an important other byproduct quantity for a large production scale. Therefore, a purification system is highly recommended.

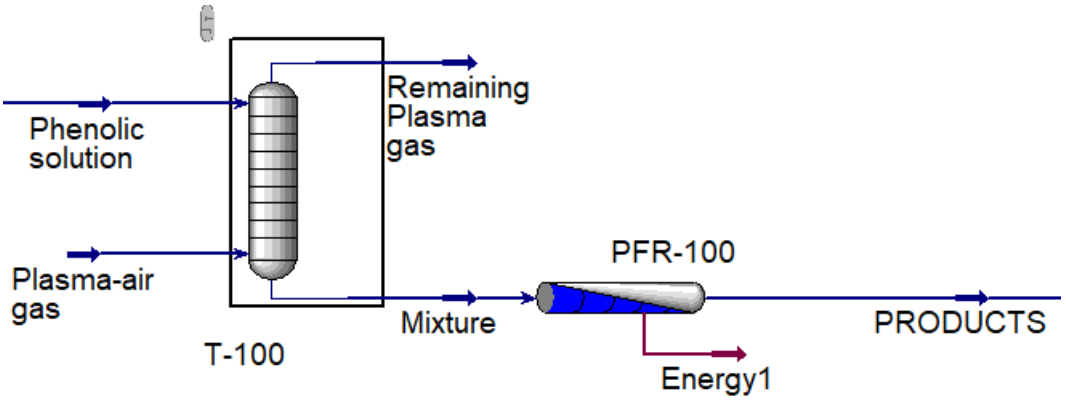

Figure 52. PFD of catechol production process using plasma reactor

3.2.3.3 Product purification

Figure 1 presents the purification system. Here, a component splitter was used to ensure the purification of the produced catechol. This unit separates phenol byproducts, water and other desirable components based on their normal boiling temperature. An energy of 6.457×10^{-3} kg h^{-1} was consumed for the outlined activity. The system provides a pure catechol flow of 8.583×10^{-6} kg h^{-1}. Table 1 shows the resulting component flowrates.

Table 21. Input and outlet stream parameters for the feeds preparation section

Feeds preparation section					
Stream	Parameters	Inlet	Outlet		
		Products	Catechol	Remaining water	Energy02
	Vapour Phase Fraction	0.000	0.000	0.000	-
	Temperature [C°]	30.00	30.00	30.00	
	Pressure [atm]	1.000	1.000	1.000	
	Volume flowrate [$m^3\,h^{-1}$]	3.120×10^{-3}	8.541e-007	3.120×10^{-3}	
	Composition (Mass fraction)	Air: 0.0003	Catechol: 1.000	Air: 0.0003	
		H2O: 0.7760			
		•OH: 0.0428		H2O: 0.6839	
		NO3-:0.0233			
		NO2-:0.1573		•OH: 0.0407	
		Cate-chol:0.0003		NO^{3-}:0.0387 NO^{2-}:0.2368	
	Heat flow rate [kJ h^{-1}]				479.8
Component splitter	Pipe diameter [m]	0.010			

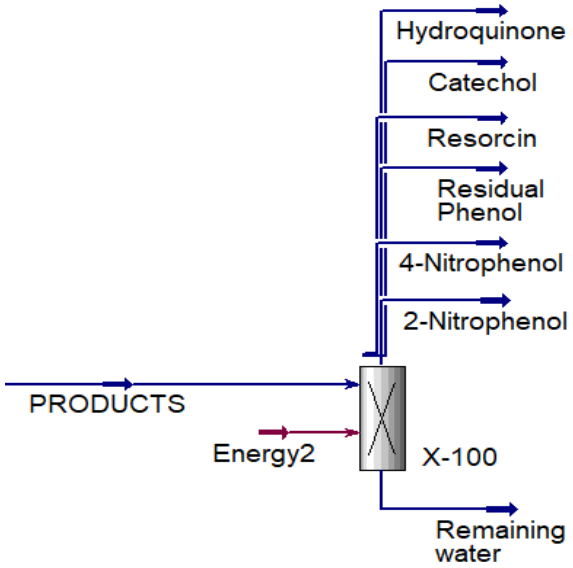

Figure 53. PFD of catechol production process using plasma reactor

4. Economic evaluation

4.1 Process economic study

An economic study was conducted using Aspen Process Economic Analyzer (APEA) software to determine the financial feasibility of the proposed process. Total capital cost, Total operating cost and total product sales were estimated concerning the process flow rates and component concentrations.

Table 19 shows the main economic assumptions used in this study. It is a production plant located in North America. The site is on the Gulf Coast in Texas, USA, for economic reasons such as market access, utility rates and corporate income tax. The project is scheduled to begin in 2025, with a construction period of 2.5 years and a commissioning and start-up (C&SU) period of one year. Once construction is 100% complete, operations can begin. The plant is expected to reach 50% of its capacity at start-up and, in subsequent years, will reach full capacity. It is estimated that the project will have a lifespan of 20 years, which is in line with other similar processes and technologies. An annual discount rate of 8.0% has been applied to consider the time value of money. In addition, the US Bureau of Labor Statistics in 2018 established an inflation rate of 1.9% for the project's life [196]. To account for plant overhauls and unscheduled shutdowns, an operating rate of 91% (7,992 operating hours per year) is assumed.

Table 22. Project economic assumptions

Component	Price	Reference
Water	17.44 USD m^{-3}	[198]
Phenol	1.1 USD kg^{-1}	[197]
Catechol	2.8 USD kg^{-1}	[197]
Hydroquinone	7.7 USD kg^{-1}	[197]
Resorcin	7.9 USD kg^{-1}	[197]
2-Nitrophenol	453.1 USD kg^{-1}	[197]
4-Nitrophenol	460.1 USD kg^{-1}	[197]

The sizing of the equipment, its cost and the estimated price of the components ensure the credibility of this study. Reference prices for the indexed API of phenol and its derivatives were obtained from the PharmaCompass organization [197]. The catechol product was 2.5 times more expensive than the phenol reagent, a significant preliminary economic indicator. In addition, the water solvent was estimated at USD 17.44 per 1 m^3 by the Canadian Water Safety Agency [198]. All prices and references are summarized in Table 23.

Table 23. Materials raw and products prices

Parameters	Values
Referenced Year of Project Initiation	2025
Project Life	25 years
Project Location	Texas, US
Inflation rate	1.9%
Annual discount rate	8.0%
Construction period	2.5 years
Start-up (C&SU) period	1 Year
Operating hours per year	7992 hours (91% on-stream factor)

Since plasma gas does not have a precise price, an estimate was made based on the input gas equipment and the energy consumed, resulting in 0.1738 USD h^{-1}. It should be noted that this competition price is based on free air used as fuel. The different methods of calculating the price are set out in Table 24.

Table 24. Plasma gas price estimating procedure

	Item cost		life time	Reference	Cost (USD h^{-1})
Equip-ment	Air com-pressor	3775	25	[199]	0,0172
	Plasma GAD	5000	5	[200]	0,114
Inlets	Air gas (0,7 $m^3 h^{-1}$)	-		-	FREE
	Electricity (0,3 kW h^{-1})	0,142 USD kWh^{-1}		[196]	0,0426
Plasma gas price	-				0,1738

The Aspen HYSYS mapping action window was used to automatically map the process equipment, except the mixer and component separator, which were mapped as a top open agitator and multi-diameter tower from the list of operating units in the HYSYS map preview. HYSYS' smoother sizing option automatically sizes the operating units according to the process flow scale.

In addition to the lab scale flow rate, nine flow rate stages were selected based on the highest masses of catechol produced, with a selectivity more significant than 95%. Table 25 shows the results calculated with the corresponding flow rates. Equipment and installation costs, which increase with the size of the equipment, are calculated by this simulation using the APEA software. Usage and operating costs are high, reaching USD 2,861,260 $year^{-1}$ for the highest process throughputs considered. Furthermore, the results demonstrate a linear increase in total raw material costs as a function of process throughputs. These improvements even result in a high overall investment cost, demonstrating increased product sales. By comparing product sales to raw materials, utilities and operating costs for flow rates of 2 and 1 $m^3 h^{-1}$ of plasma gas and phenol solution, the calculations show that the process is starting to generate a beneficial income. However, this information suggests a negative income if the total cost of capital is considered for the first year and can be balanced after 27 months of product sales. From the first year, a net profit is generated for higher flow rates, increasing from 5819269.9 to 167065826.9 USD $year^{-1}$ for flow rates of 3 to 10 $m^3 h^{-1}$.

Table 25. Catechol production economical cost and revenues summary

Nº	0	1	2	3	4	5	6	7	8	9
Plasma gas flow rate ($m^3 h^{-1}$)	0.7	2	3	4	5	6	7	8	9	10
Phenol solution flow rate ($m^3 h^{-1}$)	0.01	1	2	3	4	4	5	6	7	8
Catechol produced mass flow rate (kg h^{-1})	0.0009	115.22	226.959	348.194	460.045	554.847	576.481	692.761	790	843.173
Selectivity (%)	100	98.63	96.62	98.56	97.35	95.37	97.84	97.92	95.14	96.05
Total capital cost (USD)	4712470	4772800	4891420	4907200	4988220	4988220	5047900	5047900	5108790	5110070
Total operating cost (USD $year^{-1}$)	1644440	1798740	1950570	2102640	2253580	2253580	2407420	2556700	2711980	2861260
Total raw materials cost (USD $year^{-1}$)	1652.06	138222	276995	415218	553991	553991	692213	830435	969208	1107430
Total product sales (USD $year^{-1}$)	145155	2998090	12990600	13963900	47407800	15321700	23310600	37726400	153443000	1.76E+08
Total utilities cost (USD $year^{-1}$)	50824.7	52345.1	52345.1	53612.1	53612.1	53612.1	54879.1	54879.1	57413.1	57413.1
Desired rate of return (Percent $year^{-1}$)	20	20	20	20	20	20	20	20	20	20
P.O.Period (year)	0	0	4.8542	4.77406	3.33843	4.65891	3.96877	3.52721	2.96847	2.85559
Equipment cost (USD)	72600	101200	112600	119400	125700	125700	143100	143100	157500	157900
Total installed cost (USD)	461900	493000	533400	541500	564000	564000	595300	595300	618300	618900
Process revenues (USD $year^{-1}$)	-6264231.76	-3764017.1	5819269.9	6485229.9	39558396.9	7472296.9	15108187.9	29236485.9	144595608.9	167065826.9
Sales/cost ratio	0.0228	0.4468	1.8248	1.8806	6.0812	1.9653	2.8610	4.4725	17.4565	19.4081

Conclusion

Catechol production via a plasma hydroxylation of phenol solution can be a sustainable pathway to meet future global catechol market demands. In order to overcome the technical and economic challenges of the outlined process, this study investigated the use of plasma gliding arc discharge as a powerful hydroxylation technology. The primary objective was reached by the conceptualizing of a novel configuration called GAD-VNT. This later showed better performances in phenol conversion rate and catechol production selectivity of 48% and 97%, respectively, at 45 min of plasma exposure time. The second objective was to estimate the physicochemical properties of plasma spices and simulate the plasma chemical processes for the first time using HYSYS software. These properties help predict behaviors in different simulation conditions. The third objective was to extrapolate the proposed process to an industrial scale. Therefore, a process parametric study was conducted to fix a feasible value based on catechol selectivity and production masses. This parametric optimization was followed by a project economic feasibility, where it found that the process presents a promising revenue from the first year for a process flowrate upper than 3 and 2 $m^3 h^{-1}$ of plasma gas and phenol solution, respectively and can reach a maximum annual income of 167 million USD $year^{-1}$. The proposed process presents further advantages like eco-friendship and high safety levels by using water as process solvent instead of organic compounds, which are obviously employed in conventional productions. This study can be used as a model for large industrial companies wishing to integrate plasma reactors into their current processes.

General conclusion

This thesis focused on the control of oxidative processes in plasma reactors. For this purpose, a bibliographic study was carried out to determine and understand the different processes in non-thermal plasma, from its creation to its interaction with the target molecules, whether in gas or liquid. Plasma treatment of liquids includes a very important phenomenon which strongly influences the effectiveness of these processes, namely the absorption of plasma species into the liquid being treated. As these technologies have shown high performance in water depollution, they also present selective limitations for chemical synthesis processes. Therefore, different methods and means of controlling oxidative processes in these reactors have been widely discussed.

A new glidarc apple GAD-V configuration has been developed in this thesis. The innovation in this new configuration involves using the venturi system as the absorption system for the plasma gas produced in a GAD reservoir. Like the GAD-ST configuration, the new configuration features a spatiotemporal post-discharge treatment mode. However, the venturi system instead of the spray column and the 1 m long spiral tube increased the latter's performance.

The properties of the four Glidarc plasma configurations were evaluated. The first study determined the overall transfer coefficient by a Simulink simulation of the phenol concentration profile in a stripping experiment. Thus, experiments were carried out to monitor the acidity, conductivity, concentrations of nitrite and nitrate ions and the evolution of total oxidants during treatment. The results showed the influence of the discharge type and the absorption system on the properties of each configuration. In a second step, the efficiency in these reactors was examined by measuring the decolorization, conversion and selectivity rates. The four reactors presented different degrees of efficiency. Therefore, a more in-depth study was developed on the reaction-mass transfer competition based on the double film theory to find the right configuration for the right application. The plotting of the concentration profiles of the reactants within the liquid film explained the different properties and performances presented by the four configurations well. Subsequently, a classification of the studied configurations was carried out concerning phenol conversion rate, catechol selectivity and safety aspect (HAZOP-SIL study), where the new GAD-V reactor showed the best formula of efficiency-safety couple evaluation.

In light of the results obtained in Chapter III, a new industrial process was developed aiming at the massive production of catechol from phenol and using the GAD-V plasma reactor. The

HYSYS simulation allowed us to conduct a traffic flow optimization study to evaluate conversion rate, selectivity, and economic aspects. The calculations indicate that the process presents a beneficial income from the first year for a flow rate of 2 and 1 $m^3 h^{-1}$ of plasma gas and phenol solution, respectively. Moreover, it can recover the total capital cost for 27 months of product sales. For upper flow rates, a net profit is achieved from the first year and increases from 5.82 to 167 million USD $year^{-1}$ for the flow rates scale from 3 to 10 $m^3 h^{-1}$.

The general objective of this research thesis is to place the plasma reactor in a homogeneous classification with other conventional reactors and also to guide applications, decontamination or synthesis according to chemical control and/or a given type of reactor.

References

[1] Perucca, Massimo. "Introduction to plasma and plasma technology." Plasma Technology for Hyperfunctional Surfaces: Food, Biomedical, and Textile Applications (2010): 1-32.

[2] Yesodharan, Suguna. "Supercritical water oxidation: an environmentally safe method for the disposal of organic wastes." CURRENT SCIENCE-BANGALORE- 82.9 (2002): 1112-1122.

[3] Czernichowski, A. "Plasmas pour la destruction de l'H2S et des mercaptans." Oil & Gas Science and Technology 54.3 (1999): 337-355.

[4] B. Benstaali « Étude des propriétés chimiques des espèces $HO^{\cdot}$ et $NO^{\cdot}$ créées par un plasma non thermique d'air humide de type Glidarc. Application au traitement d'aciers inoxydables », PhD thesis, University of Sidi Bel Abbes, (2001).

[5] Depenyou, François Junior. Etude du plasma d'arc électrique glissant à pression atmosphérique dans l'air humide : Application à l'amélioration des propriétés anticorrosives d'un acier doux. Diss. Rouen, 2007.

[6] Fridman, Alexander. Plasma chemistry. Cambridge university press, 2008.

[7] Held, Bernard. Physique des plasmas froids. No. 180. Elsevier Masson, 1994.

[8] Eugen, Hnatiuc. "PROCEDES ELECTRIQUES DE MESURE ET DE TRAITEMENT DES POLLUANTS." Paris (2002).

[9] Doubla, Avaly. Étude des propriétés acido-basiques et radicalaires en phase plasma: application à la réactivité chimique du monoxyde de carbone activé par un plasma froid type décharge couronne à la pression atmosphérique. Diss. Thèse de Doctorat, Université Pierre et Marie Curie, France, 1989.

[10] Chang, J-S., Phil A. Lawless, and Toshiaki Yamamoto. "Corona discharge processes." IEEE Transactions on plasma science 19.6 (1991): 1152-1166.

[11] Van Veldhuizen, E. M., and W. R. Rutgers. "Pulsed positive corona streamer propagation and branching." Journal of Physics D: Applied Physics 35.17 (2002): 2169.

[12] Kogelschatz, Ulrich. "Dielectric-barrier discharges: their history, discharge physics, and industrial applications." Plasma chemistry and plasma processing 23.1 (2003): 1-46.

[13] Schutze, Andreas, et al. "The atmospheric-pressure plasma jet: a review and comparison to other plasma sources." IEEE transactions on plasma science 26.6 (1998): 1685-1694.

[14] J.L Cormier « dépollution des effluents gazeux », Image de la physique, 2003

[15] Allégraud, Katia. Décharge à barrière diélectrique de surface: physique et procédé. Diss. Ecole Polytechnique X, 2008.

[16] Doubla, A. "Propriétés oxydo-réductrices des plasmas non thermiques d'air humide: application à la dépollution des eaux et à la corrosion métallique." Diplôme d'Habilitation à Diriger les Recherches, Université de Rouen (2002).

[17] Chang, J-S., Phil A. Lawless, and Toshiaki Yamamoto. "Corona discharge processes." IEEE Transactions on plasma science 19.6 (1991): 1152-1166.

[18] Cao, Z., et al. "Spatially extended atmospheric plasma arrays." Plasma Sources Science and Technology 19.2 (2010): 025003.

[19] Cao, Z. W. J. L., James L. Walsh, and Michael G. Kong. "Atmospheric plasma jet array in parallel electric and gas flow fields for three-dimensional surface treatment." Applied Physics Letters 94.2 (2009).

[20] Lu, Xinpei, Mounir Laroussi, and Vincent Puech. "On atmospheric-pressure non-equilibrium plasma jets and plasma bullets." Plasma Sources Science and Technology 21.3 (2012): 034005.

[21] Czernichowski, A. "Gliding arc: applications to engineering and environment control." Pure and Applied Chemistry 66.6 (1994): 1301-1310.

[22] Peyrous, René. Simulation de l'évolution temporelle de diverses espèces gazeuses créées par l'impact d'une impulsion électronique dans de l'oxygène ou de l'air, sec ou humide. Diss. Pau, 1986.

[23] DeLand, Frank H. "CRC Handbook of Chemistry and Physics: RC West, MJ Astle, WH Beyer, Eds. Boca Raton, Florida, CRC Press, Inc., 1983, 2386 pp." (1984): 635-635.

[24] K. Meguernes, J. Chapelle, A. Czernichowski, 11th Int. Symp. Plasma Chem., (Loughborough, Grande Bretagne), Ed. J. Harry, 2, p710-715, 1993.

[25] Iya-Sou, Djakaou. Elimination de solutés organiques polluants d'effluents liquides par plasma non thermique: comparaison des processus mis en jeu à l'interface liquide-plasma dans les procédés Glidarc et DBD. Diss. Paris 6, 2012.

[26] Djakaou, Iya-Sou, et al. "Removal of model pollutants in aqueous solution by gliding arc discharge. Part II: modeling and simulation study." Plasma Chemistry and Plasma Processing 35 (2015): 143-157.

[27] Pascal, Sarah, et al. "Plasma chemical degradation of phosphorous-containing warfare agents simulants." Journal of hazardous materials 175.1-3 (2010): 1037-1041.

[28] He, Yuan, et al. "Volatile organic compounds degradation by nonthermal plasma: a review." Environmental Science and Pollution Research 30.12 (2023): 32123-32152.

[29] Gong, Xiangjie, et al. "Decomposition of volatile organic compounds using gliding arc discharge plasma." Journal of the Air & Waste Management Association 70.2 (2020): 138-157.
[30] Slamani, Samira, et al. "Initiation of Fenton process by plasma gliding arc discharge for the degradation of paracetamol in water." Journal of Photochemistry and Photobiology A: Chemistry 359 (2018): 1-10.
[31] GHEZZAR, Mouffok Redouane. Traitement par plasma glidarc de composés toxiques et de rejets industriels. Diss. Université de Mostaganem-Abdelhamid Ibn Badis, 2006.
[32] Merouani, D. R., et al. "Influence of peroxynitrite in gliding arc discharge treatment of alizarin red s and postdischarge effects." Industrial & Engineering Chemistry Research 52.4 (2013): 1471-1480.
[33] Abdelmalek, Fatiha, et al. "Bleaching and degradation of textile dyes by nonthermal plasma process at atmospheric pressure." Industrial & engineering chemistry research 45.1 (2006): 23-29.
[34] Kusano, Yukihiro, et al. "Observation of gliding arc surface treatment." Surface Engineering 31.4 (2015): 282-288.
[35] Dimitrakellis, Panagiotis, et al. "Plasma surface modification of epoxy polymer in air DBD and gliding arc." Processes 10.1 (2022): 104.
[36] Kusano, Yukihiro, et al. "Gliding arc discharge—Application for adhesion improvement of fibre reinforced polyester composites." Surface and Coatings Technology 202.22-23 (2008): 5579-5582.
[37] Hong, Seung-Hyun, Tae-Hee Kim, and Sooseok Choi. "Hydrophilic surface modification of polytetrafluoroethylene film with gliding arc plasma." Applied Science and Convergence Technology 28.4 (2019): 101-106.
[38] Men, Shangwu, et al. "Insight into the corrosion behaviors and mechanism of arc discharge plasma nitrided H13 steel in molten Al-Si." Applied Surface Science 670 (2024): 160584.
[39] Wang, Y. H., et al. "Enhancing wear resistance of TiN coating by gradient bias voltage and arc-enhanced glow discharge." Ceramics International 48.6 (2022): 8746-8750.
[40] Yang, Zhibo, et al. "Structural evolution, wear and corrosion failure mechanisms of CrN coating synthesized by applying gradient voltage and arc-enhanced glow discharge." Materials Today Communications (2024): 109361.
[41] Bacci, Tiberio, et al. "Wear resistance of Ti–6Al–4V alloy treated by means of glow-discharge and furnace treatments." Wear 240.1-2 (2000): 199-206.
[42] Wang, Jian-Qing, et al. "Double glow plasma carburization on zirconium to improve surface hardness and wear resistance." Rare Metals 36 (2017): 569-573.
[43] Ghali, Noureddine, et al. "Corrosion inhibition of carbon steel in 0.5 M NaCl aqueous solution by humid air plasma treatment." The European Physical Journal-Applied Physics 61.3 (2013): 30801.
[44] Liu, Hongbing, et al. "Corrosion and tribological behaviors of chromium oxide coatings prepared by the glow-discharge plasma technique." Surface and Coatings Technology 204.1-2 (2009): 28-36.
[45] Zhang, Hao, et al. "Plasma-enhanced catalytic activation of CO 2 in a modified gliding arc reactor." Waste Disposal & Sustainable Energy 2 (2020): 139-150.
[46] Ma, Xintong, et al. "Carbon nanosheets synthesis in a gliding arc reactor: on the reaction routes and process parameters." Plasma Chemistry and Plasma Processing 41 (2021): 191-209.
[47] Snyders, Rony, et al. "Foundations of plasma enhanced chemical vapor deposition of functional coatings." Plasma Sources Science and Technology 32.7 (2023): 074001.
[48] Martinu, Ludvik, O. Zabeida, and J. E. Klemberg-Sapieha. "Plasma-enhanced chemical vapor deposition of functional coatings." Handbook of deposition technologies for films and coatings (2010): 392-465.
[49] Sanchez, I., et al. "Plasma-enhanced chemical vapor deposition of nitrides on fluidized particles." Powder Technology 120.1-2 (2001): 134-140.
[50] Burlica, R., et al. "Bacteria inactivation using low power pulsed gliding arc discharges with water spray." Plasma Processes and Polymers 7.8 (2010): 640-649.
[51] Du, Chang Ming, et al. "The application of a non-thermal plasma generated by gas–liquid gliding arc discharge in sterilization." New Journal of Physics 14.1 (2012): 013010.
[52] Kim, Hyoung S., et al. "Use of plasma gliding arc discharges on the inactivation of E. Coli in water." Separation and Purification Technology 120 (2013): 423-428.
[53] Laroussi, Mounir, Michael Keidar, and Vladimir I. Kolobov, eds. Low-Temperature Plasma for Biomedical Applications. Frontiers Media SA, 2023.
[54] Moszczyńska, Julia, Katarzyna Roszek, and Marek Wiśniewski. "Non-thermal plasma application in medicine—focus on reactive species involvement." International Journal of Molecular Sciences 24.16 (2023): 12667.
[55] Han, Justine. "Review of major directions in non-equilibrium atmospheric plasma treatments in medical, biological, and bioengineering applications." *Plasma Medicine* 3.3 (2013).
[56] Orazov, Marat, Yukinori Sakiyama, and David B. Graves. "Wound healing modeling: investigating ambient gas plasma treatment efficacy." Journal of Physics D: Applied Physics 45.44 (2012): 445201.

[57] Montaser, S. A., et al. "Cytogenetic and biochemical investigations of cultured leukemia cells exposed to gliding arc discharges." Plasma Medicine 7.1 (2017).
[58] Roy, N. C., et al. "Atmospheric pressure gliding arc discharge plasma treatments for improving germination, growth and yield of wheat." Plasma Science and Technology 20.11 (2018): 115501.
[59] Arjunan, Krishna Priya, et al. "Non-thermal dielectric barrier discharge plasma induces angiogenesis through reactive oxygen species." Journal of the Royal Society Interface 9.66 (2012): 147-157.
[60] Ishikawa, Kenji, et al. "Generation and measurement of low-temperature plasma for cancer therapy: A historical review." *Free Radical Research* 57.3 (2023): 239-270.
[61] Sheikhlary, Sara. Effects of Atmospheric–Pressure Cold Plasma on cancer cells with the aim of cancer treatment. Diss. Kharazmi University, 2019.
[62] Subramanian, PS Ganesh, et al. "Plasma-activated water from a dielectric barrier discharge plasma source for the selective treatment of cancer cells." Plasma Processes and Polymers 17.8 (2020): 1900260.
[63] Xu, Yujing, et al. "Selective anticancer effects of plasma-activated saline in 3D tumor model co-culturing of normal cells and cancer cells." Journal of Physics D: Applied Physics 57.40 (2024): 405203.
[64] Yan, Dayun, et al. "Cold atmospheric plasma cancer treatment, a critical review." Applied Sciences 11.16 (2021): 7757.
[65] Klimek, Angelique, and Davin G. Piercey. "Nitrogen Fixation via Plasma-Assisted Processes: Mechanisms, Applications, and Comparative Analysis—A Comprehensive Review." Processes 12.4 (2024): 786.
[66] Chen, Hang, et al. "Review of low-temperature plasma nitrogen fixation technology." Waste Disposal & Sustainable Energy 3 (2021): 201-217.
[67] Hollevoet, Lander, et al. "Towards green ammonia synthesis through plasma-driven nitrogen oxidation and catalytic reduction." Angewandte Chemie 132.52 (2020): 24033-24037.
[68] Yaala, Marwa Ben, et al. "Plasma-assisted catalytic formation of ammonia in N 2–H 2 plasma on a tungsten surface." Physical Chemistry Chemical Physics 21.30 (2019): 16623-16633.
[69] Li, Sirui, et al. "Recent progress of plasma-assisted nitrogen fixation research: a review." Processes 6.12 (2018): 248.
[70] Van Alphen, Senne, et al. "Effect of N2 on CO2-CH4 conversion in a gliding arc plasmatron: Can this major component in industrial emissions improve the energy efficiency?." Journal of CO2 utilization 54 (2021): 101767.
[71] Xia, Yun, et al. "Combined steam and CO2 reforming of CH4 for syngas production in a gliding arc discharge plasma." Journal of CO2 Utilization 37 (2020): 248-259.
[72] Indarto, Antonius, et al. "Conversion of CO2 by gliding arc plasma." Environmental engineering science 23.6 (2006): 1033-1043.
[73] Li, Li, et al. "Plasma-assisted CO2 conversion in a gliding arc discharge: Improving performance by optimizing the reactor design." Journal of CO2 Utilization 29 (2019): 296-303.
[74] Zhang, Hao, et al. "Warm plasma activation of CO2 in a rotating gliding arc discharge reactor." Journal of CO2 Utilization 27 (2018): 472-479.
[75] Sun, S. R., et al. "CO2 conversion in a gliding arc plasma: Performance improvement based on chemical reaction modeling." Journal of CO2 Utilization 17 (2017): 220-234.
[76] Indarto, Antonius, et al. "Gliding arc plasma processing of CO2 conversion." Journal of hazardous materials 146.1-2 (2007): 309-315.
[77] Matra, Khanit, et al. "Enhancement of lettuce growth by PAW spray gliding arc plasma generator." IEEE Transactions on Plasma Science 50.6 (2021): 1430-1439.
[78] Chengcheng, L. I. U., et al. "Decontamination of infected plant seeds utilizing atmospheric gliding arc discharge plasma treatment." Plasma Science and Technology 23.10 (2021): 105501.
[79] Angineni, Jyothsna, et al. "Sustainable nitrogen fixation by novel gliding arc plasma reactor for the production of nitrogen fertilizers." Plasma Processes and Polymers: e2400059.
[80] Manaigo, Filippo. Study of a gliding arc discharge for sustainable nitrogen fixation into NOx. Diss. University of Antwerp, 2024.
[81] Theepharaksapan, Suthida, et al. "The Potential of Plasma-Activated Water as a Liquid Nitrogen Fertilizer for Microalgae Cultivation." IEEE Transactions on Plasma Science (2024).
[82] Wu, Sarah, et al. "Nitrate and nitrite fertilizer production from air and water by continuous flow liquid-phase plasma discharge." Journal of Environmental Chemical Engineering 9.2 (2021): 104761.
[83] Zheng, Qiyu, et al. "Plasma Agricultural Nitrogen Fixation Using Clean Energies: New Attempt of Promoting PV Absorption in Rural Areas." Processes 11.7 (2023): 2030.
[84] Ohta, T. "Plasma in agriculture." Cold plasma in food and agriculture (2016): 205-221.
[85] Chuea-uan, Siraporn, et al. "Using Plasma-Activated Water Generated by an Air Gliding Arc as a Nitrogen Source for Rice Seed Germination." Agronomy 14.1 (2023): 15.

[86] Kolev, Stanimir, et al. "Quasi-neutral modeling of gliding arc plasmas." Plasma Processes and Polymers 14.4-5 (2017): 1600110.
[87] Komarzyniec, Grzegorz, and Michał Aftyka. "Operating problems of arc plasma reactors powered by AC/DC/AC converters." Applied Sciences 10.9 (2020): 3295.
[88] Nilsson, Sebastian, et al. "Holistic analysis of a gliding arc discharge using 3D tomography and single-shot fluorescence lifetime imaging." Communications Engineering 3.1 (2024): 103.
[89] Lu, XinPei, et al. "Grand challenges in low temperature plasmas." Frontiers in Physics 10 (2022): 1040658.
[90] Ghezzar, M. R., et al. "New prototype for the treatment of falling film liquid effluents by gliding arc discharge part I: application to the discoloration and degradation of anthraquinonic Acid Green 25." Chemical Engineering and Processing: Process Intensification 72 (2013): 42-50.
[91] Benidris, El Batoul, et al. "Water purification by a new hybrid plasma-sensitization-coagulation process." Separation and Purification Technology 178 (2017): 253-260.
[92] Fridman, A. A., et al. "Modèle physique de l'arc glissant." Journal de Physique III 4.8 (1994): 1449-1465.
[93] Fridman, Alexander. Plasma chemistry. Cambridge university press, 2008.
[94] Gumuchian, Diane. Développement et étude d'un procédé d'oxydation avancée de traitement de l'eau pour composés organiques résistants par couplage plasma/catalyse. Diss. Université Pierre et Marie Curie-Paris VI, 2014.
[95] Slamani, S. Elimination de rejet pharmaceutique par procédés d'oxydation avancée POA. Diss. Thèse de doctorat. Université Abdelhamid Ibn Badis de Mostaganem, Algérie, 2018.
[96] Sobze, Eric Bertrand Tsagou. Application de décharges électriques à pression atmosphériques dans l'air humide à la destruction de composés de haute toxicité et mise au point d'un dispositif de traitement pour des composés organiques volatils| Theses. fr. Diss. Rouen, 2006.
[97] Leriche, Maud. Developpement d'un modele de chimie multiphase couple a un modele de microphysique quasi-spectral: application a un evenement nuageux echantillonne au puy de dome. Diss. Clermont-Ferrand 2, 2000.
[98] Roustan, Michel. Transferts gaz-liquide dans les procédés de traitement des eaux et des effluents gazeux. Paris, France: Tec & Doc Lavoisier, 2003.
[99] Morvan, Daniel. Les opérations unitaires: procédés industriels. Ellipses., 2009.
[100] Roizard, Chrisitn. Absorption avec réaction chimique. Ed. Techniques Ingénieur, 1997.
[101] Danckwerts, P. V. "Significance of liquid-film coefficients in gas absorption." Industrial & Engineering Chemistry 43.6 (1951): 1460-1467.
[102] Mack, John, and James R. Bolton. "Photochemistry of nitrite and nitrate in aqueous solution: a review." Journal of Photochemistry and Photobiology A: Chemistry 128.1-3 (1999): 1-13.
[103] Sweeney, Andrew J., and Y. A. Liu. "Use of simulation to optimize NOx abatement by absorption and selective catalytic reduction." Industrial & engineering chemistry research 40.12 (2001): 2618-2627.
[104] Abdelmalek, F., et al. "Gliding Arc Discharge (GAD) assisted catalytic degradation of bisphenol A in solution with ferrous ions." Separation and Purification Technology 63.1 (2008): 30-37.
[105] FERHAT, Mr Mohammed Fouad. Conception et réalisation d'un réacteur plasmagéne pour le traitement des films liquides. Diss. Université de Mostaganem-Abdelhamid Ibn Badis.
[106] Sweeney, Andrew J., and Y. A. Liu. "Use of simulation to optimize NO x abatement by absorption and selective catalytic reduction." Industrial & engineering chemistry research 40.12 (2001): 2618-2627.
[107] Ananthanarasimhan, J., et al. "Influence of gas dynamics on arc dynamics and the discharge power of a rotating gliding arc." Plasma Sources Science and Technology 28.8 (2019): 085012.
[108] Salazar-Torres, J. A., et al. "Impulse three phase power supply used for a gliding plasma discharge." Journal of Physics: Conference Series. Vol. 591. No. 1. IOP Publishing, 2015.
[109] Burlica, Radu, and Bruce R. Locke. "Pulsed plasma gliding-arc discharges with water spray." IEEE transactions on industry applications 44.2 (2008): 482-489.
[110] Lukes, P., et al. "Aqueous-phase chemistry and bactericidal effects from an air discharge plasma in contact with water: evidence for the formation of peroxynitrite through a pseudo-second-order post-discharge reaction of H2O2 and HNO2." Plasma Sources Science and Technology 23.1 (2014): 015019.
[111] Zhou, Renwu, et al. "Plasma-activated water: Generation, origin of reactive species and biological applications." Journal of Physics D: Applied Physics 53.30 (2020): 303001.
[112] Backa, Stefan, Kerstin Jansbo, and Torbjörn Reitberger. "Detection of hydroxyl radicals by a chemiluminescence method-a critical review." (1997): 557-564.
[113] Ghazi, Niloufar M., Andres A. Lastra, and Michael J. Watts. "Hydroxyl radical (OH) scavenging in young and mature landfill leachates." Water research 56 (2014): 148-155.
[114] Marouf-Khelifa, Kheira, et al. "Reduction of nitrite by sulfamic acid and sodium azide from aqueous solutions treated by gliding arc discharge." Separation and Purification Technology 50.3 (2006): 373-379.

[115] Meropoulis, S., and C. A. Aggelopoulos. "Plasma microbubbles vs gas-liquid DBD energized by low-frequency high voltage nanopulses for pollutants degradation in water: destruction mechanisms, composition of plasma-activated water and energy assessment." Journal of Environmental Chemical Engineering 11.3 (2023): 109855.
[116] Abd Allah, Zaenab, and J. Christopher Whitehead. "Plasma-catalytic dry reforming of methane in an atmospheric pressure AC gliding arc discharge." Catalysis Today 256 (2015): 76-79.
[117] Ghezzar, M. R., et al. "Gliding arc plasma assisted photocatalytic degradation of anthraquinonic acid green 25 in solution with TiO2." Applied Catalysis B: Environmental 72.3-4 (2007): 304-313.
[118] Ghezzar, M. R., et al. "Enhancement of the bleaching and degradation of textile wastewaters by Gliding arc discharge plasma in the presence of TiO2 catalyst." Journal of Hazardous Materials 164.2-3 (2009): 1266-1274.
[119] Saïm, Nacéra, et al. "New prototype for the treatment of falling film liquid effluents by gliding arc discharge part II: Plasmacatalytic activity of TiO2 thin film deposited by magnetron sputterin." Chemical Engineering and Processing: Process Intensification 98 (2015): 32-40.
[120] Lin, Kaijun, et al. "Decomposition of aqueous solutions of phenol using high energy electron beam irradiation—a large scale study." Applied radiation and isotopes 46.12 (1995): 1307-1316.
[121] Wengler, Julien. Synthèse organique en micro-réacteur plasma. Diss. Sorbonne Université, 2018.
[122] Ferhat, Mohamed Fouad, et al. "Conception of a novel spray tower plasma-reactor in a spatial post-discharge configuration: Pollutants remote treatment." Journal of hazardous materials 321 (2017): 661-671.
[123] Ghezzar, M. R. "traitement d'un rejet industriel par plasma". Thèse de doctorat, Université Abdelhamid Ibn Badis de Mostaganem, Algérie, 2007.
[124] Abdelmalek, F., et al. "Plasmachemical degradation of azo dyes by humid air plasma: Yellow Supranol 4 GL, Scarlet Red Nylosan F3 GL and industrial waste." Water Research 38.9 (2004): 2339-2347.
[125] Doubla, A., et al. "Organic pollutants abatement and biodecontamination of brewery effluents by a non-thermal quenched plasma at atmospheric pressure." Chemosphere 69.2 (2007): 332-337.
[126] Shimadzu excelence in science, Oxidation methods for TOC analyzers, 2006. https://www.shimadzu.com/an/products/total-organic-carbon-analysis/en/what/03.html. (accessed 20 Octobre 2024).
[127] Pawłat, Joanna, et al. "Evaluation of oxidative species in gaseous and liquid phase generated by mini-gliding arc discharge." Plasma Chemistry and Plasma Processing 39 (2019): 627-642.
[128] Hameedl, T. A., and S. J. Kadhem. "Gliding arc discharge for water treatment." IOP Conference Series: Materials Science and Engineering. Vol. 757. No. 1. IOP Publishing, 2020.
[129] Messai, Ridha, et al. "GAD plasma-assisted synthesis of ZnO nanoparticles and their photocatalytic activity." Materials Research Express 11.1 (2024): 015006.
[130] Lewis, Warren K., and Walter G. Whitman. "Principles of gas absorption." Industrial & Engineering Chemistry 16.12 (1924): 1215-1220.
[131] Ferhat, Mohammed Fouad, Mouffok Redouane Ghezzar, and Ahmed Addou. "Hydrodynamics and mass transfer investigations in a biphasic plasma reactor." International Journal of Chemical Reactor Engineering 19.4 (2021): 369-381.
[132] Chemical reactif products, Merck, 250, D-64293, Allemagne, Frankfuter stabe, (2000).
[133] Kudryashov, S. V., et al. "Oxidation of hydrocarbons in a barrier discharge reactor." High energy chemistry 34 (2000): 112-115.
[134] Suhr, H. "Applications and trends of nonequilibrium plasma chemistry with organic and organometallic compounds." Plasma chemistry and plasma processing 9 (1989): 7S-28S.
[135] SUHR, HARALD. "Organic syntheses under plasma conditions." Plasma Chemistry. Butterworth-Heinemann, 1974. 395-414.
[136] Suhr, Harald. "Organic reactions in the plasma of glow discharges." Angewandte Chemie International Edition in English 10.6 (1971): 422-422.
[137] Du, Yuhang, et al. "Dielectric barrier discharge plasma pretreatment: A cleaner new way to improve energy efficiency and quality of wolfberry drying." Journal of Cleaner Production 450 (2024): 141951.
[138] Li, Wenping, et al. "Non-thermal plasma assisted catalytic water splitting for clean hydrogen production at near ambient conditions." Journal of Cleaner Production 387 (2023): 135913.
[139] Haji, Aminoddin, and Maryam Naebe. "Cleaner dyeing of textiles using plasma treatment and natural dyes: A review." Journal of cleaner production 265 (2020): 121866.
[140] B. Debray et al "Méthode d'analyse des risques générés par une installation industrielle Ω-7". Study report, N° 46055-CL47569, INERIS-DRA, (2006). p 140
[141] Froquet, Laurent. "Contribution à l'analyse des risques : Proposition d'une méthode par scénarios et capitalisation de la connaissance". Diss. Institut National Polytechnique de Grenoble-INPG, 2005.
[142] Marszal, Edward M., and Eric William Scharpf. Safety Integrity Level Selection. ISA, the Instrumentation, Systems, and Automation Society, 2002.

[143] J. Dunjó, V. Fthenakis. Juan A. Vílchez and J. Arnaldos. Hazard and operability (HAZOP) analysis. A literature review. Journal of Hazardous Materials. 2010. pp19.
[144] Yalkowsky, Samuel H., Yan He, and Parijat Jain. Handbook of aqueous solubility data. CRC press, 2016.
[145] Dou, Yuan, et al. "Hydrogen sulfide inhibits enzymatic browning of fresh-cut Chinese water chestnuts." Frontiers in Nutrition 8 (2021): 652984.
[146] Rana, Md Sohel, and Marcelo I. Guzman. "Oxidation of catechols at the air–water interface by nitrate radicals." Environmental Science & Technology 56.22 (2022): 15437-15448.
[147] Yang, Da-Peng, et al. "How many drugs are catecholics." Molecules 12.4 (2007): 878-884.
[148] Dong, Lin, et al. "Sustainable production of dopamine hydrochloride from softwood lignin." Nature Communications 14.1 (2023): 4996.
[149] Koufaki, Maria, et al. "Chroman/catechol hybrids: synthesis and evaluation of their activity against oxidative stress induced cellular damage." Journal of medicinal chemistry 49.1 (2006): 300-306.
[150] Shin, Hee Soon, et al. "Catechol groups enable reactive oxygen species scavenging-mediated suppression of PKD-NFkappaB-IL-8 signaling pathway by chlorogenic and caffeic acids in human intestinal cells." Nutrients 9.2 (2017): 165.
[151] Fukazawa, Nobuyuki, et al. "Catechol derivatives and pharmaceutical preparations containing same." U.S. Patent No. 5,232,923. 3 Aug. 1993.
[152] Motiejunaite, Justina, Laurence Amar, and Emmanuelle Vidal-Petiot. "Adrenergic receptors and cardiovascular effects of catecholamines." Annales d'endocrinologie. Vol. 82. No. 3-4. Elsevier Masson, 2021.
[153] Kinoshita, Kosaku. "Traumatic brain injury: pathophysiology for neurocritical care." Journal of intensive care 4 (2016): 1-10.
[154] Chesnut, Randall M., et al. "The role of secondary brain injury in determining outcome from severe head injury." 50 Landmark Papers every Trauma Surgeon Should Know. CRC Press, 2019. 63-66.
[155] Gubbi, Sriram, et al. "Catecholamine physiology and its implications in patients with COVID-19." The Lancet Diabetes & Endocrinology 8.12 (2020): 978-986.
[156] Pak, Chang Sik, et al. "Effects of a catechol-functionalized hyaluronic acid patch combined with human adipose-derived stem cells in diabetic wound healing." International journal of molecular sciences 22.5 (2021): 2632.
[157] Zhang, Wei, et al. "Catechol-functionalized hydrogels: biomimetic design, adhesion mechanism, and biomedical applications." Chemical Society Reviews 49.2 (2020): 433-464.
[158] Gao, Hongcai, et al. "Mussel-inspired synthesis of polydopamine-functionalized graphene hydrogel as reusable adsorbents for water purification." ACS applied materials & interfaces 5.2 (2013): 425-432.
[159] Karthik, P., et al. "A visible-light active catechol–metal oxide carbonaceous polymeric material for enhanced photocatalytic activity." Journal of materials chemistry A 5.1 (2017): 384-396.
[160] Joshi, Saurabh, et al. "Functional catechol–metal polymers via interfacial polymerization for applications in water purification." ACS applied materials & interfaces 12.16 (2020): 19044-19053.
[161] Patil, Nagaraj, Christine Jerome, and Christophe Detrembleur. "Recent advances in the synthesis of catechol-derived (bio) polymers for applications in energy storage and environment." Progress in Polymer Science 82 (2018): 34-91.
[162] Payra, Debabrata, et al. "Bioinspired adhesive polymer coatings for efficient and versatile corrosion resistance." RSC advances 5.21 (2015): 15977-15984.
[163] Li, Jiao, et al. "A novel sol-gel coating via catechol/lysine polymerization for long-lasting corrosion protection of Mg alloy AZ31." Colloids and Surfaces A: Physicochemical and Engineering Aspects 656 (2023): 130361.
[164] Feng, Cheng-yuan, et al. "Metallization of polyphenylene sulfide by low-cost mussel-inspired catechol/polyamine surface modification." ACS Applied Polymer Materials 4.6 (2022): 4445-4453.
[165] Bouad, Vincent, et al. "Utilization of catechol end-functionalized PMMA as a macromolecular coupling agent for ceramic/fluoropolymer piezoelectric composites." ACS Applied Polymer Materials 4.10 (2022): 7258-7267.
[166] Sakib, Sadman, et al. "Surface functionalization of metal oxide semiconductors with catechol ligands for enhancing their photoactivity." Solar RRL 5.10 (2021): 2100512.
[167] Karthik, P., et al. "A visible-light active catechol–metal oxide carbonaceous polymeric material for enhanced photocatalytic activity." Journal of materials chemistry A 5.1 (2017): 384-396.
[168] Casado, Nerea, and David Mecerreyes, eds. Redox polymers for energy and nanomedicine. Vol. 34. Royal Society of Chemistry, 2020.
[169] Patil, Nagaraj, Christine Jerome, and Christophe Detrembleur. "Recent advances in the synthesis of catechol-derived (bio) polymers for applications in energy storage and environment." Progress in Polymer Science 82 (2018): 34-91.
[170] Zhu, Limin, et al. "Recent Developments in Safety-Enhancing Separators for Lithium-Ion Batteries." Journal of The Electrochemical Society 168.10 (2021): 100524.

[171] Khezraqa, Homayun, et al. "A review on polydopamine as an efficient material in different components of rechargeable ion batteries." Journal of Energy Storage 79 (2024): 110170.
[172] Ryou, Myung Hyun, et al. "Mussel-inspired polydopamine-treated polyethylene separators for high-power Li-ion batteries." Advanced materials 23.27 (2011): 3066-3070.
[173] Kang, Sung Min, et al. "Mussel-and diatom-inspired silica coating on separators yields improved power and safety in Li-ion batteries." Chemistry of Materials 24.17 (2012): 3481-3485.
[174] Lingappan, Niranjanmurthi, et al. "A comprehensive review of separator membranes in lithium-ion batteries." Renewable and Sustainable Energy Reviews 187 (2023): 113726.
[175] Tyman, John HP. "Chapter 14 Synthesis of natural phenols (and their derivatives) of pharmaceutical, medicinal or technical interest." Studies in Organic Chemistry 558-661 52 (1996): 0165-3253.
[176] Suzuki, Toshisada, et al. "A catechol-type lignan and neolignans are specifically present in the seed coat of tung trees." Journal of Wood Science 66 (2020): 1-6.
[177] Çiğdem, Ayhan, and Uğur Güller. "Purification and characterization of catechol oxidase from Posof Badele apple (Malus domestica L): in vitro and in silico studies." International Journal of Food Engineering 18.7 (2022): 513-524.
[178] Link, Karl Paul, and Jo C. Walker. "The isolation of catechol from pigmented Onion scales and its significance in relation to disease resistance in Onions." (1933): 379-383.
[179] Ma, Zhiqiang, Ekaterina Troussard, and Jeroen A. Van Bokhoven. "Controlling the selectivity to chemicals from lignin via catalytic fast pyrolysis." Applied Catalysis A: General 423 (2012): 130-136.
[180] Zhang, Min, et al. "Pyrolysis of lignin extracted from prairie cordgrass, aspen, and Kraft lignin by Py-GC/MS and TGA/FTIR." Journal of Analytical and Applied Pyrolysis 98 (2012): 65-71.
[181] Yang, Le, et al. "Green and efficient synthesis route of catechol from guaiacol." Journal of Molecular Catalysis A: Chemical 368 (2013): 61-65.
[182] Ivanov, D. P., et al. "New way of hydroquinone and catechol synthesis using nitrous oxide as oxidant." Advanced Synthesis & Catalysis 344.9 (2002): 986-995.
[183] Tao, Ying, et al. "Oxidation of benzene to phenol, catechol, and 1, 2, 3-trihydroxybenzene by toluene 4-monooxygenase of Pseudomonas mendocina KR1 and toluene 3-monooxygenase of Ralstonia pickettii PKO1." Applied and Environmental Microbiology 70.7 (2004): 3814-3820.
[184] Mi, Wei, et al. "Direct hydroxylation of benzene to phenol by dielectric barrier discharge plasma." Russian Journal of Physical Chemistry A 93 (2019): 2812-2816.
[185] Pamin, Katarzyna, et al. "Hydroxylation of phenol by hydrogen peroxide catalyzed by heteropoly compounds in presence of glycerol as green solvent." Catalysis Today 257 (2015): 80-85.
[186] Azizi, Ahmed, Mahmoud Abouseoud, and Abdeltif Amrane. "Phenol Removal by a Sequential Combined Fenton-Enzymatic Process." Nature Environment & Pollution Technology 16.1 (2017).
[187] Shi, Huixian, et al. "Photocatalytic hydroxylation of phenol to catechol and hydroquinone by using organic pigment as selective photocatalyst." Current Organic Chemistry 16.24 (2012): 3002-3007.
[188] Song, Guotian, et al. "High-level production of catechol from glucose by engineered Escherichia coli." Fermentation 8.7 (2022): 344.
[189] Jeenpadiphat, Sirima, Isara Mongkolpichayarak, and Duangamol Nuntasri Tungasmita. "Catechol production from lignin by Al-doped mesoporous silica catalytic cracking." Journal of Analytical and Applied Pyrolysis 121 (2016): 318-328.
[190] Wang, He-Fang, Ye-Yu Wu, and Xiu-Ping Yan. "Room-temperature phosphorescent discrimination of catechol from resorcinol and hydroquinone based on sodium tripolyphosphate capped Mn-doped ZnS quantum dots." Analytical chemistry 85.3 (2013): 1920-1925.
[191] J.E. Lyons, 1976. U.S. Patent No. 3,987,112. Washington, DC: U.S. Patent and Trademark Office.
[192] 焦宁梁雨锋宋颂. “Synthesis method for catechol compound.” China Patent. CN105801381A. 2016.
[193] K. Matsuzawa, A. Matukuma, I. Takagishi, K. Yoshida, 1974. U.S. Patent No. 3,825,604. Washington, DC: U.S. Patent and Trademark Office.
[194] Higbie, Ralph. "The rate of absorption of pure gas into a still liquid during short periods of exposure." Trans. Am. Inst. Chem. Engrs. 31 (1935): 365-389.
[195] Renon, Henri, and John M. Prausnitz. "Local compositions in thermodynamic excess functions for liquid mixtures." AIChE journal 14.1 (1968): 135-144.
[196] U.S BUREAU OF LABOR STATISTICS, 1995. Midwest Information Office. 749 https://www.bls.gov/regions/midwest/data/averageenergyprices_selectedareas_table.htm / 750 (accessed 02 January 2023).
[197] Pharmacompass, 2015. price. https://www.pharmacompass.com/search/q=price/ (accessed 729 20 Octobre 2023).
[198] Water security agency, 1993. industrial-water-use-charges. https://www.wsask.ca/permits731 approvals/regulatory-information/industrial-water-use-charges/(accessed 20 Octobre 2023).

[199] Made in China, 1998. Products. https://shkingair.en.made-in744 china.com/product/txqpjlVyr-FWb/China-High-Quality-15kw-20HP-20bar-VSD-Permanent745 Magnet-High-Pressure-Electric-AC-All-in-One-Industry-Rotary-Screw-Air-Compressor.html 746 / (accessed 02 January 2024).
[200] ebay, 1995. items. https://www.ebay.com/itm/134213120941/ (accessed 02 January 2023).
[201] Kawasaki, Toshiyuki, et al. "Detection of reactive oxygen species supplied into the water bottom by atmospheric non-thermal plasma jet using iodine-starch reaction." Japanese Journal of Applied Physics 54.8 (2015): 086201.
[202] Rodier, Jean, et al. "L'analyse de l'eau. 7eme édition." Paris, France (1984).

Annexes II.1 The determination of total oxidants by the KI method [201]

The potassium iodide-starch (KI-Starch) test, is a detecting method of the oxidizing agents. It is often applied to measure total oxidative species (TOS) in plasma. The test relates to the oxidation of iodide (I^-) to iodine (I_2), which forms a blue complex with starch. The intensity of the color is proportional to the amount of oxidizing species present in the sample.

The principle of the analysis of total oxidants by the KI-Amidon method is based on two main stages, such as:

The oxidation of iodide ions (I^-) into iodine (I_2):

In an acidic medium and in the presence of anions iodide, plasma oxidants have an oxidation-reduction potential greater than that of the I2/I- redox couple (E°= 0.621 V), are capable of oxidizing the iodide anion I- into iodine (I2), to give water (H2O).

The reaction between the iodine and the starch:

Starch is a carbohydrate found in plants. It consists of two different types of polysaccharides that are made up of glucose units which are connected in two different ways.

When iodine (usually in the form of potassium iodide solution, KI) comes into contact with amylose, it inserts itself into the amylose spiral, causing a color change, often a deep blue hue. This indicates the presence of oxidants.

Example : Hydrogen pyroxide oxidizer

Redox couple involved:

- H_2O_2 / H_2O, E° = 1.77V.
- I_2 / I^- E° = 0.53V.

Note: this reaction is slow, but can be accelerated by the addition of a catalyst, ammonium or sodium molyb-date.

Equations:

$$H_2O_2 + 2H^+ + 2e^- \leftrightarrow 2\,H_2O \qquad \textbf{(R 75)}$$

$$I_2 + 2e^- \leftrightarrow 2I^- \qquad \textbf{(R 76)}$$

Bilan : $$H_2O_2 + 2H^+ + 2I^- \rightarrow 2\,H_2O + I_2 \qquad \textbf{(R 77)}$$

Reduction of I_2 by starch:

$$I_2 + \text{starch} \rightarrow \text{Iodine} - \text{Starch (Darc bleu complex)} \quad \textbf{(R 78)}$$

Procedure:

Preparation of KI-Starch solution:

- Weigh 240 g of ioded potassium and 120 g of starch, both were purchased from sigma Al-drich.
- Dissolve the starch powder in 20 mL of warmed ultrapure water and stir with a magnetic stirrer until the solution is homogenized.
- After heating the prepared solution to 40 C°, add the weighted KI powder and shake until being homogeneous again.

Total oxidant analysis:

- After plasma treatment of ultrapure water, collect 1.5 mL of treated water and introduce into a 3 mL UV-Visible analysis cell.
- Add a drop of 0.1 N chloridric or sulfuric acid to accelerate the reaction.
- Make a 10-fold dilution for short treatment times and a 20-fold dilution for long treatment times.
- Measure the absorbance of the diluted samples at a wavelength of 680 nm.

Note: Only the ultrapure water was added to KI-Starch solution as control sample.

NB: The KI method is suitable for all oxidizing agents. We have therefore assimilated the results obtained by this method to total oxidants.

Annexe II.2 Nitrite determination [202].

Sulfanilic acid in hydrochloric medium, in the presence of ammonium ions and phenol (ZAMBELLI reagent), forms a yellow complex with nitrite ions, the intensity of which is proportional to the nitrite concentration.

Procedure

The yellow-colored complex absorbs at wavelength 435 nm, so the intensity, which is proportional to nitrite concentration, can be evaluated spectrophotometrically. A standard solution of 0.0023% Nitrite is used as the starting point. g L^{-1}.

Reagents

- Pure ammonia.
- ZAMBELLI reagents:
- Hydrochloric acid (d=1.19) 260 mL;
- Sulfanilic acid 5 g;
- Crystallized phenol 7.5 g;
- Ammonium chloride 135 g;
- Distilled water 625 mL.

Place the HCl acid in a 1-liter flask, add distilled water and dissolve the sulfanilic acid and phenol, heating gently in a water bath. After complete dissolution, add ammonium chloride and stir until dissolved. After cooling, make up with distilled water.

- NO2- stock standard solution 0.23 g L^{1}
- Sodium nitrite 0.345 g L^{-1}
- Distilled water 1000 mL
- Daughter solution 0.0023 g L^{-1}

Into 6 vials introduce the different standard daughter solutions.

Table 26. Nitrite calibration curve

N°	Indicator	1	2	3	4	5
Standard daughter solution (mL)	0	1	5	10	15	20
Distilled water (mL)	50	49	45	40	35	30
Zambelli reagent	2	2	2	2	2	2
10 minutes						
Pure ammonia (mL)	2	2	2	2	2	2

Procedure

Take 50 mL of the sample to be analyzed, add 2 mL of ZAMBELLI reagent and allow to stand for 10 minutes, then introduce 2 ml of pure ammonia. The calibration curve obtained is shown in figure 53.

Table 27. Absorbance at 435 nm as a function of nitrite concentration

ABS_{435nm}	0	0,097	0,413	0,907	1,247	1,621
$[NO_2^-]$	0	0,046	0,230	0,460	0,690	0,920

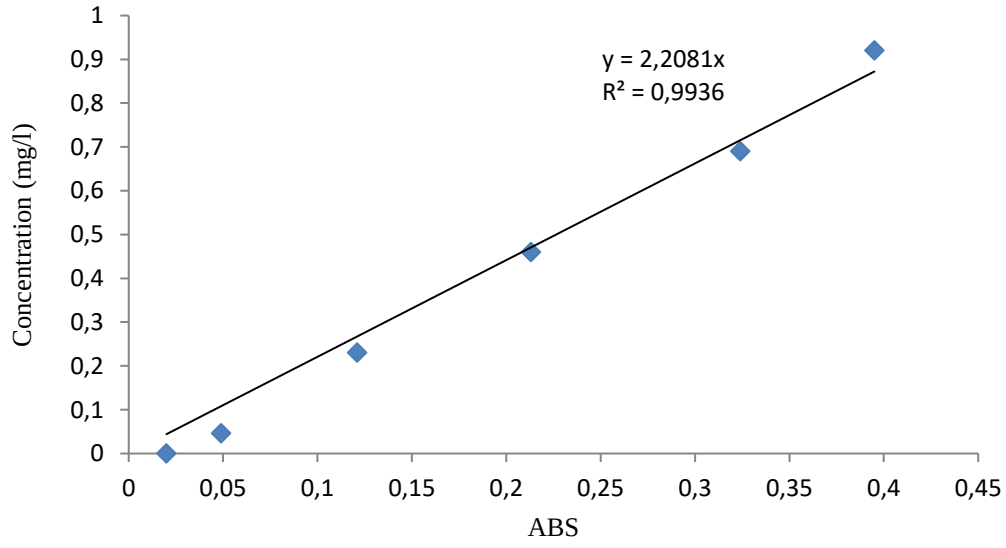

Figure 54. Nitrite ions calibration curve

Annexe II.3 Nitrate determination-Sodium salicylate method [202]

In the presence of sodium salicylate, nitrates react to give sodium paranitrosalicylate, which is suitable for colorimetric determination.

Reagents

- 0.5% salicylate solution, repeated every 24 hours;
- Sulfuric acid (d=1.84);
- Sodium hydroxide, sodium tartrate and potassium tartrate solution;
- Sodium hydroxide 400 g;
- Sodium potassium tartrate 60 g;
- Distilled water 1000 mL;
- Dissolve salts and allow to cool
- Standard stock solution 0.1 g L^{-1} ;
- Potassium nitrate 0.722 g;
- Distilled water 1000 q s;
- Daughter standard solution 0.005 g L^{-1}.

Into 5 flasks, introduce the different daughter standard solutions,

Table 28. Nitrate calibration curve

N°	Indicator	1	2	3	4
Standard daughter solution (mL)	0	1	2	5	10
Distilled water	10	9	8	5	0
Sodium salicylates	1	1	1	1	1

Evaporate to dryness in a water bath heated to 75-80°C, moisten the dry material with 2 mL sulfuric acid, leave to stand for 10 min, then add 15 mL distilled water and 15 mL sodium hydroxide solution and sodium potassium tartrate, which develops a yellow coloration. Read at 415 nm.

Procedure

Introduce 10 mL of the sample to be analyzed, add 1 mL of sodium salicylate, then continue with the same assay as for the calibration curve. Prepare a control with 10 mL distilled water. For a 10 mL sample, the calibration curve directly gives the ex-pressed nitrate nitrogen content in (mg. L^{-1}), to obtain the nitrate concentration, multiplied by 4.43.

The calibration curve obtained is shown in figure.54

Table 29. Absorbance at 415 nm as a function of nitrate concentration

ABS_{415nm}	0	0,173	0,291	0,697	1,359
$[NO_3^-]$	0	0,5	1	2,5	5

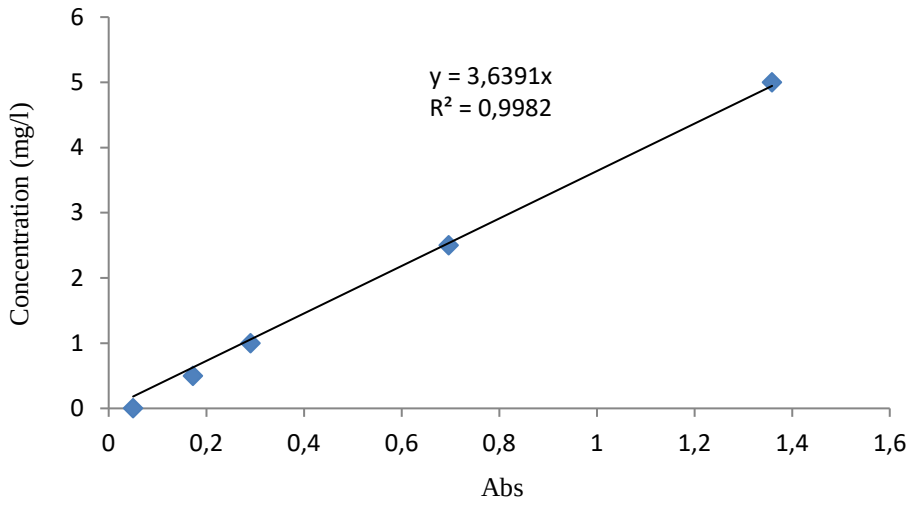

Figure 55. Nitrate ions calibration curve

Annexe II.4 Analysis of phenol and its by-products

Chromatograms of the various phenol samples analyzed during processing show numerous peaks of reaction intermediates, the by-products of phenol oxidation.

The chromatographic detection conditions (mobile phase composition, retention time, wavelength, etc.) for the various references studied are shown in Table 30.

Table 30. Chromatographic analysis parameters for reference products

Compound	Mobil phases		Flowrate (mL min^{-1})	Wavelength (nm)	Retention time (min)
	Aqueous phase (%)	Organic phase (%)			
Phenol	60	40	1	270	6.34
Hydroquinone	60	40	1	254	3.37
Catechol	60	40	1	254	4.20
Resorcinol	60	40	1	270	3.70
2-Nitrophénol	60	40	1	247	12.0
4-Dinitrophénol	60	40	1	247	9.34
***p*-Benzoquinone**	60	40	1	254	4.87

Intermediates are identified by comparing the retention times of the reference products. When the chromatogram characteristics of the intermediate match those of the reference product, a third sample containing a mixture of phenol and reference product is analyzed by HPLC. When the area of the chromatogram peak corresponds to the retention time of the intermediate studied, we can consider that the intermediate and the reference are identical. Concentrations are calculated from calibration curves obtained under the same conditions as the samples taken.

The calibration curves obtained are presented in figure.55.

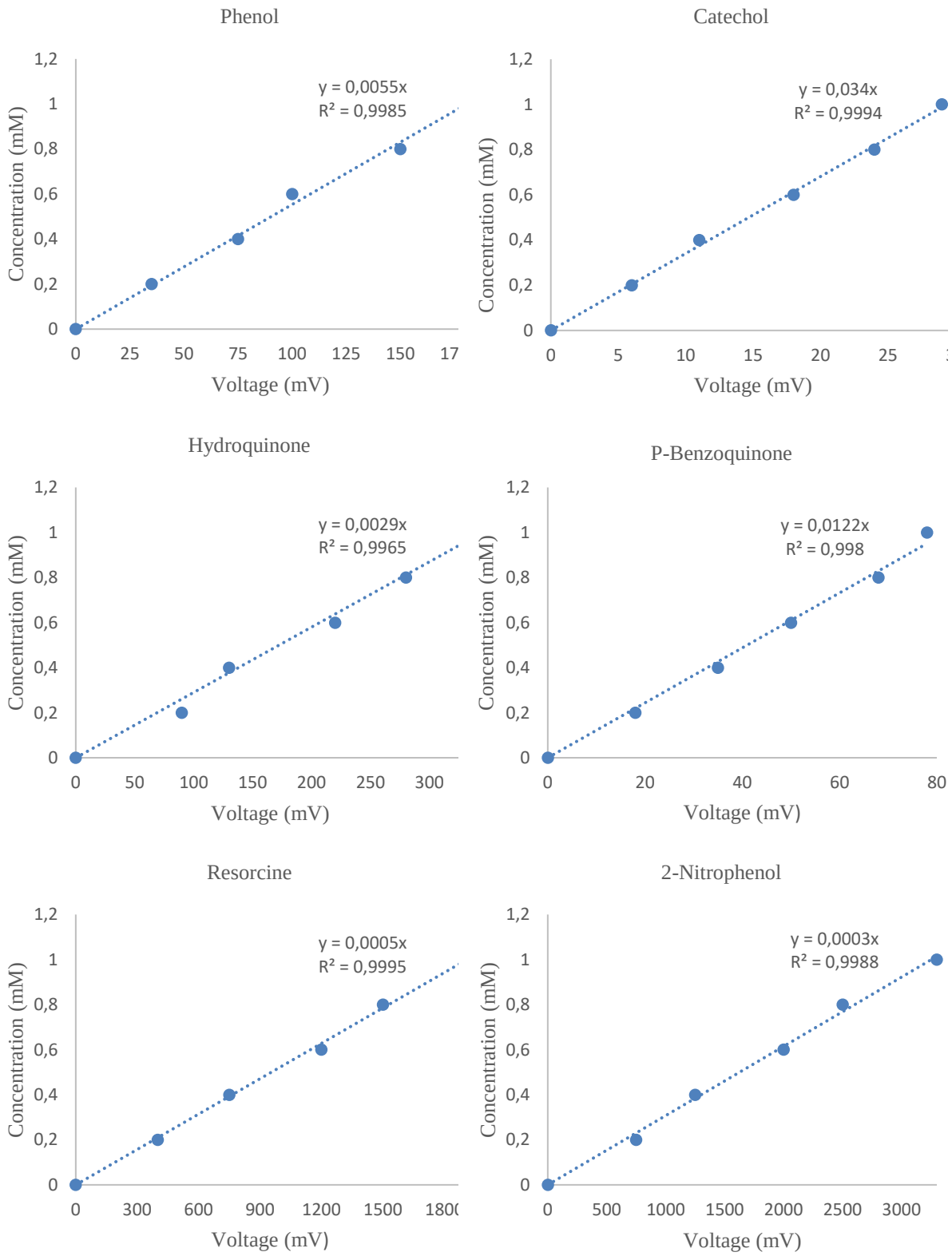

Figure 56. Phenol and its by-products calibration curves.